RCA REVIEW

a technical journal

RADIO AND ELECTRONICS
RESEARCH · ENGINEERING

VOLUME XIII JUNE 1952 NO. 2

RCA REVIEW, published quarterly in March, June, September and December by RCA Laboratories Division, Radio Corporation of America, Princeton, New Jersey. Entered as second class matter July 3, 1950 at the Post Office at Princeton, New Jersey, under the act of March 3, 1879. Subscription price in the United States, Canada and Postal Union; one year $2.00, two years $3.50, three years $4.50: in other countries; one year $2.40, two years $4.30, three years $5.70. Single copies in the United States, $.75; in other countries, $.85.

RCA REVIEW

a technical journal

RADIO AND ELECTRONICS
RESEARCH • ENGINEERING

Published quarterly by
RCA Laboratories Division
Radio Corporation of America
in cooperation with

RCA Victor Division
Radiomarine Corporation of America
RCA International Division
RCA Communications, Inc.
National Broadcasting Company, Inc.
RCA Institutes, Inc.

VOLUME XIII | JUNE, 1952 | NUMBER 2

CONTENTS

RCA REVIEW is regularly abstracted and indexed by *Industrial Arts Index, Science Abstracts* (I.E.E.-Brit.), *Electronic Engineering Master Index, Chemical Abstracts, Proc. I.R.E.*, and *Wireless Engineer.*

RCA REVIEW

BOARD OF EDITORS

I. R. E.—The First Forty Years

On the night of May 13th, 1912, a group of 46 pioneers, devoted to the new, rapidly growing science of wireless communication, gathered together to found the Institute of Radio Engineers. Forty years later the membership of the Institute is 30,000, a remarkable growth which has kept pace with the great advances of electronics itself. The Institute has, in fact, had an outstanding part in the pattern of events which has brought the field of electronics to its present high state of development.

Through the Institute of Radio Engineers, scientists and engineers have been able to give their work wide publication. They have formed Technical Committees, Standardization Committees, Professional Groups devoted to specialized fields, and have fostered a number of other cooperative activities which have made contributions to engineering, to industry, and to the public at large.

On the occasion of the 40th Anniversary of the founding of the Institute of Radio Engineers, the Editors of *RCA Review* wish to join its readers in extending congratulations to the Institute on its accomplishments and in predicting a future of ever-increasing usefulness.

SOME TYPES OF OMNIDIRECTIONAL HIGH-GAIN ANTENNAS FOR USE AT ULTRA-HIGH FREQUENCIES*

By

J. Epstein, D. W. Peterson, and O. M. Woodward, Jr.

Research Department, RCA Laboratories Division,
Princeton, N. J.

Summary—The construction and operation of three types of UHF transmitting antennas are described, two of which utilize a quadrature feed system and the third an in-phase drive. All of these constructions provide simple means of integrating the design of the supporting structure and radiating elements. In addition, considerable simplification of the feed system is obtained by energizing each vertical row at one end. The two primary drawbacks of all of the models are their frequency sensitivity and the multiplicity of feed points. Both of these defects can be overcome by the development of a unit antenna having a large radiating aperture for a single feed point.

The advantages of using a quadrature feed are quite significant in that it provides a simple method of matching the input transmission lines, maintaining equal power division in the radiating elements, and diplexing two signals into the common antenna.

DURING 1946 it became evident that the most likely frequency range for the extension of television broadcasting services lay between 500 and 900 megacycles. Consequently, a program was initiated with the object of developing transmitting antennas for this band of frequencies.

The following tentative specifications for antenna characteristics were drawn up at that time: (1) a circular azimuth pattern; (2) a power gain of twenty; (3) a power handling capacity of 50 kilowatts; (4) a flat impedance characteristics for at least six megacycles.

Requirement (1) was based on the assumption that the transmitting antenna would be centered in its service area. A circular azimuth pattern can be obtained by two methods. One uses the required number of in-phase radiating elements disposed symmetrically around a circle. The other uses four elements, equally spaced on the circumference and

* Decimal Classification: R326.7.

fed in quadrature. The power gain is, of course, determined by the number of layers of the basic units. The power gain and power handling capacity requirements were a recognition of the fact that propagation characteristics in this range stress the need for all the radiated power that can be obtained.

It is assumed that both picture and sound signals will be diplexed into the same antenna. In view of the fact that the transmitting antenna will generally be located quite a distance from the transmitter, it would appear to be highly desirable to use a single line between the transmitters and the antenna because of economical and operational considerations. However, the advantages thus gained are somewhat offset by the fact that such an arrangement will require the use of a frequency selective circuit in order to diplex both picture and sound transmitters into the single line. This becomes rather serious in the transmission of color television signals with the attendant necessity of maintaining adequate high-frequency response. The alternative is to use a turnstile type of antenna which requires two transmission lines but which permits the diplexing to be done with a bridge network[1] which has a broader frequency response. The details of such a circuit will be discussed.

It was decided to concentrate the development work on radiating structures which utilize quadrature feed; however, the use of structures utilizing in-phase drive were not eliminated from consideration and a novel design along these lines is described. Basically this decision was made because a quadrature-fed antenna permits the use of a network which has the property of providing a perfect termination for the input transmission line and of insuring a circular azimuth radiation pattern.

First, consider a single layer of the slot antenna as shown in Figure 1. It consists of a metal cylinder with four equally spaced axial slots. Diametrically opposite slots are fed out of phase with one another and in quadrature with the other set. Each slot is energized at its center by means of a coaxial transmission line. The electric field component of the radiated field is parallel to the width of the slot. Each set of diametrically opposite slots is located in a zero potential plane with respect to the other set and, as a consequence, there is no coupling between them. The relative azimuth pattern produced by each set of diametrically opposite slots is given by the expression[2]

---

[1] R. W. Masters, "A Power-Equalizing Network for Antennas," *Proc. I.R.E.*, Vol. 37, p. 735, July, 1949.

[2] G. Sinclair, "The Patterns of Slotted-Cylinder Antennas," *Proc. I.R.E.*, Vol. 36, p. 1487, December, 1948.

$$E_\phi = \sum_{n=1,3,5}^{n=\infty} j^n \frac{\sin(n\alpha)}{n\alpha} \frac{\cos(n\phi)}{\left[J'_n \frac{(\pi d)}{\lambda} - jN'_n \frac{(\pi d)}{\lambda} \right]},$$

where $\alpha = \frac{1}{2}$ of the angle subtended by width of slot, in radians,

$d/\lambda =$ diameter of pole, in wave lengths,

$\phi =$ azimuth angle.

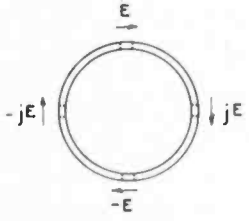

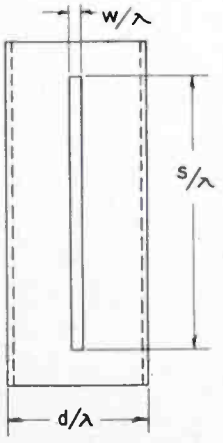

Fig. 1—Single layer of cylindrical slot antenna.

$$J'_n \frac{(\pi d)}{\lambda} = \frac{J_{(n-1)} \frac{(\pi d)}{\lambda} - J_{n+1} \frac{(\pi d)}{\lambda}}{2},$$

Bessel function of first kind.

$$N'_n \frac{(\pi d)}{\lambda} = \frac{N_{n-1} \frac{(\pi d)}{\lambda} - N_{(n+1)} \frac{(\pi d)}{\lambda}}{2}.$$

Bessel function of second kind.

For small values of d/λ, E_ϕ can be represented by the first term of the expansion, since $N'_n\ (\pi d)/\lambda$ becomes very large for $n > 1$. Hence, the

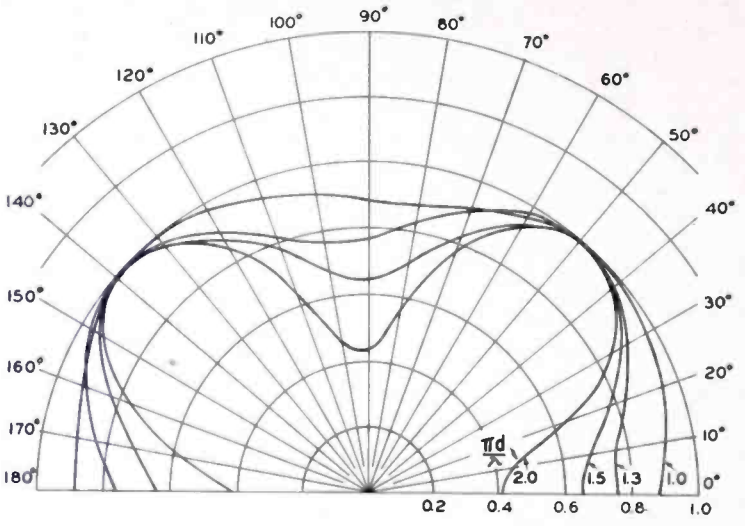

Fig. 2—Azimuth patterns of a cylindrical slot antenna as a function of diameter to wave length ratio.

field produced by one set of diametrically opposite slots is proportional to cos ϕ, while the other set radiates a field proportional to sin ϕ. Since the two fields are fed in quadrature, the total field is proportional to $[\cos \phi + j \sin \phi]$ which is, of course, constant for all values of ϕ. A series of azimuth patterns as a function of d/λ has been calculated and is shown in Figure 2. The ratio of minimum to maximum fields for the various azimuth patterns has been plotted against d/λ in Figure 3. The variation of E as a function of the elevation angle θ, as deter-

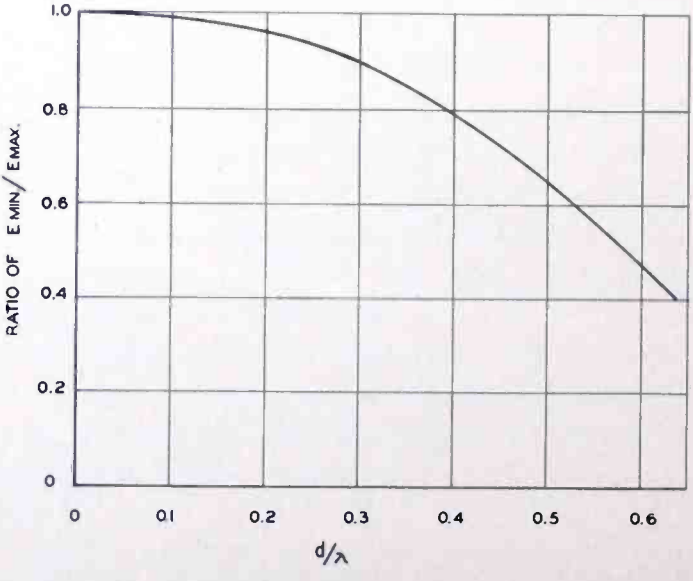

Fig. 3—Ratio of minimum to maximum fields of azimuth patterns of cylindrical slot antenna as a function of d/λ.

mined experimentally, very closely approximates the radiation pattern of a dipole having the same electrical length as the slot.

Although several workers, notably C. H. Holt,[3] have made contributions to the theoretical formulation of the input impedance of a slotted cylinder, no satisfactory solution has been given for the range of d/λ which is of interest here. Consequently, considerable time was devoted to an experimental determination of the impedance characteristic of slots. A typical impedance curve as a function of the length of the

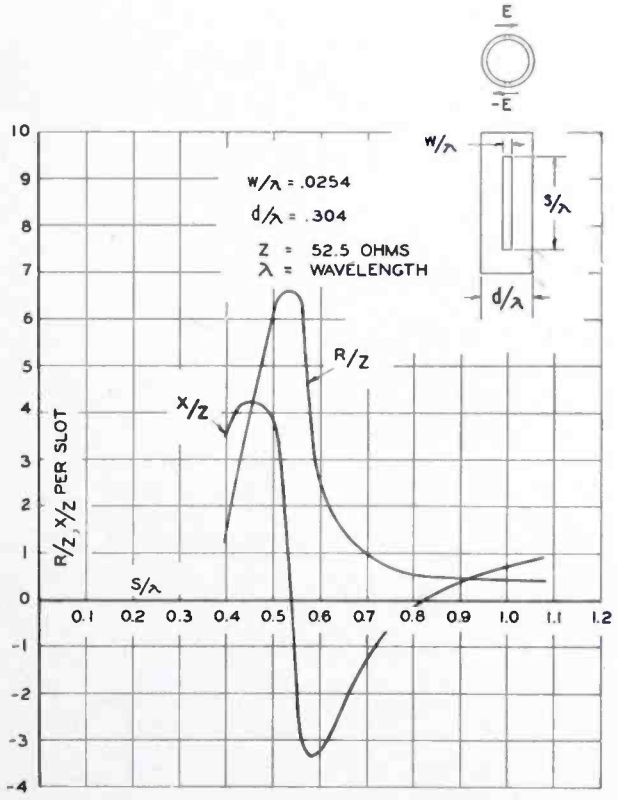

Fig. 4—Typical impedance curve of a cylindrical slot antenna.

slot in wave lengths for $d/\lambda = .304$ is shown in Figure 4. s/λ is chosen so that the slot is operating around the second resonance point since this is the region of flattest impedance-frequency response.

In the spring of 1948,[4] a field test was initiated involving transmissions on frequencies in the vicinity of 500 megacycles. In anticipation of these field tests, a slot antenna with a nominal power gain of 10 was developed. The antenna structure was made from a seamless steel tube

[3] C. H. Holt, "Input Impedance of Slotted-Cylinder Antenna," University of Illinois Bulletin, Vol. 47, No. 51, March, 1950.

[4] G. H. Brown, "Field Test of Ultra-High-Frequency Television in the Washington Area," *RCA Review*, Vol. IX, p. 585, December, 1948.

six inches in diameter and over twenty feet in length. For tests in Washington, D. C., it seemed logical to place the antenna on top of the channel 4 antenna used by television station WNBW. A study of the mechanical problem revealed that it would be desirable to design and construct a 500-megacycle antenna of smaller dimensions in order that the existing supporting pole not be stressed unduly. Hence, an antenna having a power gain of 5 was specially constructed. A picture of this antenna, which is also constructed of 6-inch seamless steel tubing, is shown in Figure 5. The over-all height of the structure shown, which

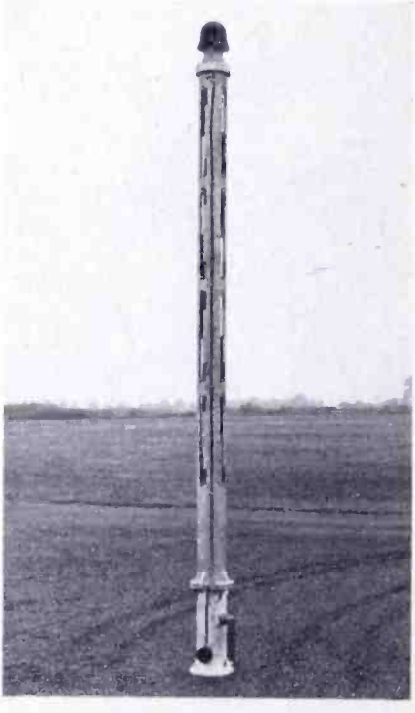

Fig. 5—500-megacycle slot antenna.

comprises the antenna and housing for a power equalizing circuit, is approximately 10 feet. The required power gain is obtained with four layers of slot radiators with a separation of one wave length between layers. Each vertical row is energized by a solid dielectric coaxial line which is secured to the inside wall of the steel tubing. The input voltages to the lines are obtained from a bridge circuit called a power equalizing network. The reason for this name and a detailed explanation of its operation is given in Appendix A. A view of the equalizer with the housing removed is shown in Figure 6. The phasing and matching network is shown in Figure 7a which view would be obtained by making an axial cut along the tube and then unrolling it.

The indicated input voltages are derived from the equalizer net-

work. The slots in a given row are in phase and the rows are phased relative to each other as indicated in Figure 1. Some details of the electrical circuitry are of interest. The outer conductor of the coaxial line feeding each row is bonded to the inner surface of the wall. The drive voltage for each slot is obtained by removing the outer conductor at the midpoint of each slot. Since the electrical length of the coaxial line between adjacent slots is 3/2 wave lengths, this effectively puts the impedances of the radiators in series. In order to facilitate matching the antenna to the feed lines, a series stub which can be used to

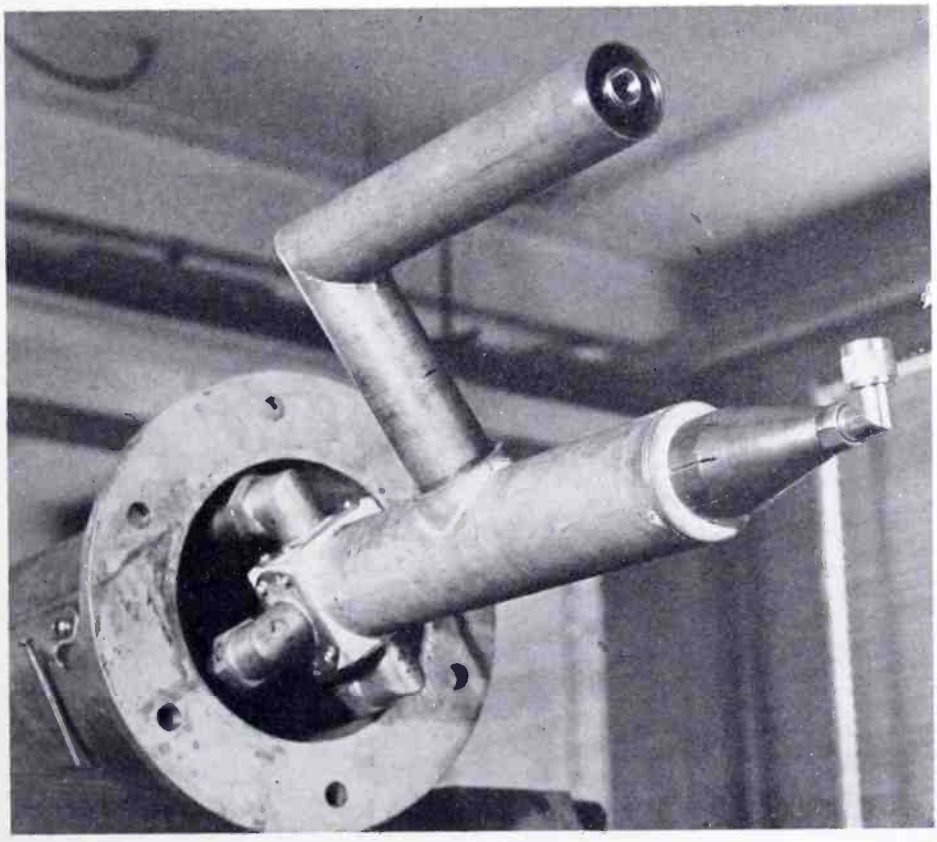

Fig. 6—Power equalizer used with 500-megacycle slot antenna.

resonate the antenna reactance is inserted as indicated. Since the radiation impedance of each slot is approximately 25 ohms, the total input impedance is 100 ohms and consequently a ¼-wave-length transformer is used to match to the 52.5-ohm coaxial feed lines. The quadrature phasing is obtained by simply extending the length of two of the feed lines by ¼ wave length.

A simple bridge network, as described in Appendix A, may be used to feed the picture and sound signals into the same antenna. It was intended that the diplexer used for this purpose be mounted in the

base of the antenna with separate transmission lines from the sound and picture transmitters. However, because of the short time available to construct the special transmission line needed at these frequencies, as well as the installation problem on the tower, it was decided to use only one line from the transmitter room to the antenna and to couple the two transmitters to this line through an isolating filter. The bridge diplexer was, nevertheless, mounted at the base of the antenna and one of its inputs terminated in 52 ohms in order to obtain the advantages

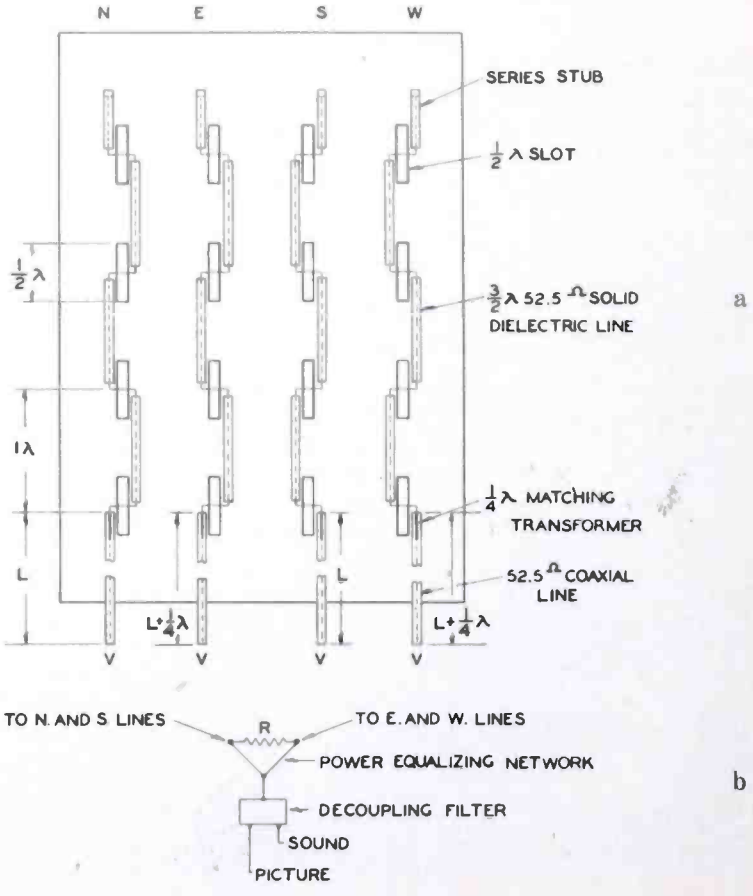

Fig. 7—Schematic of 500-megacycle antenna and equalizing network.

indicated by this procedure in Appendix A. A schematic diagram of the equalizer circuit is shown in Figure 7b.

The input impedance to the power equalizer is flat for the channel used (504-510 megacycles). The antenna proper is adjusted to provide perfect matching of its four feed lines at picture carrier of 505.25 megacycles. At the sound frequency of 509.75 megacycles, the reflection coefficient k of the individual feed lines is 0.18 and consequently the power equalizer absorbs k^2 or 3.2 per cent of the input power.

The azimuth field pattern had a deviation of ± 5 per cent from

circularity. The elevation beam width at ½ field was equal to 18 degrees. The measured power gain compared to a ½-wave-length dipole was 4.8 at picture frequency and 3.85 at sound frequency.

After the Washington tests were concluded, work was resumed on the general project of developing a high-power-gain antenna. The first problem was that associated with the design of a feeder system required to energize the radiators. Normally, each vertical row would be energized from its center point; i.e., a single coaxial line, similar to that described for the four-layer slot antenna, would be used to connect the radiators in a given vertical row and this line would be energized from its center point. This condition insures that the phase and amplitude characteristics of both halves of the antenna will be symmetrical about its center and consequently that the main lobe will be perpendicular to the axis of the pole. However, this method of feed is very difficult to attain simply because of lack of sufficient internal pole space to house the necessary transmission lines. It was realized that considerable simplification would result if a given vertical row could be end-fed. The principal drawback in end-feeding a large number of loads spaced a wave length apart at center frequency is the large deviation in amplitude and phase of the load currents with frequency. This results in tilting in elevation of the main lobe for antennas of large vertical aperture. A theoretical investigation showed that this variation could be greatly reduced if a large ratio of load to transmission line impedance were used (Appendix B).

Three basic radiating structures were evolved to utilize this type of feed and designed to operate at 850 megacycles. The first was a slot radiator and was an extension of previous principles with a novel configuration used in the construction of the transmission lines which energize the individual slots. The second is an array of inverted turnstile dipoles arranged so that the supporting structure, which also doubles as coaxial lines for feeding power to the radiators, is external to the dipoles. The third is a novel configuration of three symmetrically oriented in-phase dipoles.

Slot Antenna

A close-up of the bottom of a developmental slot antenna is shown in Figure 8. The pole has an outside diameter of 4⅛ inches, giving a d/λ of 0.3 and, according to Figure 3, would have an azimuth pattern which varied ± 5 per cent from its average value. Each vertical row, containing sixteen ½-wave-length slots spaced a wave length apart between centers, is fed in quadrature with respect to adjacent rows. Theoretically this aperture will have a power gain of 20 with respect

to a ½-wave-length dipole. The radiation impedance of each slot is high (Figure 4), thus fulfilling the condition required to minimize phase and amplitude variations for an end-fed antenna. The vertical feed lines with one of the inner conductors removed may be seen in Figure 8. Observe in particular the structure of this transmission line. There are two basic advantages in using this type of construction. First, the internal space occupied by the line is less than for a conventional coaxial line of equal power handling capacity. Second, a line

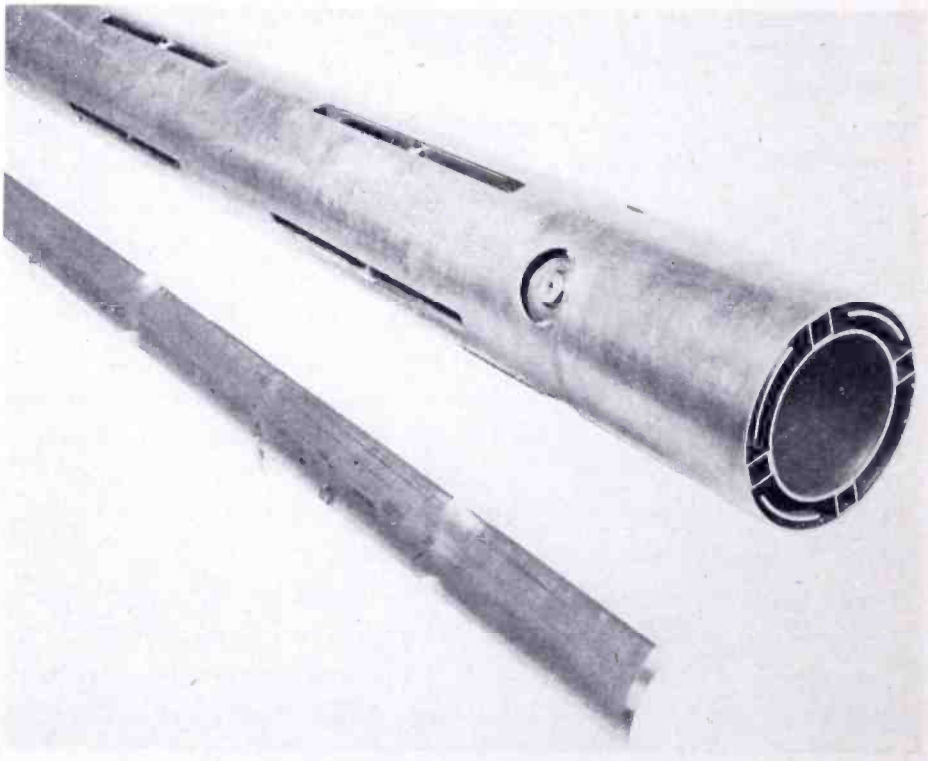

Fig. 8—Close-up of the bottom of the slot antenna.

of low characteristic impedance of 25 ohms is obtained which is desirable since a high ratio of antenna to transmission line impedance is a condition required for end-feeding. The 1⅝-inch coaxial lines, which are used to tie the power equalizing network to the antenna, are attached at the openings shown near the bottom of the antenna. The section of flat transmission line which extends past this point is short-circuited ¼ wave length away and consequently acts as a high impedance paralleling the antenna impedance. The picture shown in Figure 9 is another close-up of the bottom of the antenna and indicates how the phasing lines are attached between the antenna and power equalizer balun.

Since the velocity of propagation along a transmission line is in practice less than the free-space velocity, some estimate of the velocity must be made in order to insure that all the feed points are in phase at the required frequency. A check of the accuracy of this estimate can be made by determining the amount of beam tilt of the main pattern as a function of frequency. A measurement of this sort is shown in Figure 10 and indicates that zero tilt occurs at 843 megacycles. Since the actual spacing between slot feed points was 13.85 inches, this would indicate that the ratio of v/v_0 (v is actual and v_0 is free-space velocity) is .975.

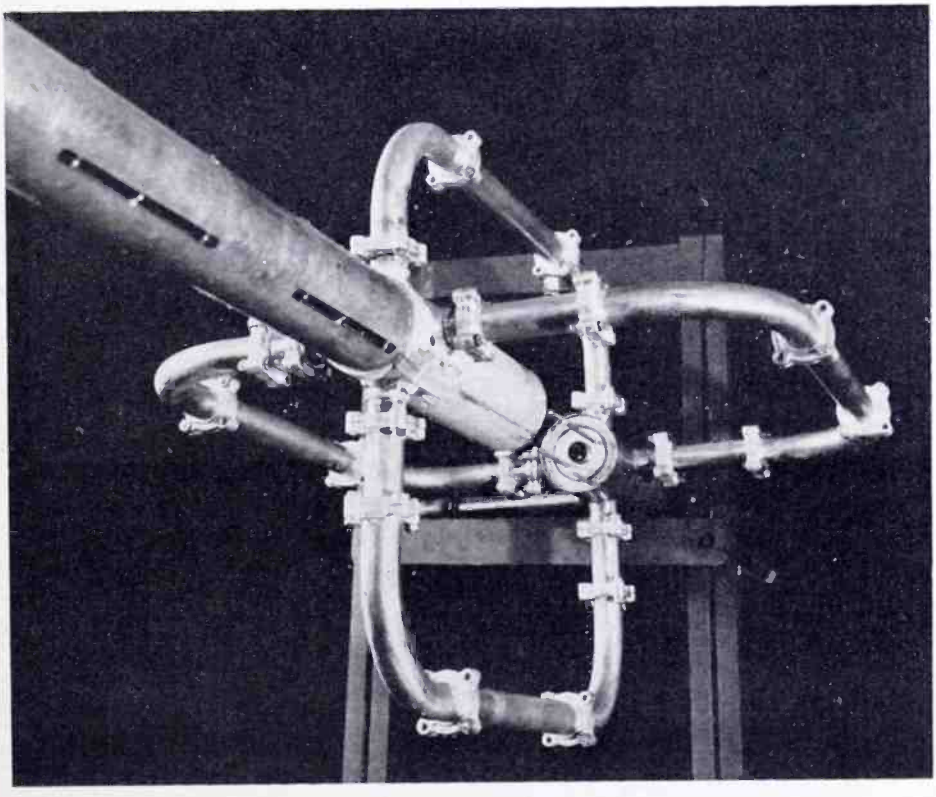

Fig. 9—Close-up of bottom of slot antenna showing how the phasing lines are attached between antenna and power equalizer.

The elevation beam widths at ½ field strength are also shown in Figure 10 and are slightly larger than those predicted theoretically. The power gain as computed from radiation patterns is equal to 15 at both picture and sound frequencies. The azimuth patterns for both frequencies are shown in Figure 11 and the elevation pattern in Figure 12. Matching of the four 1⅝-inch lines connecting the antenna to the power equalizer was done simply by adjusting the length of the individual slots by means of movable shorting bars until the reflected voltage measured across the equalizing resistance was zero. The ratio of the

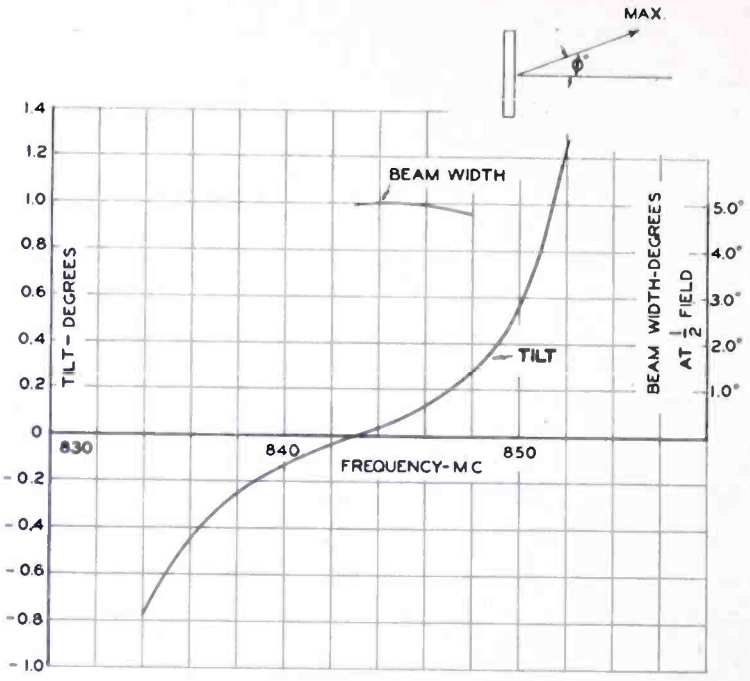

Fig. 10—Variation of beam width and tilt of the slot antenna as a function of frequency.

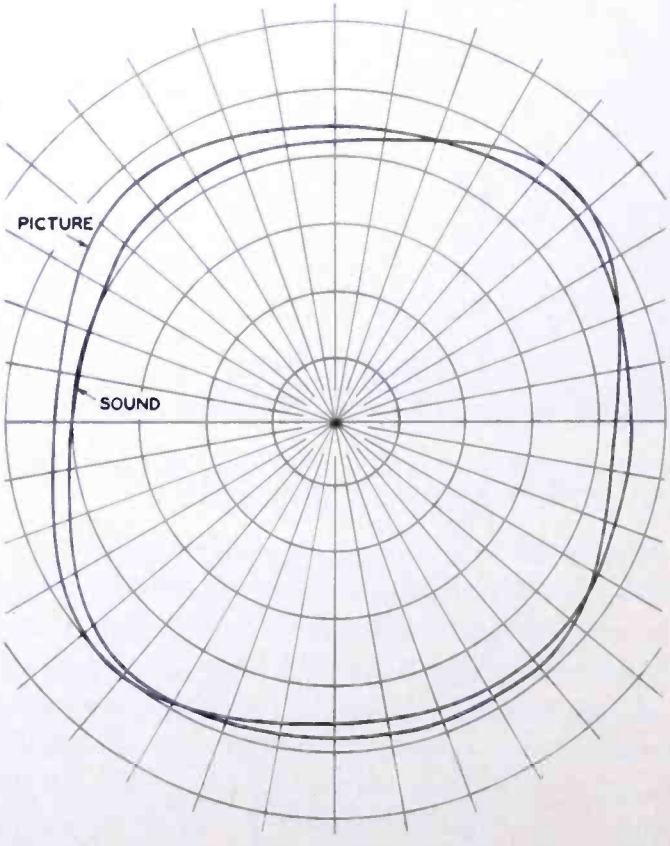

Fig. 11—Azimuth patterns of slot antenna.

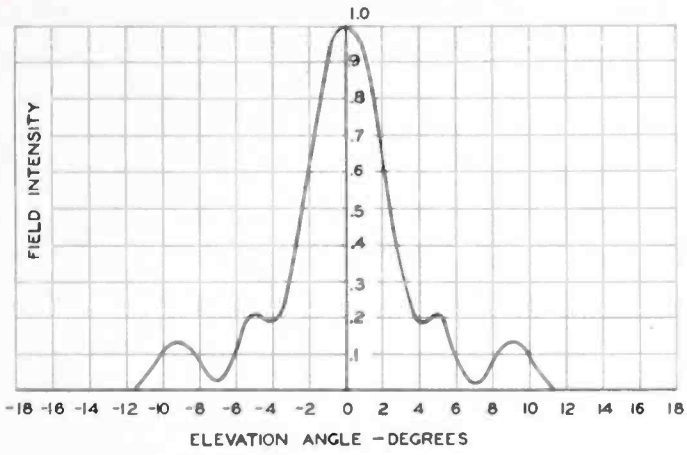

Fig. 12—Elevation pattern of slot antenna.

input power to the power equalizer to that delivered to the antenna is shown in Figure 13. This curve permits the computation of the relative field strength for constant power input to the equalizer also shown in Figure 13. Although these curves indicate that the antenna impedance is relatively frequency sensitive, the input impedance to the balun is equalized as indicated in Appendix A by means of the absorbing resistance.

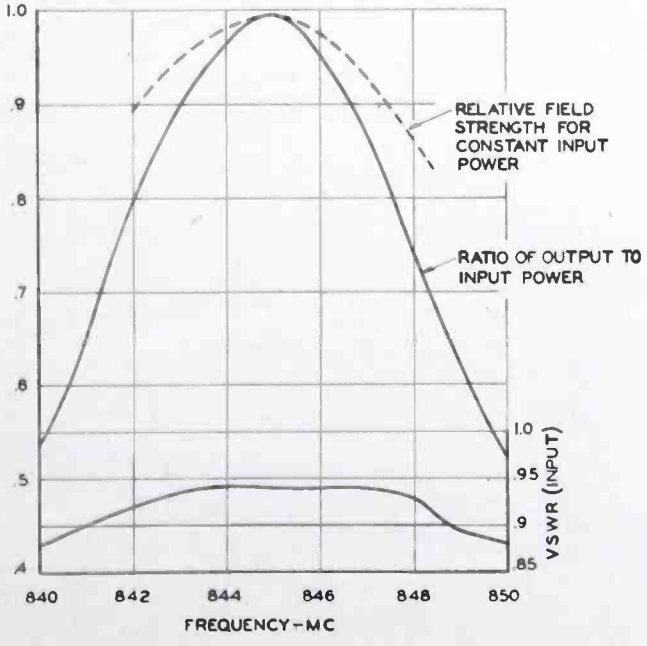

Fig. 13—Operational characteristics of slot antenna.

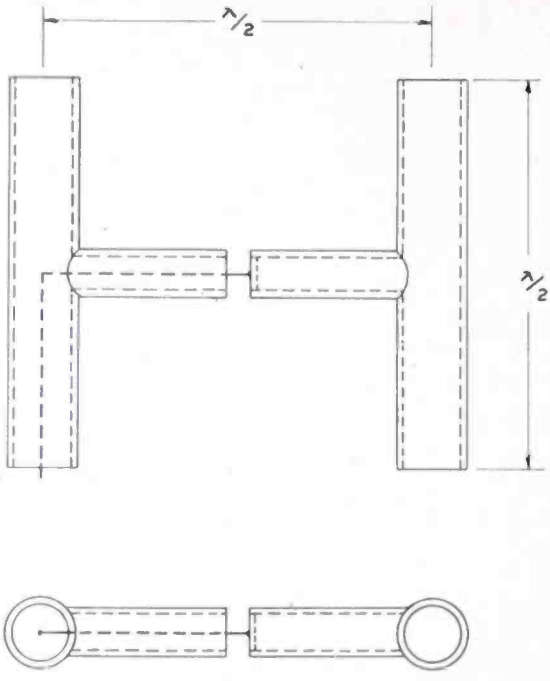

Fig. 14—Basic radiating element of the inverted turnstile antenna.

Inverted Turnstile

The basic radiating element of this design is shown in Figure 14 and, as seen, is essentially a top-loaded center-fed dipole. A picture of a single element which was used in obtaining impedance and radiation characteristics is shown in Figure 15. A ¼-wave-length sleeve is inserted on the exterior of the feed line to isolate the dipole from the transmission line. The azimuth pattern has an essentially cosine

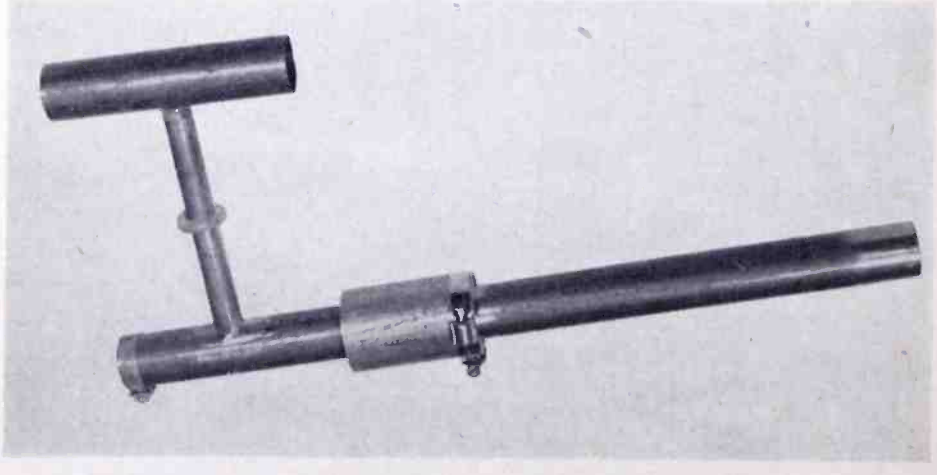

Fig. 15—Picture of experimental inverted turnstile antenna element.

variation which insures that an omnidirectional pattern will be obtained when the antennas are used in a turnstile arrangement.

A high impedance will be desired at point "*A*" when these elements are used in an end-fed array. An arrangement by which this impedance can be controlled is shown in Figure 16. The center point of the dipole is connected to point "*A*" of the transmission line by two cascaded ¼-wave-length transformers. The impedance at "*A*" is then equal to

$$Z_A = Z_d \frac{Z_2^2}{Z_1^2},$$

where Z_d is equal to the radiation impedance of the dipole, and Z_2 and Z_1 are the characteristic impedances of the two ¼-wave-length transformers. The equation indicates that for a given Z_d, Z_A is determined by the ratio of $\frac{Z_2^2}{Z_1^2}$. A typical curve obtained under these conditions is shown in Figure 17.

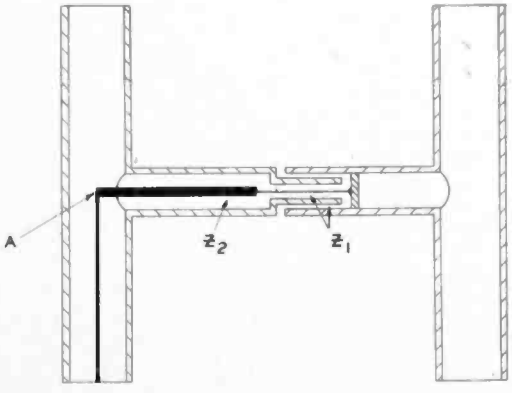

Fig. 16—Details of the construction of a single inverted turnstile element.

The procedure for constructing a turnstile array with these elements is shown in Figure 18. The dipoles in the north-south structure are spaced ½ wave length apart and are in phase, since alternate dipoles are fed from the same transmission line. The metal sheet has the dual function of providing mechanical strength for the structure and for isolating electrically the active array as shown in the drawing from the remaining external configuration. The number of such groups would, of course, be determined by the power gain required. A similar arrangement is used for the east-west array, except that all elements are displaced mechanically ¼ wave length. A model of a turnstile bay is shown in Figure 19.

An antenna embodying the above principles was built to operate at 850 megacycles and is shown in Figure 20. Just one half of the antenna was constructed to demonstrate and evaluate the feasibility of its application to an array design. The antenna is 20½ wave lengths long and has four bays with eight radiators per bay. The beam width of the elevation pattern at ½ field strength is equal to 3½ degrees and the power gain of a turnstile of this aperture is 25.

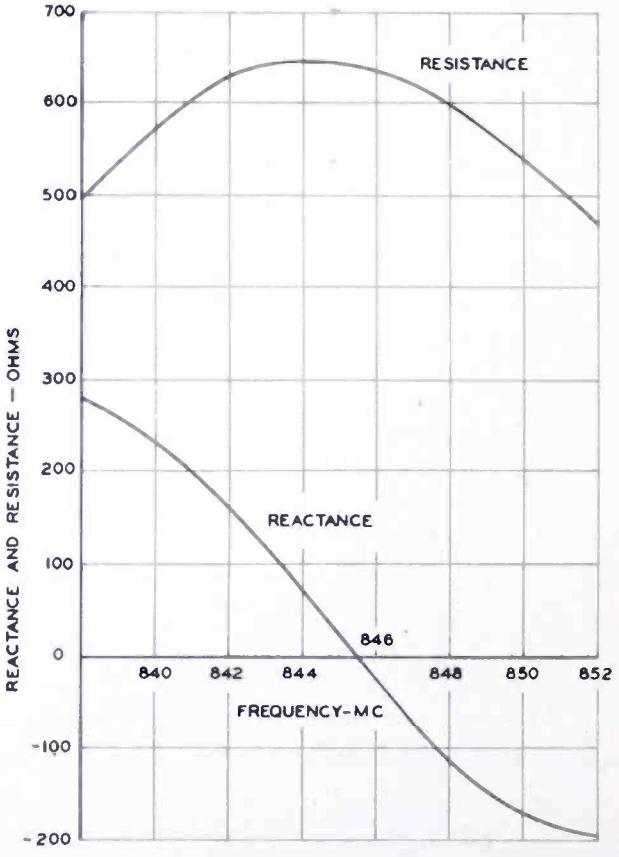

Fig. 17—Typical impedance curve of inverted turnstile element.

Disk Loop Antenna

This design utilizes novel unit radiators spaced vertically a wave length apart to obtain the required power gain. Mechanical support for the layers is provided by three equally-spaced vertical tubes. Three end-fed, balanced transmission lines supply power to the radiators. A truncated section of the array is pictured in Figure 21 showing a single layer with support tubes and feed lines attached.

A plan view of the layer construction is given in Figure 22. Three equally spaced holes (a) and notches (b) cut out of a circular metal

disk provide a loop of three half-wave dipoles (c) joined at their mid-points by the sections (d) forming a symmetrical Y webbing. Three sets of vertical, balanced transmission lines (f) with polarities as indicated join to the dipole ends to drive the elements as a circular loop radiator.

The vertical support tubes pass through holes (e) which are zero potential points with this type of excitation, thus preventing vertical

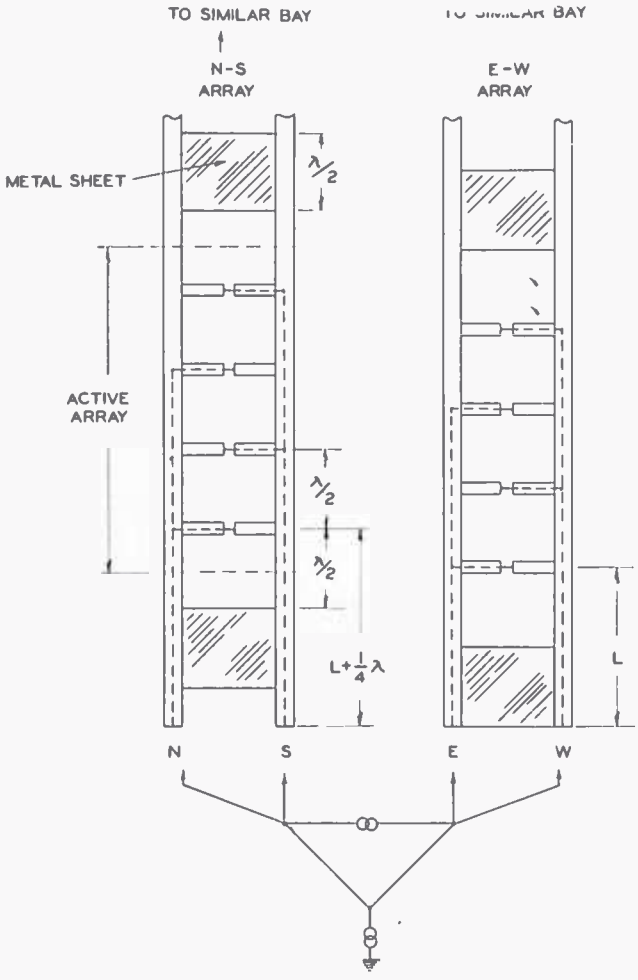

Fig. 18—Diagram showing the elemental details in the construction of an inverted turnstile antenna.

currents on the tubes. Likewise, current flow in the dipole support legs (d) is reduced to a minimum since a symmetrical radial Y is decoupled from a circular loop.

As the layers are spaced one wave length apart, all elements are fed in phase at the mid-band frequency. The three transmission lines are connected in parallel at the base of the array. A balun transforms

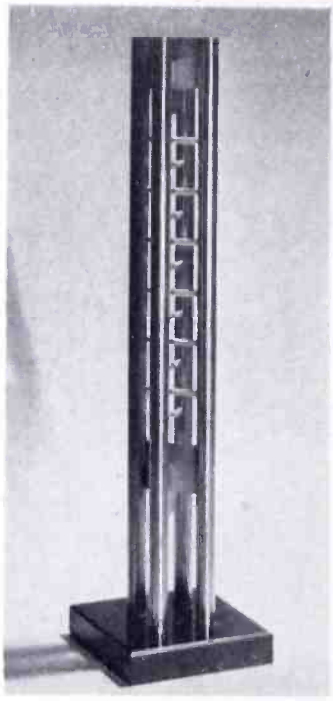

Fig. 19—Model of a single bay of inverted turnstile antenna.

this parallel junction to the main coaxial feed line leading to the transmitter.

As each dipole is fed at its ends with the mid-point at ground potential, the impedance at the transmission line terminals will be quite high in value. In the present antenna, using a nine-inch-diameter disk, the individual radiator impedances are in the order of 1200 ohms. The transmission line characteristic impedance is approximately 70 ohms, thus maintaining a high ratio of radiator to line impedance.

Fig. 20—Experimental four-bay inverted turnstile.

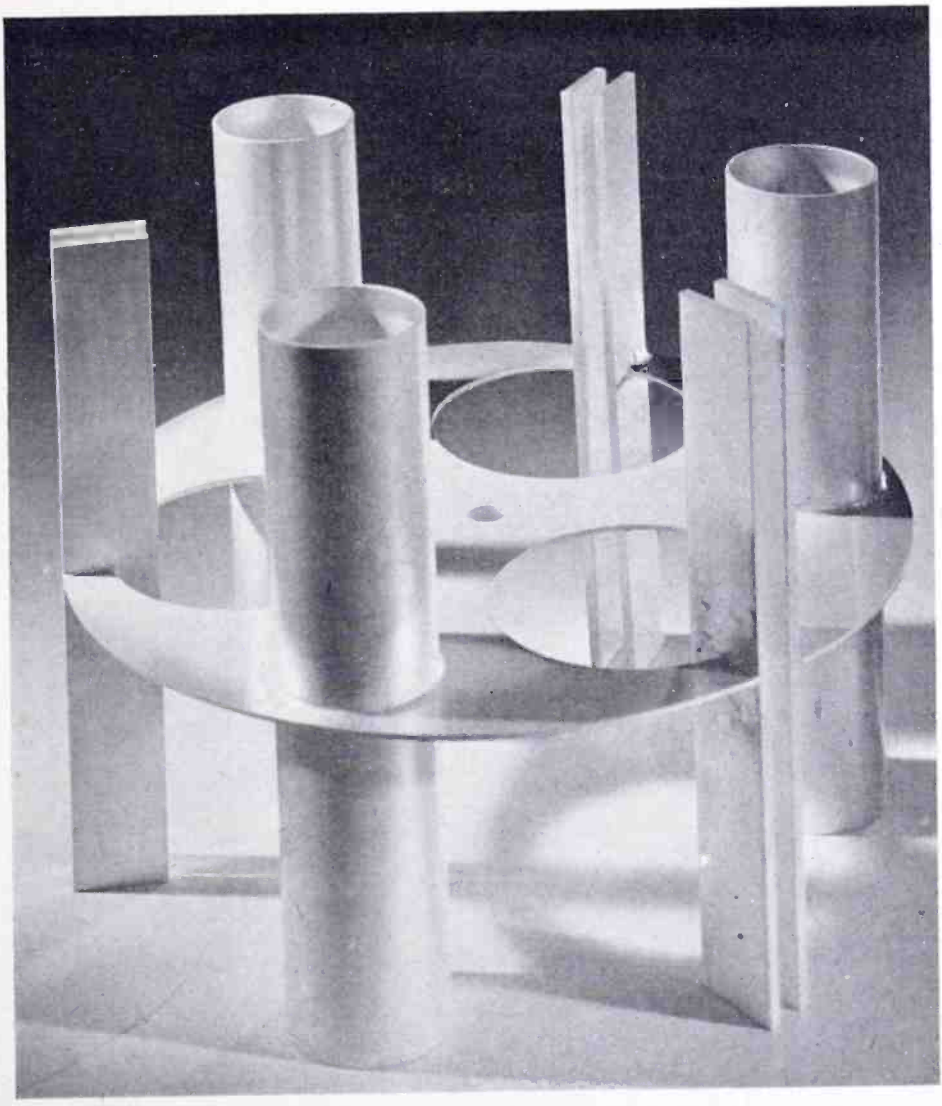

Fig. 21—Truncated section of single layer of disk-loop antenna.

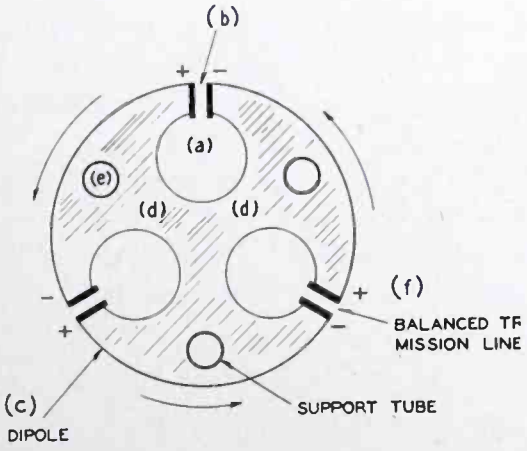

Fig. 22—Plan view of element of disk-loop antenna.

Previous work has shown the desirabilty of this high ratio in improving the band width of the antenna.

The voltage-standing-wave-ratio characteristic of the array as measured on the 52-ohm coaxial input line is given in Figure 23. Considerable improvement in band width could be expected by a somewhat more complicated feed system. For example, the three vertical support tubes could be used as coaxial transmission lines to feed the array at its mid-point. Several other variations are possible, none of which have yet been tried.

The horizontal field pattern of the array is shown in Figure 24. For comparison, the equivalent root-mean-square circular pattern is

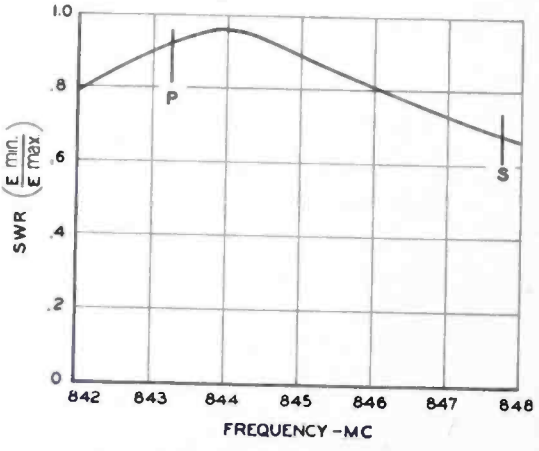

Fig. 23—Input voltage-standing-wave ratio of 16-layer disk-loop antenna.

shown. The measured pattern is seen to be somewhat triangular in shape. Experiments have indicated that this noncircularity is caused by the irregular shape and size of the individual dipole elements and also by the presence of the 1½-inch-diameter support tubes. Maximum, root-mean-square, and minimum relative field values as taken from this measured pattern are 1.00, 0.84, and 0.77, respectively.

The measured elevation field pattern of the array is plotted in Figure 25, showing a beam width at one-half field of 4.8 degrees. Mechanical integration of this pattern gave power gains (relative to a half-wave dipole) of 20.4, 14.4, and 12.1, at the maximum, root-mean-square, and minimum fields, respectively. Actual power-gain measurements in the field checked these calculated values quite closely.

Conclusions

The construction and operation of three types of ultra-high-frequency transmitting antennas, two of which utilize a quadrature

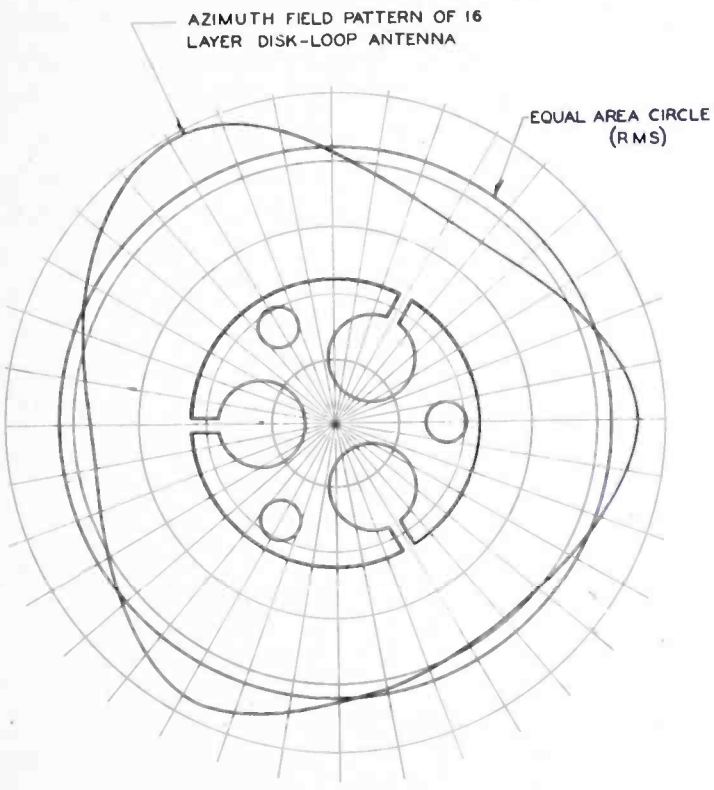

Fig. 24—Azimuth field pattern of 16-layer disk-loop antenna.

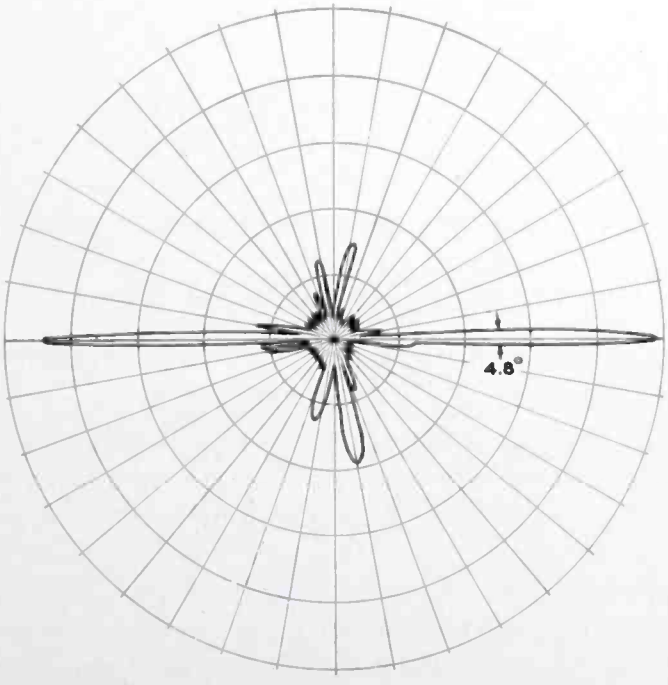

Fig. 25—Elevation field pattern of 16-layer disk-loop antenna.

feed system and the third an in-phase drive have been described. All of these constructions provide a simple means of integrating the design of the supporting structure and radiating elements. In addition, considerable simplification of the feed system is obtained by energizing each vertical row at one end. The two primary drawbacks of all of the models are their frequency sensitivity and the multiplicity of feed points. An obvious method of overcoming both defects would be the development of a radiating element having a large aperture for a single feed point.

The advantages of using a quadrature feed are quite significant in that it provides a simple method of matching the input transmission lines, maintaining equal power division in the radiating elements, and diplexing two signals into the common antenna.

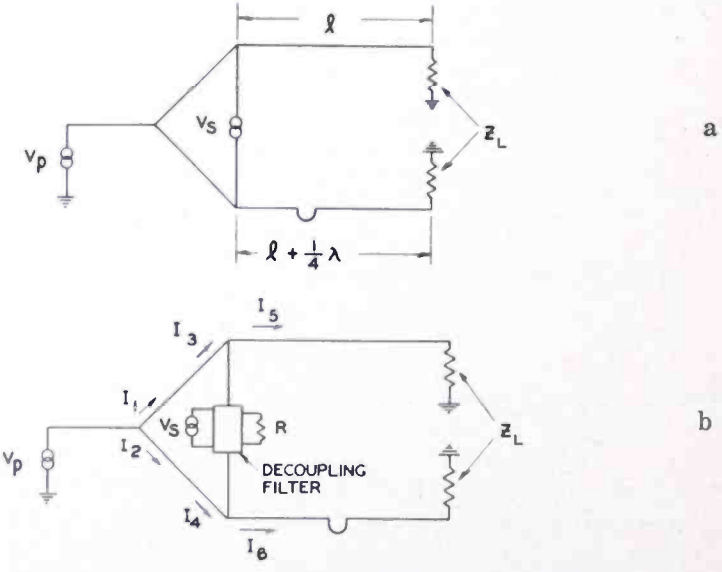

Fig. 26—Schematic diagrams of power equalizer.

Appendix A—Power Equalizer Network

In the introductory remarks it was stated that one of the advantages of a turnstile antenna is the fact that two signals can be diplexed into it by means of a simple bridge network. As will be shown later, there are several other important advantages which can be obtained by its use and these have influenced the choice of the name of power equalizer network.

The equalizer is essentially a bridge network which has two decoupled inputs connected to common loads. Schematically, the bridge and the equivalent loads of the turnstile can be represented as shown in Figure 26a. Physically, the operation of this circuit can be analyzed

in the following way. All of the incident energy from V_p divides equally between the two loads Z_L. If Z_L is equal to Z, the characteristic impedance of the feed line, all of the incident energy is absorbed. If $Z_L \neq Z$, then all of the reflected energy is directed toward V_s. Suppose, now, a means of absorbing this reflected energy in a resistance completely decoupled from V_s by means of a filter is provided. This circuit is shown in Figure 26b. It will be assumed that the characteristic impedance of all transmission lines, exclusive of those connected to the generators, is equal to Z. If $Z_L = Z$, then $Z_p = Z/2$ and $Z_s = 2Z$. If R is adjusted to absorb all of the incident energy, the following results are obtained:

1. The impedance presented to the generator V_p is independent of Z_L and equal to $Z/2$.
2. The power dissipated in the loads Z_L is equally divided between them.

The conditions necessary to achieve the above are obtained if $R = 2Z$ and if $Z_5 Z_6 = Z^2$. The last relation is obtained by making one of the lines to the load Z_L ¼ wave length longer than the other. To derive the results stated in 1 and 2, the following circuit relations may be written:

$$V_p = jI_3 Z,$$

$$V_p = jI_4 Z,$$

$$I_1 = j\frac{I_5 Z_5}{Z},$$

$$I_2 = j\frac{I_6 Z_6}{Z},$$

$$O = -I_5 Z_5 + (I_3 - I_5)\, R + I_6 Z_6,$$

$$O = I_3 - I_5 + I_4 - I_6.$$

Solving by determinants,

$$I_1 = V_s \frac{Z_5}{Z^2} \frac{[R + 2Z_6]}{[R + Z_5 + Z_6]},$$

$$I_2 = V_s \frac{Z_6}{Z^2} \frac{[R + 2Z_5]}{[R + Z_5 + Z_6]},$$

$$I_5 = -j\frac{V_s}{Z} \frac{[R + 2Z_6]}{[R + Z_5 + Z_6]},$$

$$I_6 = -j \frac{V_s}{Z} \frac{[R + 2Z_5]}{[R + Z_5 + Z_6]}.$$

Since the two conditions (1) $R = 2Z$, and (2) $Z^2 = Z_5 Z_6$ have been specified, the impedance seen by the generator V_p is equal to

$$Z_p = \frac{V_s}{I_1 + I_2} = \frac{Z}{2},$$

and the power division between the two loads is

$$\frac{P_5}{P_6} = \frac{I_5^2 Z_5}{I_6^2 Z_6} = 1,$$

and the power dissipated in R is

$$P_R = (I_3 - I_5)^2 R = \frac{2V_p^2}{Z} k_5^2,$$

where k_5 = reflection coefficient on Z_L lines. Power input is

$$P_p = \frac{2V_p^2}{Z}.$$

Hence,

$$\text{per cent power lost} = \frac{P_R \times 100}{P_p} = k_5^2 \times 100.$$

Under similar conditions the same results can be obtained for generator V_s.

Appendix B—Analysis of Amplitude and Phase Variation of Currents in a Large Number of Loads Which Are End-Fed by Means of a Transmission Line

The particular configuration to be analyzed is shown in Figure 27. This consists of n identical loads separated θ degrees and fed from one end. Since the currents through the loads will be proportional to the voltages across the individual loads, only the expression for the voltage at any point on a transmission line is needed. The following set of equations is obtained:

$$E_2 = E_1\left[\cos\theta + j\frac{Z_c}{R_1}\sin\theta\right]$$

$$E_3 = E_2\left[\cos\theta + j\frac{Z_c}{R_2}\sin\theta\right]$$

$$E_n = E_{n-1}\left[\cos\theta + j\frac{Z_c}{R_{n-1}}\sin\theta\right] \qquad (1)$$

where R_{n-1} is the impedance measured at the $(n-1)$ terminal. Hence, for $\theta = 360$ degrees, $E_1 = E_2 = E_3 = E_n$ which indicates that the loads will have equal in-phase currents. Now suppose that the frequency is varied so that $\theta = 360\ (1 \pm \delta) = 360 \pm \Delta\theta$ where $\delta = \Delta f/f_0$. Assume also that δ is sufficiently small so that $R_2 = R/2$, $R_3 = R/3$,

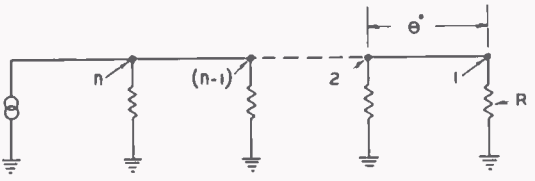

Fig. 27—Schematic of n equal loads separated θ degrees and fed from one end of a transmission line.

and $R_{n-1} = \dfrac{R}{(n-1)}$. Then Equation (1) reduces to

$$E_2 = E_1\left[\cos\Delta\theta \pm j\frac{Z_c}{R}\sin\Delta\theta\right]$$

$$E_3 = E_2\left[\cos\Delta\theta \pm j\frac{2Z_c}{R}\sin\Delta\theta\right]$$

$$E_n = E_{n-1}\left[\cos\Delta\theta \pm j\frac{(n-1)Z_c}{R}\sin\Delta\theta\right]. \qquad (2)$$

From the above it is again seen that for $\Delta\theta = 0$, $E_1 = E_2 = E_3 = E_n$, but that for $\Delta\theta \neq 0$, the amplitude and phases of all the voltages will, in general, not be equal. Note, however, that the phase variation can

be minimized by making $R \gg Z_c$. As an extreme case, if R is sufficiently large compared to Z_c so that the j terms can be neglected, the phase variation will be eliminated, and only an amplitude variation of the currents in the loads will be obtained. In order to evaluate qualitatively the dependence of the radiation pattern for a given $\frac{R}{Z}$ and $\Delta\theta$, simply sum vectorially the voltages as given by Equation (2) after having properly accounted for the delay introduced by the path length difference.

To illustrate the procedure involved in the above calculations some parameters that might be used in a typical case are assumed and the results summarized. Let $n = 16$ and $\delta = .005$. The vector expression

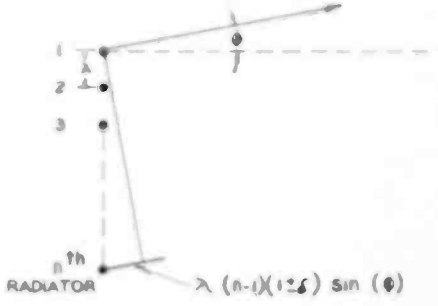

Fig. 28—Diagram illustrating method of obtaining radiated field of n end-fed radiators.

for the field of the n^{th} radiator with respect to the 1^{st} radiator is given by the expression

$$E_n = E_{n-1}\left[\cos(\Delta\theta) \pm j\frac{(n-1)Z}{R}\sin\Delta\theta\right]e^{-j\frac{2\pi}{\lambda}d_n},$$

where θ = elevation angle and $d_n = \lambda(n-1)(n \pm \delta)\sin\theta$ = path-length difference (Figure 28). For $R/Z = 1.0$, the main beam will be tilted upward 2.5 degrees, while for $R/Z = 10$, the tilt is only 0.5 degree. It is of some interest to note that the tilt angle measured experimentally for the 16-layer slot antenna, which has an $R/Z = 13$, for $\delta = .005$ is equal to 0.15 degree.

STUDIES OF EXTERNALLY HEATED HOT CATHODE ARCS*

Part II — The Anode-Glow Mode

By

W. M. Webster, E. O. Johnson, and L. Malter

Summary—In Part I of this series, the qualitative aspects of the various modes of operation assumed by an externally heated hot cathode arc were treated. This present paper is concerned with a more detailed treatment of one of these — the anode-glow mode — wherein all ionization and excitation occur in a thin electron sheath close to the anode surface.

The processes of ion generation and loss in a cylindrical diode are treated analytically and then equated to obtain an expression for the volt-ampere characteristic of the discharge. It is found that the anode current varies as the fourth power of the excess of the applied anode voltage over the ionization potential. It is also found that the ratio of anode current to the rate of ion generation is dependent only upon the nature of the gas filling and the tube geometry. The correspondence between this analysis and experiment is found to be good if ion losses to the oxide cathode are taken into account. These losses are ascribed to nonuniformities of potential along the cathode surface.

Experimental evidence is presented to show that the plasma density distribution is one in which the lowest diffusion mode predominates. Measurements of ion and electron currents to segmented electrodes which bound the plasma show that the distribution is cosinusoidal in the axial direction and characteristic of a zero-order Bessel function in the radial direction.

I. Introduction

PART I[1] of this series described various possible modes of the hot cathode arc. Characteristics of the different modes such as plasma potential distribution and electron temperatures were presented. This paper will be concerned primarily with detailed studies of the anode-glow mode. This is the mode which occurs at low current values and at pressures in excess of about 300 microns.† It is characterized by the following features: The light emission is entirely from a thin skin on the anode surface; the plasma occupies all of the tube except for the sheaths at walls or electrodes; the plasma is close

---

* Decimal Classification: R337.1.

[1] L. Malter, E. O. Johnson, and W. M. Webster, "Studies of Externally Heated Hot Cathode Arcs, I—Modes of the Discharge," *RCA Review*, Vol. XII, pp. 415-435, September, 1951.

† The plasma conditions which determine whether or not a hot cathode arc can assume the anode-glow mode will be discussed in a later paper of the series.

to cathode potential; the tube drop occurs primarily in the anode sheath; the excitation and ionization occur close to the anode surface only.

II. Ion Generation in the Anode-Glow Mode

The ions generated within the anode sheath are ultimately lost by diffusion to walls or electrodes, or by recombination within the plasma or by a combination of these processes. The relations governing the balance between ion generation and ion loss are of value in later determinations of plasma density distribution and in studies of the

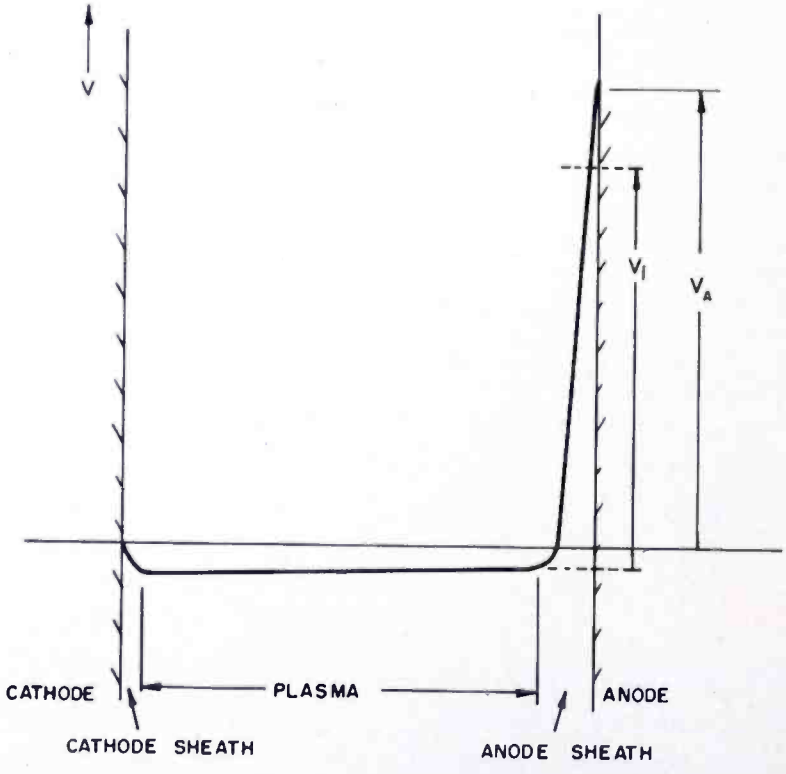

Fig. 1—Potential distribution in the anode-glow mode.

conditions which result in a transition of the discharge out of the anode-glow mode. The process of ion generation is considered first.

As was shown in Part I, the potential distribution between cathode and anode for the anode-glow mode is roughly of the form shown in Figure 1.

It is assumed that all the ionization occurs beyond the point where $V = V_i$ (the ionization potential), and that it obeys the differential ionization law[2]

[2] J. D. Cobine, *Gaseous Conductors*, First Edition, p. 79. McGraw-Hill Publishing Co., New York, N. Y., 1941.

$$n = ap(V - V_i). \tag{1}$$

Then, in a distance ds, an electron current j_e generates an ion current dj_p given by

$$dj_p = j_e\, ap(V - V_i)\, ds \tag{2}$$

where V is the electron energy, n is the number of ion pairs produced per centimeter of path length per electron, and p is the gas pressure in millimeters of mercury. Values of the coefficient a for various gases are given on page 80 of Reference (2).

In order to make use of Equation (2) in computing the ion generation in the anode sheath, it is necessary to postulate a potential distribution in the sheath, particularly beyond $V = V_i$. Since this distribution is unknown, we compute the generation for the two possible limiting cases. In both cases it is assumed that the sheath is so thin that planar theory applies, but in the first case it is further assumed the ionization within the sheath is so small that the 3/2-power law for space-charge flow of particles of one sign applies. Then since the current flow is essentially electronic, the potential distribution within the sheath satisfies the relation

$$j_e = \frac{k\, V^{3/2}}{s^2} \text{ amperes per square centimeter,} \tag{3}$$

where j_e is the current density and $k = 2.33 \times 10^{-6}$. V and s are defined in Figure 2, which is an expanded version of the sheath region of Figure 1. It is seen that both V and s are measured from the plasma-sheath boundary. The error introduced by measuring V_A from the sheath edge instead of from cathode potential, as well as the error introduced by contact potential and cathode coating drop, is corrected for later in the analysis.

Langmuir[3] has treated the problem of the simultaneous flow of electrons and ions in opposite directions between two planar sources. He considers the case wherein the cathode emits a surplus of electrons but the anode emits positive ion current of density j_p. He shows that the saturated electron current density, j_e, increases with j_p until the quantity

$$\alpha = \frac{j_p}{j_e}\left[\frac{m_p}{m_e}\right]^{1/2}$$

[3] I. Langmuir, "The Interaction of Electron and Positive Ion Space Charges in Cathode Sheaths," *Phys. Rev.*, Vol. 33, p. 954, June, 1929.

attains the value of unity. When this happens, the positive ion current, as well as the electron current, is saturated. Further increase in the ion emission results in no further changes in electron and ion currents or in the potential distribution. The case just discussed wherein $j_p = 0$, is the one for which $\alpha = 0$. Since the ionization in the anode sheath occurs very close to the anode, the actual situation corresponds to a case for which $\alpha \neq 0$. As a second limiting case we adopt (with Langmuir) $\alpha = 1$.

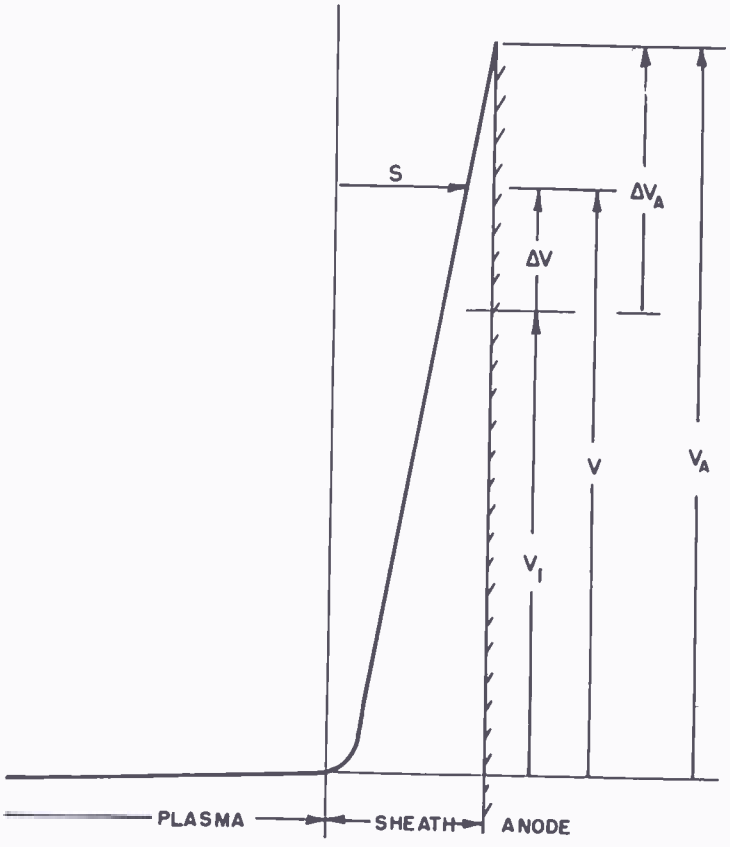

Fig. 2—Detailed view of the potential distribution in the anode sheath.

We consider first the case $\alpha = 0$. From Equation (3),

$$ds = \frac{3}{4}\left[\frac{k}{j_e}\right]^{1/2} V^{-1/4}\, dV. \tag{4}$$

Substitution of Equation (4) in Equation (2), and integration over the ionizing region, yields

$$j_p = \frac{3}{4} ap \sqrt{k j_e} \int_{V_i}^{V_A} \frac{(V - V_i)\, dV}{V^{1/4}}. \tag{5}$$

If we make the substitutions $\Delta V = V - V_i$ and $dV = d(\Delta V)$, we can rewrite this equation as

$$j_p = \frac{3}{4} ap \sqrt{kj_e} \int_0^{\Delta V_A} \frac{\Delta V d(\Delta V)}{(\Delta V + V_i)^{1/4}}, \tag{6}$$

where $\Delta V_A = V_A - V_i$. Integration is simplified by neglecting ΔV with respect to V_i. Upon integration, Equation (6) then yields

$$j_p = \frac{3}{8} ap \sqrt{kj_e} \left[\frac{(\Delta V_A)^2}{V_i^{1/4}} \right] = (j_p)_{\alpha = 0}. \tag{7}$$

Langmuir[3] has solved for the potential distribution for $\alpha \neq 0$, the result being expressed in integral form in his Equation (11). It was found possible to integrate this expression for the region close to the anode for the case $\alpha = 1$ and $\Delta V_A \ll V_A$. The result is

$$(j_p)_{\alpha = 1} = ap \sqrt{kj_e} \left[\frac{4}{7} (\Delta V_A)^{7/4} + \frac{1}{15} \frac{(\Delta V_A)^{9/4}}{V_A^{1/2}} \right]. \tag{8}$$

The actual value of j_p must lie between those of Equations (7) and (8). A quantity of interest is the ratio

$$B = \frac{(j_p)_{\alpha = 1}}{(j_p)_{\alpha = 0}} = \frac{\frac{4}{7} (\Delta V_A)^{7/4} + \frac{1}{15} \frac{(\Delta V_A)^{9/4}}{V_A^{1/2}}}{\frac{3}{8} \frac{(\Delta V_A)^2}{V_i^{1/4}}}. \tag{9}$$

B has been computed for Helium and Argon and the results are plotted in Figure 3.

Tests of the ion generation theory as outlined above were carried out in a cylindrical tube of the form shown in Figure 4. The tube contained helium at a pressure of 1 millimeter.

At any value of V_A for which the tube is operating in the anode-glow mode the ions, which are generated close to the anode, are lost primarily to the negative end shields. We assume, as a first approximation that the ion current generated in accordance with the preceding theory appears as the current i_p flowing to the end shields. The electron current i_e which generates this ion current, plus a current equal to the ion current (made up of the electrons liberated in forming the ions) is that which flows to the anode. However, the contribution to i_e of

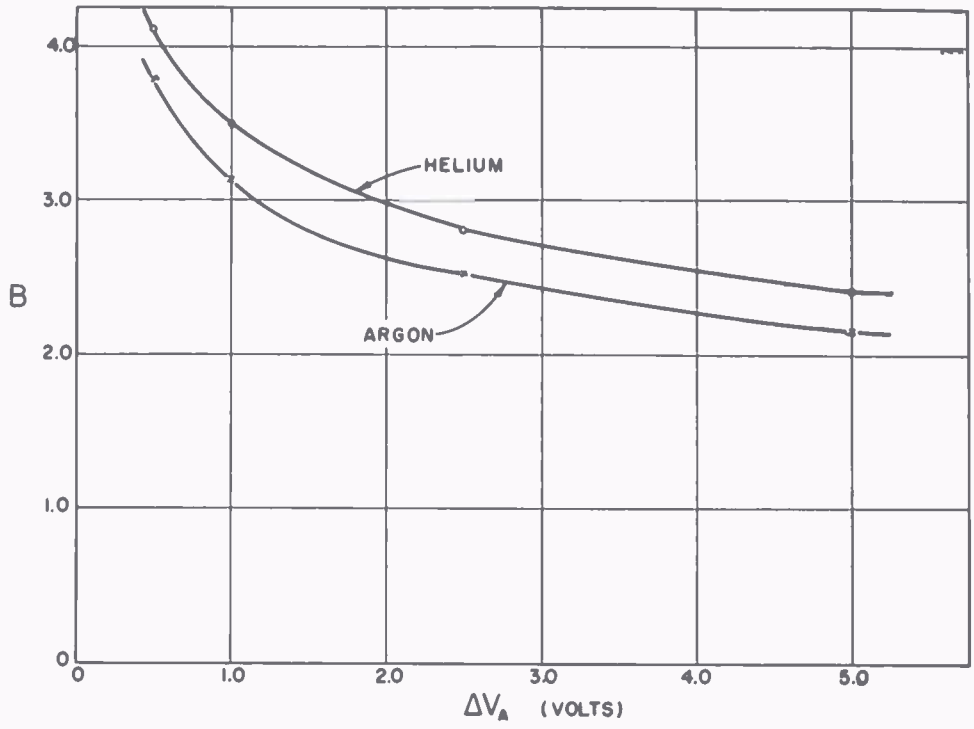

Fig. 3—Correction factor for the ionization in the anode sheath.

the latter electron current is negligible. A typical set of data is presented in Table I. The various columns will be considered seriatim. The meaning of columns 1, 2, and 3 is indicated in Figure 4. Column 4 is the ratio of the anode electron current to the ion current flowing to the end shields. For $\alpha = 1$, this ratio would be 85.7. Thus, in the case at hand, $\alpha = 0.14$. Since this is closer to zero than to unity, we shall

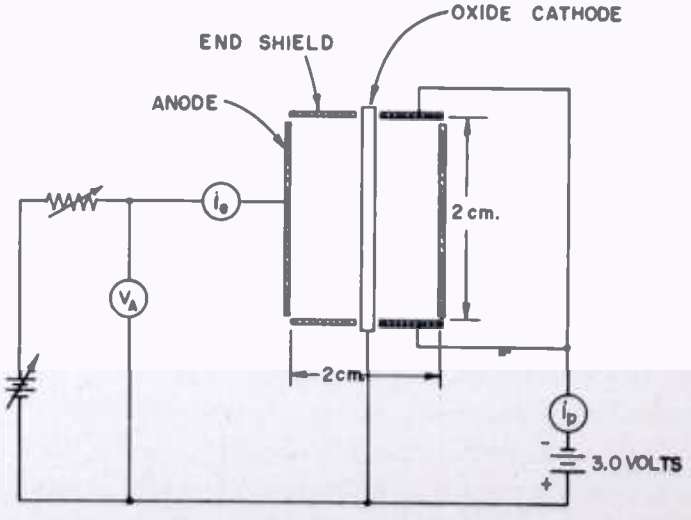

Fig. 4—Schematic of the experimental setup.

use Equation (7) to compute a theoretical value for the ion current generated at the anode.

Due to the small ion currents flowing to the end shields, the sheath thickness there will be appreciable. Assuming that ion current density is uniform over the end shields, an average ion sheath thickness can be computed from the 3/2-power law. A number of these are listed in column 6. In order that the ion current to the end shields could be measured, the bias on these electrodes was made just large enough to repel the plasma electrons. The discharge conditions were then negligibly different from those wherein the end shields "float."

Table I

1	2	3	4	5	6	7	8	9	10	11	12
V_A (volts)	i_e (ma)	i_p (μa)	i_e/i_p	j_p AT END SHIELDS ($\mu a/cm^2$)	ION SHEATH THICKNESS AT SHIELDS (cm)	j_e AT ANODE (ma/cm^2)	ANODE SHEATH THICKNESS (cm)	ΔV_A (volts)	j_p AT ANODE (CALC.) $= i_p/A_a$ ($\mu a/cm^2$)	j_p AT ANODE ($\mu a/cm^2$)	$j_p = \frac{i_p}{A_a}\frac{\tau_{cal.}}{\tau_{msd.}}$ ($\mu a/cm^2$)
25.5	5.0	5.1	975	0.81		.40		2.0	0.96	0.405	0.91
26.8	20.0	27.2	736	4.32		1.60		3.3	5.23	2.16	4.86
27.9	50.0	75.0	666	11.6	.11	3.98	.30	4.4	14.5	5.95	13.4
28.1	60.0	92.0	653	14.6		4.76	.26	4.6	17.4	7.30	16.4
28.3	70.0	108	649	17.2		5.65	.25	4.8	20.7	8.59	19.3
28.5	80.0	127	630	20.2	.084	6.36	.21	5.1	24.6	10.1	22.7
28.9	100	164	610	26.1	.074	7.95	.20	5.5	32.1	13.0	29.2
29.2	120	196	613	31.2	.068	9.52	.18	5.8	39.0	15.6	35.1
29.5	140	232	603	36.9	.064	11.3	.17	6.0	45.3	18.4	41.4
29.8	160	269	595	42.7	.059	12.7	.16	6.3	53.0	21.4	48.2
30.1	180	315	571	50.0	.055	14.3	.15	6.6	61.9	25.0	56.3
30.4	200	356	562	56.5	.051	15.8	.04	6.9	71.5	28.2	63.5

ANODE AREA = A_a = 12.6 cm^2; TOTAL END SHIELD AREA = 6.3 cm^2
END SHIELD VOLTAGE = − 3.0 volts
$\tau_{calc} = 270 \times 10^{-6}$ sec.; $\tau_{msd} = 120 \times 10^{-6}$ sec.; $\frac{\tau_{calc.}}{\tau_{msd.}} = 2.25$

Similarly, one can compute the electron sheath thickness at the anode. Again, assuming that the electron current density is uniform over the entire anode surface, one computes average current densities and sheath thicknesses as given in columns 7 and 8 respectively. It is seen from columns 6 and 8 that the sheath thicknesses are not insubstantial and that for exactitude, corrections to effective tube length and diameter should be applied when computing ion and electron densities. However, in view of the other approximations involved in both theory and experiment, we shall neglect the effects of sheath thickness for the present. To minimize the error, we shall restrict our checks of theory and experiment to the cases where $i_e > 50$ milliamperes.

Because of the uncertainty arising from contact potentials and

potential drop through the cathode coating, one cannot set the point for onset of ionization at the ionization potential V_i (24.5 volts for helium). A reasonable value can be obtained from Equation (7) by noting that

$$\Delta V_A = V_A - V_i' = \left[\frac{8V_i^{1/4}}{3\,apk^{1/2}}\right]^{1/2} \frac{j_p^{1/2}}{j_c^{1/4}}, \tag{10}$$

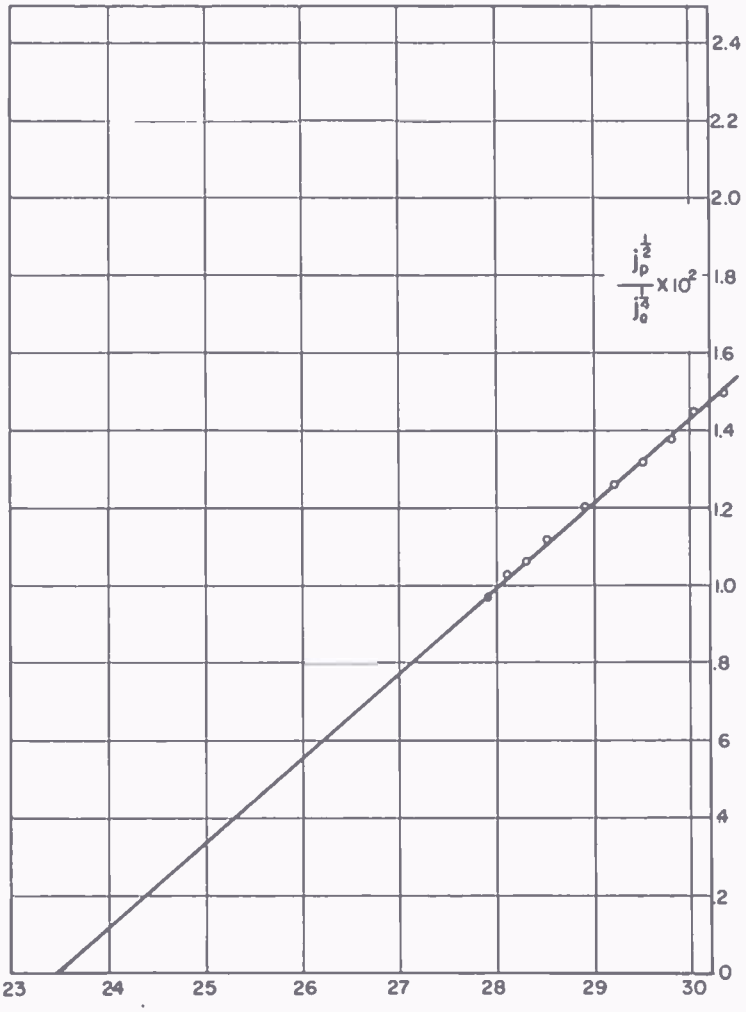

Fig. 5—Plot for the determination of the effective ionization potential.

where V_i' is the ionization potential uncorrected for contact potentials, etc.

Thus if we plot $j_p^{1/2}/j_c^{1/4}$ versus V_A, its intercept will give us the desired value for V_i', from which one can then obtain ΔV_A. Figure 5 is the desired graph from which it is seen that $V_i' = 23.5$ volts. From this and column 1, one obtains the values of ΔV_A. These values are

given in column 9. Substitution of these values of ΔV_A and the values of j_e from column 7 into Equation (7) yields the computed values of j_p presented in column 10. It is seen that these run about 150 per cent higher than the measured values of column 11. Actually, since in the experiment $\alpha > 0$, the computed values of j_p should be multiplied by a factor lying between 1.0 and B of Figure 3. Thus the discordance between theory and experiment is actually worse than is indicated by the table. This discrepancy can be accounted for in a number of ways: (1) The values of ΔV_A used are too large. This would require that ΔV_A be in error by over one volt. In view of the good linearity of the data of Figure 5, it is unlikely that the error in ΔV_A can be that large. (2) The measured value of j_p does not include all the ion currents flowing out of the plasma. Some ion current flows to the mica sheets which support the end shields. This cannot, however, account for the observed discrepancy. (3) A very effective sink for ions occurs in regions, or patches, of the oxide cathode surface which have such a combination of work function, emission, and ohmic resistance that they are at a potential below that of the plasma. Justification for this belief stems from experiments with tubes having very nearly unipotential cathodes. Such tubes which contain tungsten filamentary cathodes arranged so that measurements can be made when the heating voltage is zero, yield data that differs from theory by only about 10 per cent. However, the difficulty in getting such tubes to operate over a sufficiently wide range of the parameters has largely precluded their use. Further evidence in support of this belief will be presented later in the paper. (4) Recombination may account for unmeasured losses. Computation shows that this is very unlikely under the conditions of these experiments.

It is of interest to compare the experimental and theoretical values for the slope of the characteristic of Figure 5. From that figure we obtain

$$\frac{\Delta V_A}{j_p^{1/2}/j_e^{1/4}} = 455.$$

From Equation (10) we obtain, for the same quantity,

$$\frac{\Delta V_A}{j_p^{1/2}/j_e^{1/4}} = \left[\frac{V_i^{1/4}}{3/8\, apk^{1/2}}\right]^{1/2} = \left[\frac{8 \times 2.22}{3 \times .046 \times 1.0 \times 1.53 \times 10^{-3}}\right]^{1/2} = 290. \quad (10a)$$

Actually, since $\alpha \neq 0$, Equation (10a) should contain in its denominator not the factor 3/8, but one somewhat larger. Even though this causes

a larger discrepancy between theory and experiment than indicated above, it is felt that the concordance between theory and experiment is good and that this picture of the ionization process appears sound. The error is seen to be in the direction that one would expect if an anomalous ion loss were present.

III. Plasma Balance in the Anode-Glow Mode

In the preceding section expressions have been developed for the ion generation in the anode-glow mode. Under equilibrium conditions the ion generation must be balanced by ion loss. By equating these two, some interesting relations follow.

Experimental evidence will be presented below showing that if the discharge is interrupted at any instant, the remaining plasma will then decay according to the law

$$N = N_o e^{-t/\tau}, \tag{11}$$

where N is the total number of ions or electrons within the plasma.

Then $$\frac{dN}{dt} = -\frac{N}{\tau}.$$

The ion current flowing out of the plasma is given by

$$i_p = -e\frac{dN}{dt} = \frac{Ne}{\tau}. \tag{12}$$

The actual plasma density distribution in the tube will be discussed to some extent later in this paper, and in greater detail in the next paper of this series. A brief treatment is in order at this point.

In the most general case, the plasma density distribution in a decaying plasma is given by[4]

$$n\,(x, y, z) = \sum_{m=1}^{\infty} n_{om}\,(x, y, z)\; e^{-t/\tau m} \tag{13}$$

where $\tau_1 > \tau_2 > \tau_3 > \cdots\cdots\cdots$.

At $t = 0$, $n = \sum n_{om}$, and $N = \int \sum n_{om}\, dv$ taken throughout the plasma.

[4] M. A. Biondi and S. C. Brown, "Measurements of Ambipolar Diffusion in Helium," *Phys. Rev.*, Vol. 75, pp. 1700-1705, June, 1949.

Since experiments show a nicely exponential decay, the actual situation in the anode-glow plasma during operation can be characterized by Equation (11) where a single mode predominates. As one would expect, this is the fundamental mode, the one with the longest decay constant, τ. The τ of Equation (11) is the τ of Equation (13). In structures of the form of the tube of Figure 4, the density distribution is one in which the axial distribution is close to being cosinusoidal and the radial distribution is close to a Bessel function of zero order. The density decreases as one approaches the outside cylinder or the end shields and falls off at the plasma-sheath boundaries to values whose ratio to the maximum values within the tube depends on the nature of the gas, the pressure and the tube geometry.

Let n_a be the average plasma density at the plasma-sheath boundary along the cylindrical anode surface of the tube of Figure 4. Let v be the total plasma volume. Then $N = n_a v \psi$ where ψ is a factor depending on the gas, its pressure and the tube geometry, and which relates the ratio of the average density throughout the plasma to the average in the plasma close to the anode surface. Means for the determination of ψ will be presented in the next paper of this series. For the tubes studied here, it lies between 1 and 20. From Equation (12) we now obtain

$$i_p = \frac{Ne}{\tau} = \frac{n_a v \psi e}{\tau}. \tag{14}$$

From kinetic theory,

$$i_e \cong \frac{n_a e \bar{c}_e}{4} A, \tag{15}$$

where $\bar{c}_e$ is the average electron velocity in the plasma and A is the effective anode area. Combining Equations (14) and (15) we obtain

$$\frac{i_e}{i_p} = \frac{c_e A \tau}{4 v \psi}. \tag{16}$$

It is of interest to note that the ratio i_e/i_p does not depend upon V_A or i_e except insofar as alterations in their magnitude cause secondary effects on the quantities on the right hand side of Equation (16). Increasing V_A or i_e causes:

(1) A to increase by decreasing the sheath thicknesses.

(2) v to increase due to thinning of sheaths at anode and end shields.

(3) τ to increase as v increases.

(4) ψ to increase as v increases.

All these changes are small and effects (3) and (4) tend to cancel each other. From Table I it is seen that, except for very low values of i_t where sheath thicknesses are appreciable, i_e/i_p is substantially constant, as predicted by this analysis.

It is of interest to see how Equation (16) checks with experiment. We set

$$\bar{c}_e = 1.87 \times 10^{-8} \sqrt{\frac{T_e}{m_e}}.$$

For T_e (the electron temperatures), 1400°K is chosen. This is based on studies described in Part I. m_e is the electron mass.

$$\frac{A}{v} = \frac{2\pi r_b h}{\pi r_b^2 h} = \frac{2}{r_b} = \frac{2}{1} = 2 \text{ cm}^{-1}.$$

Actually, due to the effect of sheath thickness at the anode, $r_b < 1$ centimeter, so that $A/v > 2 \text{ cm}^{-1}$.

The method outlined by Biondi and Brown[4] was used to compute τ. Since the ion losses are assumed to occur only to the end plates, the diffusion geometry is that of a pair of infinite plane parallel plates whose spacing is $h = 2$ centimeters. Setting $T_e = 1400°\text{K}$ and T_p (positive ion temperature) $= 350°\text{K}$ (the gas temperature), we obtain $\tau = 270 \times 10^{-6}$ second.

Integration of the density distribution gives the value of ψ. For the case at hand, $\psi \simeq 4.5$. Substitution of the above values in Equation (16) yields $i_e/i_p = 700$. This is in particularly good agreement with the values of column 4 of Table I.

We are now in a position to arrive at the desired expression relating the applied potential to the electron current flowing between cathode and anode. Under steady state conditions, the ion generation and the ion loss must balance. Thus we can equate i_p in Equation (7) and Equation (16) (this assumes that $\alpha = 0$). Then:

$$\frac{4 i_e v \psi}{\bar{c} A \tau} = \frac{3}{8} \frac{a p [k A i_e]^{1/2} (\Delta V_A)^2}{V_1^{1/4}}. \tag{17}$$

Solving this for i_e,

$$i_e = \left[\frac{3}{32}\frac{a\,p\,\bar{c}}{\psi V_i^{1/4}}\sqrt{k}\right]^2 \frac{A^3}{v^2}\tau^2\,(\Delta V_A)^4. \tag{18}$$

Thus we see that in the anode-glow mode of discharge, the anode current should vary as the fourth power of the voltage excess above the ionization potential. This will now be checked. We set

$$j_e^{1/4} = \left(\frac{i_e}{A}\right)^{1/4} = \left[\frac{3}{32}\frac{a\,p\,\bar{c}\,\sqrt{k}\,\tau}{\psi V_i^{1/4}}\frac{A}{v}\right]^{1/2} \Delta V_A = \gamma \Delta V_A \tag{19}$$

$$j_e^{1/4} = \gamma \Delta V_A = \gamma (V - V_i).$$

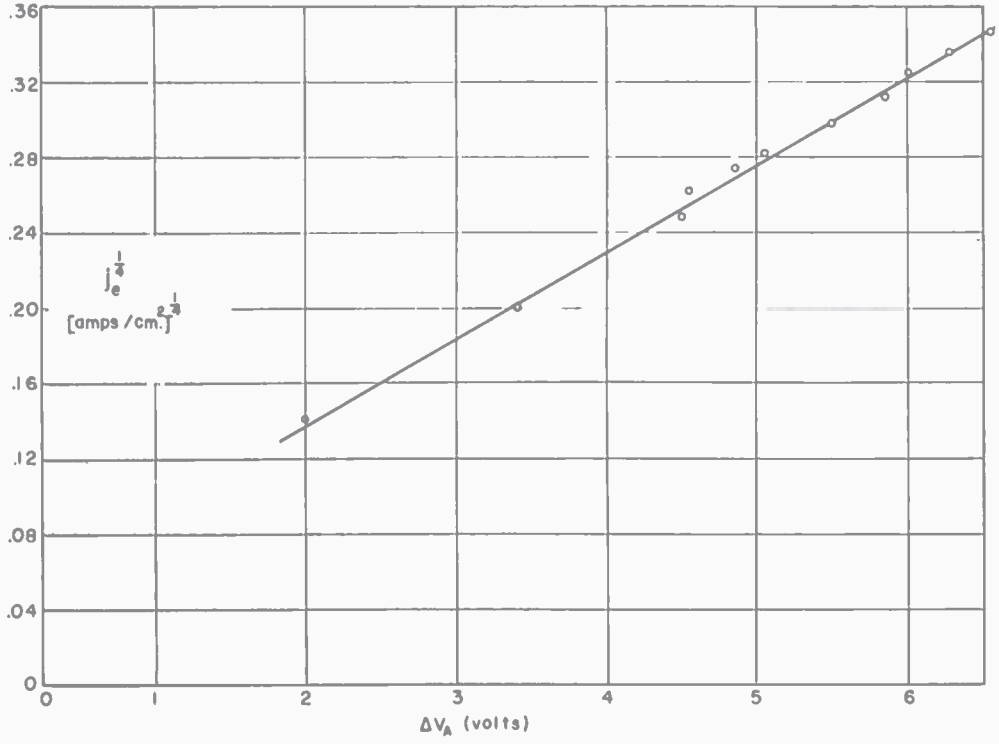

Fig. 6—Volt-ampere characteristic of the anode-glow mode.

Thus a plot of $j_e^{1/4}$ versus ΔV_A should yield a straight line of slope γ. This has been done in Figure 6, from which one finds $\gamma = 0.045$. Substitution of the various quantities in the coefficient of ΔV_A in Equation (19) yields $\gamma = 0.096$. If for τ in Equation (19) we substitute the experimental value 120×10^{-6} second rather than the theoretical value, we obtain $\gamma = 0.064$, which is in better agreement with the value of 0.045 obtained from Figure 6. This measured value of τ,

roughly 45 per cent of the calculated value, suggests that the true rate of ion loss is about double that observed by measuring i_p. As is outlined below, the oxide cathode is far from an ideal equipotential surface and acts as an ion sink. Other experiments have indicated that more or less ion current unquestionably flows to the cathode depending on the uniformity of the cathode surface. One can attempt to correct the data for the ion current flowing to the cathode by multiplying i_p by the ratio of the calculated to measured values of τ. This has been done in column 12 of Table I resulting in excellent agreement with the values of column 10. This further substantiates our model of the anode glow mode of discharge.

IV. Plasma-Decay Constant

Following the interruption of a discharge, the remanent plasma decays according to the relation expressed in Equation (13). In Equation (13) it is assumed that the plasma losses are by diffusion to the walls and that recombination is negligible. Such is the case in these studies. When $t = 0$, i.e., at the moment of discharge interruption, $n = n_o\,(x, y, z) = \sum_{m=1}^{\infty} n_{om}\,(x, y, z)$. Studies of the plasma distribution presented in Section V indicate that in the case of the anode-glow mode, the distribution is very closely given by the first term of the series of Equation (13). In that case, the plasma density following the interruption of an anode glow discharge is given by $n = n_1\, e^{-t/\tau_1}$. Since only the fundamental term of the series exists, we omit subscripts, and write

$$n = n_o\, e^{-t/\tau}. \tag{20}$$

For the cylindrical structures studied here, wherein ion losses occur largely to the end plates, it can be shown that[4]

$$\tau = \frac{1}{\frac{\pi^2}{h^2}\,(D_a)_{1400}}, \tag{21}$$

where $(D_a)_{1400}$ is the ambipolar diffusion coefficient (ADC) for the case where the electron temperature is 1400°K. The ratio between the ADC for the case of electrons at 1400°K and the ADC for electrons at 300°K (the ions being at 300°K in both cases) is

$$\frac{(D_a)_{1400}}{(D_a)_{300}} = \frac{1 + \dfrac{1400}{300}}{1 + \dfrac{300}{300}} = \frac{5.67}{2} \simeq 2.8.$$

Now, for a pressure of 1 millimeter, $(D_a)_{300} = 540$ in helium.[4] Thus in our case, $(D_a)_{1400} \simeq 1500$. Then from Equation (21), since $h = 2$ centimeters,

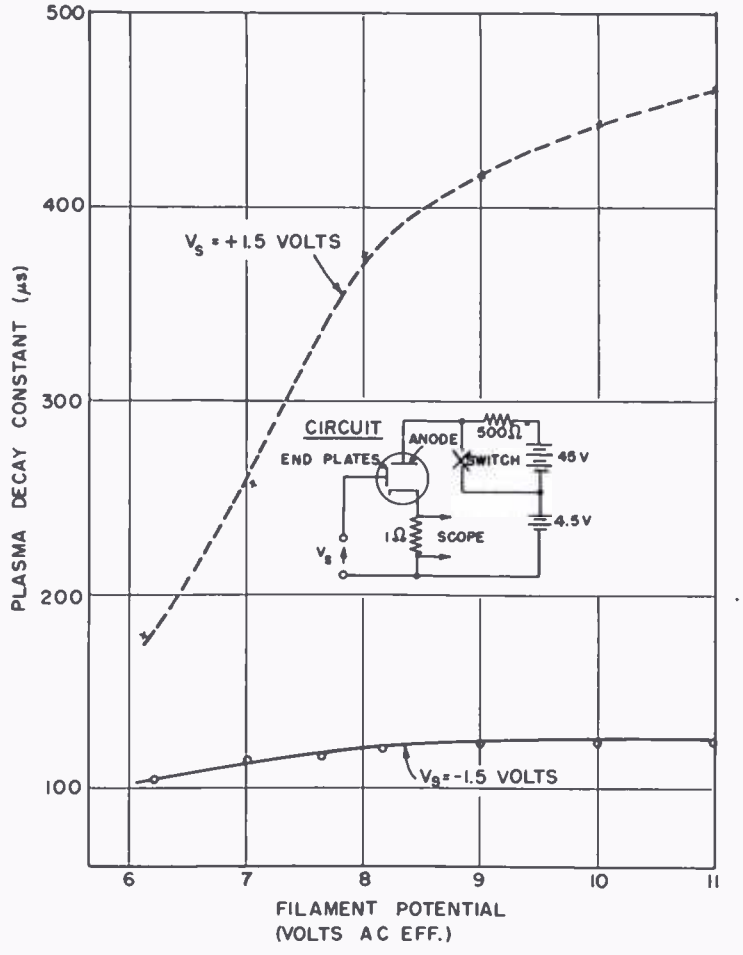

Fig. 7—Effect of the heater input on plasma decay constant.

$$\tau = \frac{4}{1500\,\pi^2} \simeq 270 \times 10^{-6} \text{ second.}$$

The plasma decay constant of the tube used in these studies was measured with the circuit shown in Figure 7. In this setup the anode of the tube was connected alternately to + 49.5 volts (through a limit-

ing resistor) and to + 4.5 volts. The shifting was accomplished by means of a high-speed relay driven by a 60-cycle source. The display on the scope shows a flat-top section during the discharge and then a period of decay following the interruption of the discharge. It is found that the decay can be described very closely by a simple exponential function of the form of Equation (20), thus substantiating the minuteness of modes other than the fundamental in the anode glow discharge.

Using the circuit of Figure 7, τ was measured as a function of E_f, the heater voltage. The results are plotted on the same figure. It is

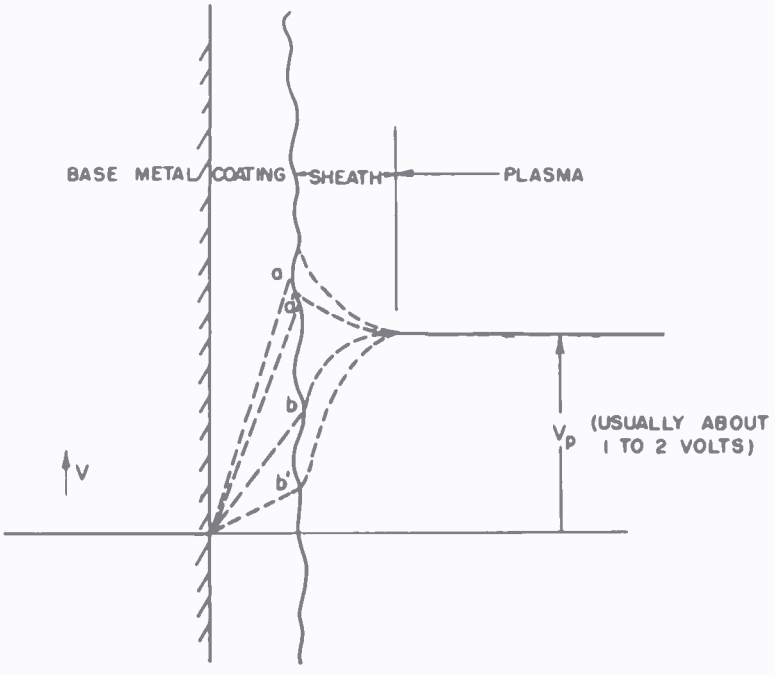

Fig. 8—Detailed view of the potential distribution in the cathode region.

seen that the measured values of τ are less than half the computed value. This difference is ascribed mostly to ion losses at the cathode.

It is seen that τ increases with increasing cathode temperature. This effect was made more dramatic by setting the end shields at a potential of + 1.5 volts so that they could no longer act as ion sinks. In this case the portions of the cathode which can accept ions play a more dominant role. The measured values of τ in this case are given by the dashed line of Figure 7. It is seen that as E_f is varied between 6.2 and 11 volts, τ varies by a factor of almost 3 as against a change of less than 20 per cent in the case where $V_s = -1.5$ volts.

The influence of cathode temperature upon ion loss, and consequently upon τ, can be explained by reference to Figure 8, where the

electric potential in the vicinity of the cathode is portrayed. The surface of oxide cathodes is notoriously patchy with regard to electron emission, work function and probably also with regard to resistance. Let us suppose that the average effect of all the patches is such as to fix plasma space potential at the value V_p shown in the figure.* The patches such as a and a', whose potentials are a tenth of a volt or more above plasma potential, cannot be reached by ions from the plasma. However, other patches, such as b and b', which have a different combination of work function, emission, and resistance are located below plasma potential and so act as ion sinks. The ion loss to such patches is greatly out of proportion to the size of the patch since the plasma density near the cathode is generally many times its value elsewhere. Now as the cathode temperature is increased by an increase in the filament voltage, the ohmic resistance which connects a patch to the base metal will decrease.** Furthermore, the electron emission from each patch will increase. Consideration of the resulting current and voltage relations will show that the overall effect is such as to reduce the number of patches that can act as ion sinks. Hence τ should increase with filament voltage.

V. Plasma Density Distribution in the Anode-Glow Mode

A picture has been presented of the mechanism of the anode glow, a feature of which is the fact that the plasma density distribution is very nearly in the fundamental or lowest order mode of the series solution of Laplace's equation for the cylindrical structures employed. The bases thus far presented for this belief are twofold: (1) A theoretical analysis, publication of which is reserved for a later paper in this series. This analysis is used to determine the total plasma content within the tube from measured electron and ion currents flowing to electrodes. (2) Measurements of plasma decay following the interruption of the discharge indicate the virtual nonexistence of higher order modes at the moment of the discharge interruption. This is strong evidence for their nonexistence at earlier times.

It was felt desirable to secure a less ambiguous confirmation of this view. As a first thought it might appear that the density distribution could be determined by means of a number of suitably placed probes or by means of movable probes. However, experiment and analysis indicates that probes can and do exercise a profound effect upon the

---

* The potential relationships in a cathode-plasma-anode system similar in all essentials to the one above are treated analytically by E. O. Johnson and W. M. Webster in a forthcoming paper.

** Private communication from L. S. Nergaard of these laboratories.

plasma density in their vicinity, reducing the density from the value in the absence of the probe by a factor of as much as ten or more. (It is expected that these probe studies will be described in a subsequent publication.) One concludes from this that any means for studying the plasma density distribution must be one which in no way influences the discharge. The only obvious method that meets this requirement is to measure the current distribution to the bounding electrodes and to compare the data obtained with the results predicted by the theoretical analysis.

Two tubes were built, one with a segmented anode and the other with segmented end shields. Each was operated in the anode glow

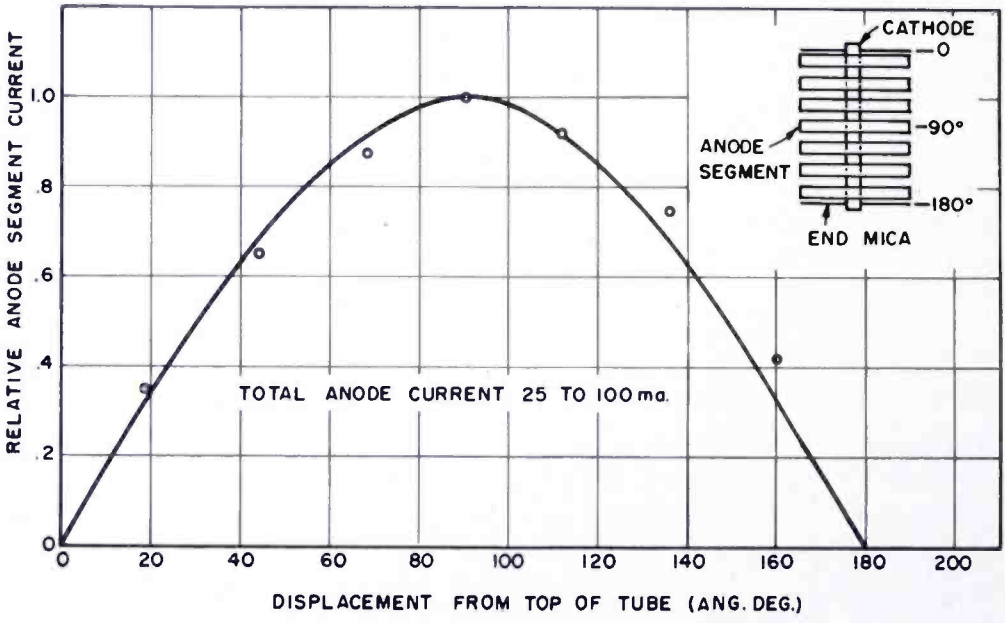

Fig. 9—Axial plasma density distribution.

mode and the electron currents measured to the anode segments and positive ion currents to the end shield segments.

A sketch of the tube with segmented anode is shown in Figure 9. It is seen that the anode consists of seven closely spaced rings. The currents to the various segments are plotted on the same figure using as abscissas the angular value of the segment midpoints; the scale being chosen so that the anode height corresponds to 180 degrees. This scale was chosen because the theory indicates that the axial distribution should be cosinusoidal. A cosine function (normalized to the current value at the central segment) is plotted on the same figure. It is seen that theory and experiment are in good agreement. The tendency for divergence at the end segments is ascribed to the fact that the plasma density should not and does not fall to zero at

the edge of the end shield sheaths. Thus, the cosine function should be drawn on a slightly more expanded horizontal scale. It was not felt necessary to add this refinement or be concerned with more detailed averaging due to the fact that each segment extends over a finite portion of the distribution. This tube as well as the one described below has the same over-all dimensions, gas, and gas pressure as the tube associated with Figure 4.

The segmented-end-shield tube is sketched in Figure 10. If ion generation and loss within the plasma are negligible (which is the case in the anode-glow mode), then the plasma density is governed

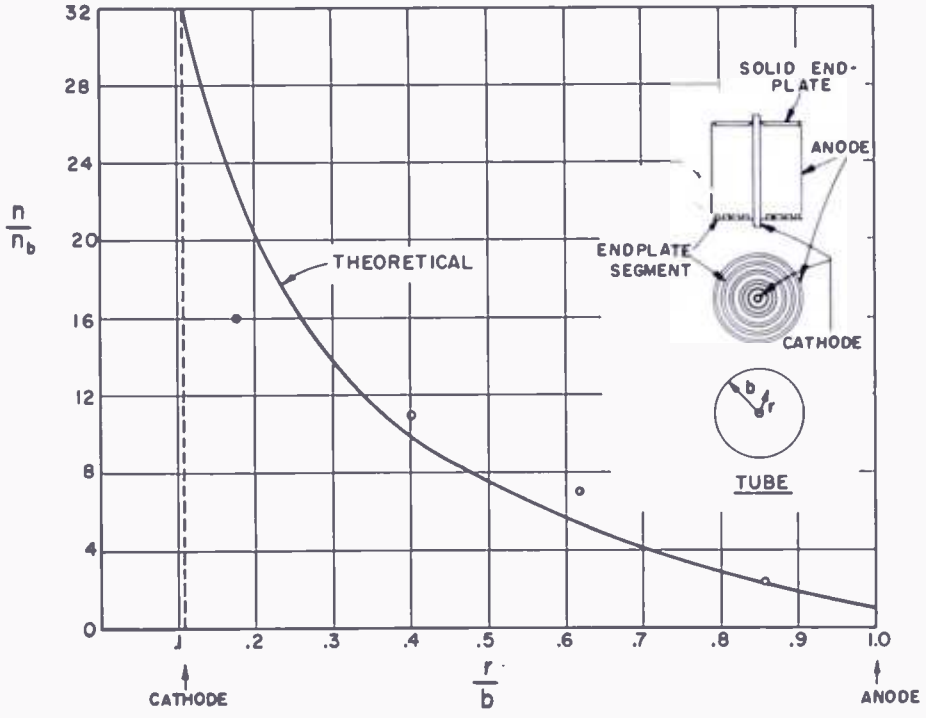

Fig. 10—Radial plasma density distribution.

by Laplace's equation. The solution of this equation* for the cylindrical geometry employed, with boundary conditions appropriate to the anode-glow mode, is plotted as a smooth curve in Figure 10. The abscissas represent the fractional distances r/b from the axis of the tube to the anode edge of the plasma; the ordinates represent the normalized plasma density, that is to say, n divided by the plasma density n_b at the anode edge of the plasma. On the same figure are plotted quantities which are proportional to the ion currents to the end plate segments and hence to the plasma densities directly above

* The details of this solution will be presented in a later paper of this series.

each segment. These have been plotted on a scale to scatter about the theoretical curve. The agreement can be said, at best, to be fair. Considering the small number of rings employed, it is felt that the view that the plasma distribution conforms to the lowest mode is reasonably well substantiated. The maximum divergence occurs at the innermost ring. The divergence is in the direction to be expected if the cathode acts as an ion sink. (In the simple theory it is assumed that no ions are lost to the cathode.) Thus, the data of Figure 10 may be considered as offering further evidence for marked nonuniformity of the oxide cathode with consequent ion loss thereto.

VI. Conclusion

This paper treats the anode-glow mode of the hot cathode discharge. In this mode a "dark" plasma substantially at cathode potential fills the major portion of the space between cathode and anode. The applied potential appears across a double sheath at the anode. The ion generation occurs very close to the anode surface.

Using this picture it is possible to compute the ion generation associated with a given electron flow and the relation between electron current and applied potential. It appears that the ratio of electron current to ion generation should be almost constant. Experiment confirms this. The electron current should vary as the fourth power of the potential excess above the ionization potential of the gas. This is reasonably well confirmed by experiment.

Theory and experiment combine to indicate that the density distribution in the dark plasma conform to the fundamental term of the solution of Laplace's equation for the geometry employed.

Studies of the decay of the dark plasma following the interruption of the discharge show that ion losses take place to the oxide cathode even when the plasma appears to be negative with respect to the cathode. This is ascribed to nonuniformities in emission, work function, and resistivity along the cathode surface.

Later papers will treat more fully the matter of plasma density distribution in the anode-glow mode as well as the conditions which determine when the discharge will "break" out of this mode. In addition, it will be shown that the gas pressure must exceed a critical value for the anode glow to occur.

STATIC MAGNETIC MATRIX MEMORY AND SWITCHING CIRCUITS*

By

Jan A. Rajchman

Research Department, RCA Laboratories Division,
Princeton, N. J.

Summary—Information bits are stored in terms of the direction of magnetization of a multitude of saturated cores connected in a matrix array. Access to any core, for registry or interrogation, is by simultaneous excitation of its defining matrix lines. Bivalued signals, identifying the information bit and corresponding core, select these lines by activating magnetic switches, likewise composed of saturable cores. This memory is characterized by an access time of several microseconds, indefinitely long storage requiring no holding power, and the possibility of large storage capacity at low cost. An operating experimental model with a capacity of 256 bits has been built.

Introduction

IT IS GENERALLY recognized that the internal memory is the most critical element in the present-day art of digital computing and information handling machines. In fact, its nature dictates the type of machine being built.

Most memory systems use time as a switching variable, that is, the information is available serially in the order in which it was stored. This creates an intrinsic dilemma between access time and storage capacity. The problem is resolved, in engineering practice, by judicious combination of devices with long access and large capacity, with ones with short access but small capacity. There is no such dilemma in a matrix type memory in which access to any bit of information is by multiple coincidence of signals specifying its label or address within the storage device. Such a matrix type memory would be highly desirable if large capacities could be obtained simply and at low cost.

Two problems are encountered in a matrix memory; storage, and switching. The storing cell must have two (or more) possible physical stable states, and it must be possible to change these states by the coincidence of several input signals. While many possible physical effects exhibit inherent stable states, most lack the necessary nonlinearity required for switching, so that actually the real problem of the matrix memory is one of switching rather than one of storage. Multiple coincidence can be obtained by multiple nonlinear effects, each

* Decimal Classification: R282.3.

with an effective threshold such as the control of electron current in a tube. This is the principle of selection in the selective electrostatic storage tube which was the first rapid access matrix memory device made.[1] The multiple coincidence switching can also be achieved with a threshold effect of a single variable obtained as a linear combination of the address selecting signals, coincidence occurring when the single threshold is exceeded. Resistive matrices[2] switches are based on that idea and so are the devices to be discussed.

Magnetic cores have intrinsically the two requisites for a storing element of a matrix memory: stable states of residual magnetization; and nonlinear variations of magnetic induction with respect to magnetizing force. These properties are closest to ideal when the hysteresis loop approaches a rectangle. The advent, several years ago, of nickel-iron alloys with extraordinary loop rectangularity stirred the imagination of workers in the field of digital computers. The first pioneering application, announced by the Harvard Computation Laboratory in 1947, was a static delay line operating as serial memory.[3] The realization that the saturable cores were ideally suited for a matrix memory occurred to several men, as far as is known, at about the same epoch. R. L. Snyder, Jr. considered the broad idea in 1947. J. W. Forrester published a proposal to that effect in 1951,[4] and results of the Massachusetts Institute of Technology work were reported by W. N. Papian at the National Convention of the Institute of Radio Engineers in 1951. The resistive matrix switch and the selective electrostatic storage tube, mentioned above, were conceived in 1941 and 1946 respectively. As a natural development we have, for several years, been studying matrix-type memories using nonlinear elements with inherent stable states and most particularly ferromagnetic materials. This paper describes some of the more recent findings.

Principle

Consider an array of magnetic cores arranged in rows and columns. Each core is linked by three windings. Two of the windings are connected in series by rows and columns and the third is a common series winding, as shown in Figure 1. All cores are magnetized to one or

---

[1] J. Rajchman, "The Selective Electrostatic Storage Tube," *RCA Review*, Vol. XIII, p. 53, March, 1951.

[2] J. Rajchman, U. S. Pat. 2,428,811.

[3] A. Wang, "Magnetic Storage and Delay Line," *Jour. Appl. Phys.*, Vol. 21, pp. 49-54, January, 1950.

[4] J. W. Forrester, "Digital Information Storage in Three Dimensions Using Magnetic Cores," *Jour. Appl. Phys.*, Vol. 22, pp. 44-48, January, 1951.

the other of the two remanant inductions represented by points P and N on the idealized hysteresis loop of Figure 1. In this state, the array is holding information previously stored. In order to set any given core to the desired remanance (P or N), pulses of current in one or the other direction are simultaneously applied to the row and column of the core. The amplitude of these currents is so adjusted that their additive, i.e., doubling effects, produce sufficient magnetomotive force to exceed the knee of the loop for the selected core at the intersection of the lines but insufficient to exceed the knee for the other cores on the selected lines where they act singly. Consequently, the selected core will be magnetized in the desired direction while all other cores in the

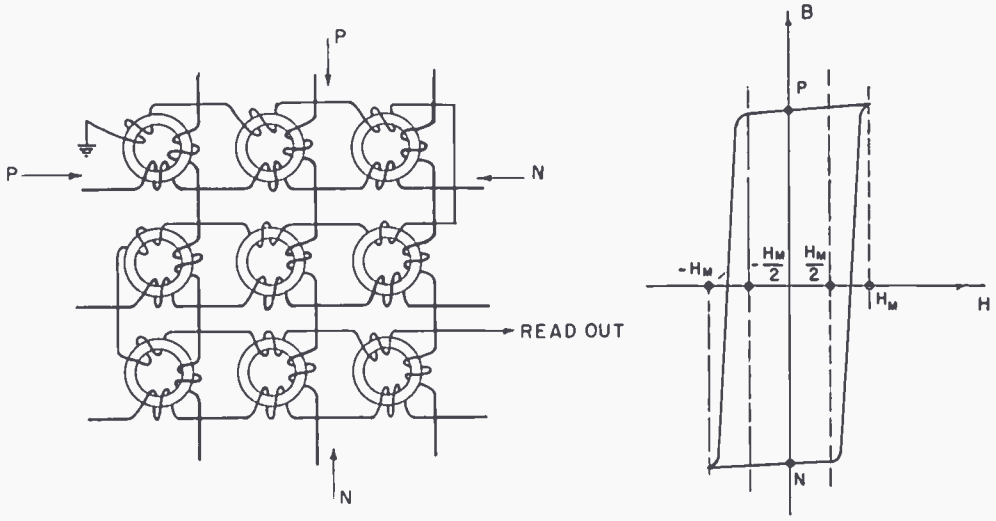

Fig. 1—Double coincident magnetic matrix memory and idealized hysteresis loop.

matrix will remain unaffected. The read-out is obtained by applying read-in current pulses of a standard direction, e.g., toward P, on the lines of the core being interrogated, and observing whether or not the flux changes in that core. A change of flux induces a voltage in the common winding. If a voltage is observed, as a result of the change of flux from N to P, in the interrogated core, this core is restored to its initial state N, by circuits activated by the reading signal.

The operation of the matrix arrangement just described depends on high discrimination between the changes of induction produced in the cores for magnetomotive forces varying in the ratio of 2 to 1. Actually, it is possible to have an arrangement depending on a ratio of excitations of 3 to 1. There are also many combinatorial possibilities in which more than two signals must coincide on any core to switch its direction of magnetization. A survey of these various possibilities follows.

Combinatorial Systems

A ratio of 3 to 1 in the excitations of the selected and unselected cores may be obtained by sending a current in the unselected lines in the opposite direction to that of the selected lines. By choosing the amplitude of that current to be one-third of the selecting current, it is easy to verify that the excitation of the unselected cores on the selected lines is one-third of the excitation on the selected core, and the excitation of the unselected cores in the rest of the matrix is also one-third of that on the selected core but in the opposite direction. This is illustrated in Figure 2. A similar arrangement consists in

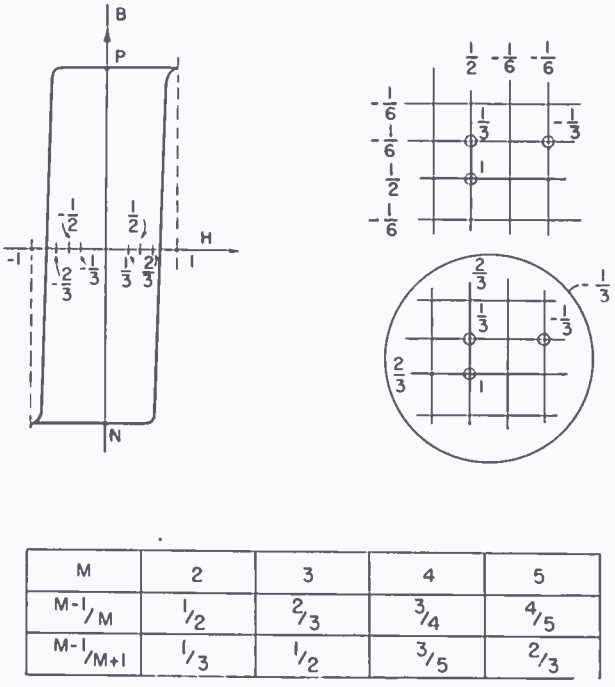

M	2	3	4	5
$M-1/M$	$1/2$	$2/3$	$3/4$	$4/5$
$M-1/M+1$	$1/3$	$1/2$	$3/5$	$2/3$

Fig. 2—Partial excitation of unselected cores to both polarities and multi-coincidence switching.

having an additional winding linking all the cores of the matrix and sending through it an opposing current equal to one-third of that required on the selected cores and using an increased drive on the selected lines equal to two-thirds that required in the selected core. Both of these systems utilize more effectively the range of magneto-motive excitations below the coercive force by extending it to both polarities, as illustrated in Figure 2.

The possibility of using both polarities of partial excitation on all the unselected cores including those on unselected lines can be utilized also to increase the number of coincident signals from two to three.

For example, in the winding common to all the cores, an opposing current equal to one of the selected lines currents can effectively inhibit the matrix, the excitation on the selected core being ½ (of the excitation required on the selected core); the excitation on the unselected cores in the rest of the matrix is $-\frac{1}{2}$. The coincidence of two pulses and anti-coincidence of the third is required for the core to change its direction of magnetization. All three signals may be also of the same polarity and equal to ½ of the selected core turn-over unit current, when an equal opposing current on all cores of the matrix is present at every entry. The matrix operates in that case on a straight triple coincidence. In both of these methods of obtaining triple, rather than double, coincidence switching, the ratio of effective magnetomotive drives on the selected and unselected cores is two-to-one.

It can be seen by these examples that partial excitation of the unselected cores to both polarities can be utilized to either increase the absolute ratio of excitations to 3 to 1 in a double coincidence system or to obtain a triple coincidence system with an absolute ratio of excitations equal to 2 to 1. This can be generalized to a greater number, M, of coincident signals for which an absolute ratio of excitations of unselected to selected cores equal to $(M-1)/(M+1)$ can be obtained by several different means. For example, for four coincident signals the discriminating ratio is $\frac{3}{5}$, or 60 per cent, and for five signals it is $\frac{2}{3}$ or 66 per cent. This indicates that the closer the hysteresis loop approaches rectangularity and the more uniform the magnetic properties from core to core, the greater the number of coincident signals which may be used to switch into the memory matrix. Because multiple coincidence switching can be obtained so easily in a switch described below, triple coincidence is likely to be the highest used in practice even when materials with superlative magnetic properties are available.

Switching the Memory Matrix

The double coincidence array of cores reduces the problem of switching into n^2 cores, to that of switching into $2n$ channels. In each channel, two electronic devices—such as tubes or crystals—are required, since current can flow in only one direction through these devices. While the number of tubes required ($4n$) may be relatively small compared to n^2, when n is large it is still a large number of tubes.

It was recognized at the outset that efficient means to further reduce the number of input channels was indispensable and that this could be accomplished by using cumulatively the coincident means used in the memory matrix, that is, by using sets of cores driving other sets. When considering possible systems of driving the matrix by sets of cores,

an important fact was realized, namely, that information is stored in the final array only, and that, in the driving sets of cores, either all cores are in state N, or a single core is state P while others are at N. Consequently, in these driving sets it is possible to have large magnetizing currents on all unselected cores in the direction N while the selected core is driven to P. This is in contradiction to the very limited

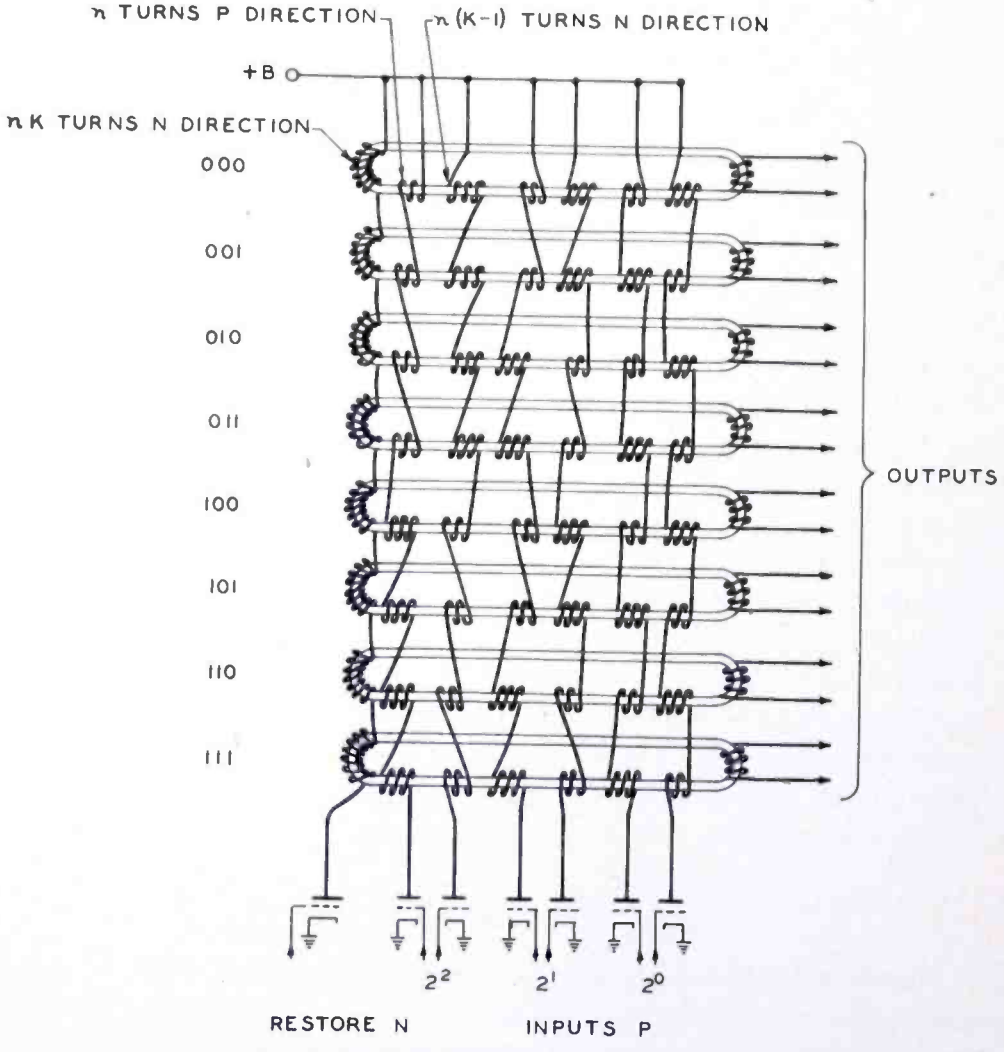

Fig. 3—Magnetic commutator switch.

spread to the opposite polarity on the excitation of the unselected cores which was permissible in the information storing matrix.

Switching into each side of the information storing matrix can be by means of commutator switches in which one core out of 2^K is selected by K channels. A typical commutator switch with three inputs and eight outputs is illustrated in Figure 3. Every input channel has

a pair of windings, one of which links one half of the cores in one direction and the other half in the other direction, while the other winding links the same halves in the opposite direction from the first winding. The division in halves of the various inputs pairs is by actual geometrical halves for one input, interlaced quarters for the next input, interlaced eighths for the next, etc. A current pulse is sent through one winding or the other in each pair. As a result, for every combination of inputs, one core will have K windings driving it in the P direction, some with $(K\text{-}S)$ driving in the P direction and S in the N direction, S being 1, 2, . . . K. The number of turns of the N windings is chosen to be $(K—1)$ times that on the P windings, so that a single core, the selected core, is driven to P while all other cores have either no excitation or are driven to N, some with large excitation. Consequently, only the selected core will change its direction of magnetization from N to P, provided all cores were initially magnetized in direction N. To restore the selected core to its initial direction of saturation N, there is a common restoring winding linking all cores. When it is excited, it tends to magnetize all cores in the direction N, restoring the selected core from P to N and subjecting all other cores to a fairly large current tending to magnetize them in the direction of their existing remanant induction. This method to avoid doubling the selecting channel driving tubes is based on recognition of the fact that the restoration need not be selective.

Each core of the commutator has an output winding. The outputs may be heavily loaded, that is, considerable power may be transmitted through the switch. The primary driving currents are, of course, correspondingly large. In fact, the selected core acts in a similar manner to a conventional transformer, sufficient primary current (and power) must be provided both to magnetize the transformer and to supply the secondary currents (and power). The increased current in the N windings of the unselected cores automatically compensates for the increased P driving currents so that the power transmitted through the switch may be varied arbitrarily without any adjustments. It is worth mentioning also that current from all selecting power tubes add their magnetizing effects on the selected core, consequently the greater the number of inputs, the smaller the required current from each driving channel selecting tube.

There are many variations of possible distributions of the windings according to the binary system as outlined above. They all depend on the fact that it is possible to drive the unselected cores to an arbitrarily large excitation in the direction of their remanant induction.

The commutator switches are used to drive a memory matrix, one

driving the rows and one the columns, as illustrated in Figure 4. Such a system may be operated as follows: Assume that initially all cores of both commutators are in state N and that some cores of the memory matrix are in state N and some in state P. The writing into the memory is in two or three steps. In the first step, all inputs to both commutators are excited simultaneously, that is, current is sent through one winding in each input pair. This will cause one core in each commutator to turn over from N to P, and this, in turn, will cause currents

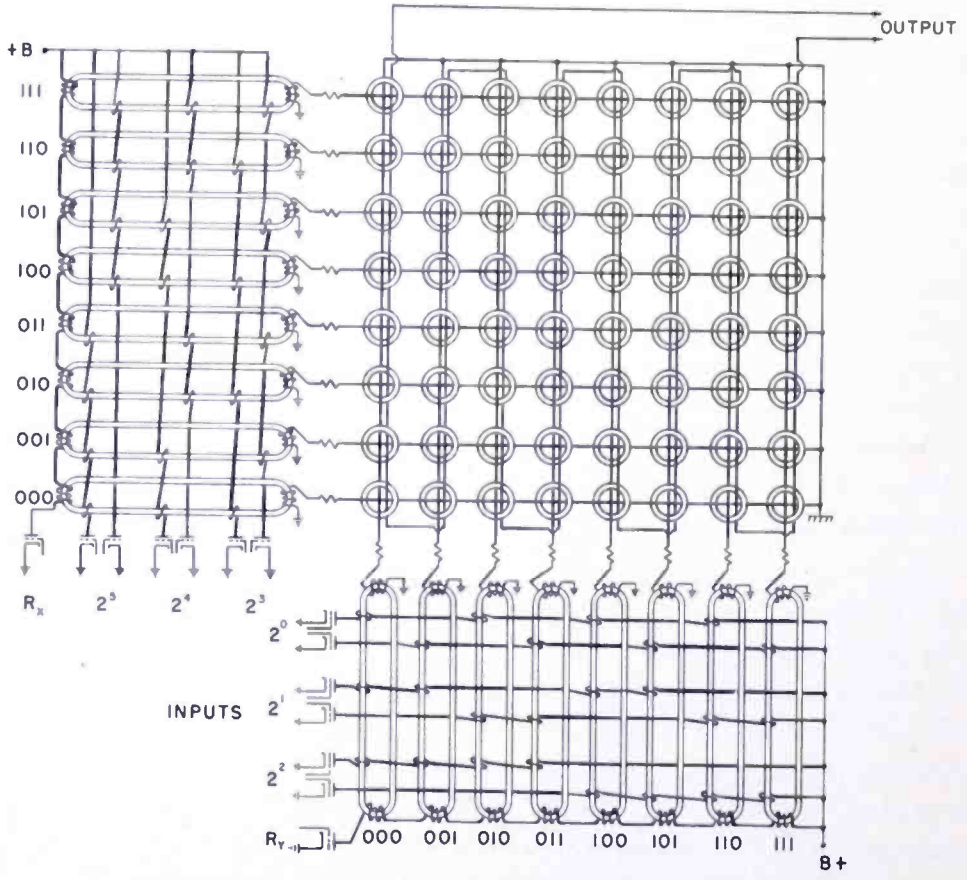

Fig. 4—Double coincidence magnetic matrix memory driven by multi-coincidence magnetic commutator switches.

to be induced in the lines of the memory matrix which are linked to these cores. The currents induced in the lines are adjusted to have the proper amplitude to cause the core at the intersection to be magnetized in direction P (regardless of its previous direction of magnetization) while leaving all other cores on the same lines unaffected. The second step is conditioned by the polarity of the information signal which is to be stored. If the core is to be left at N, both commutators are restored simultaneously to N by exciting their restoring windings.

This will induce currents in the selected lines of the matrix equal to but in opposite direction from those of the first step, and the selected core at the intersection of the lines will be driven to state N. If, on the other hand, the selected core is to be left at state P, only one of the commutators is restored to N in the second step, while the other is restored in the third step. Of course, the excitation of only one line of the matrix leaves all cores unaffected, since it provides only half the magnetomotive force required to turn over any core. The reading or interrogating proceeds by the same two or three steps. In the first step, when the interrogated core is driven towards P, a large signal or practically no signal is observed in the reading winding, depending on whether the interrogated core was initially in state N or P. If a signal is observed, it is utilized to restore simultaneously both commutators in step 2 and thereby restore the interrogated core to its initial state N. If no signal is observed, the commutators are restored successively in steps 2 and 3, and the interrogated core is left at its initial state, P, from which it was not disturbed.

This three-step operating schedule was chosen for the first experiments with a complete system, but it is possible to use different schedules of operating pulses of the combination of the commutator switches and memory matrix, some requiring only two steps. This can be accomplished, for example, by using an additional winding linking all cores of the matrix. The first step is as before—both sets of inputs to the commutator are driven simultaneously and magnetize the selected core of the matrix to P. In the second step, both commutators are restored simultaneously, and an inhibiting current pulse, equal in amplitude to the matrix line currents, may be sent through the common winding. When the inhibiting pulse is sent, the selected core remains at P; when the pulse is not sent, the core is driven to N, as was explained in the triple-coincidence mode of operation. For reading, the absence or presence of a signal in the reading winding in the first step determines whether an inhibiting pulse is or is not used in the second step, so that the interrogated core is restored to N if disturbed to P in the first step, but is left undisturbed if its initial state was P.

In this two-step schedule, the commutator excitation is not dependent on the polarity of read and write. Polarity selection is obtained in this case by the presence or absence of the inhibiting pulse in the matrix winding. This renders the schedule particularly suitable for driving many information storing matrices from a single pair of commutators. Similar lines in all matrices are driven by the same commutator cores and similar points are selected in all matrices. The polarity of write-in, and the restoration of the interrogated core on

reading out, are determined by the presence or absence of the inhibiting pulses in the individual matrices.

The use of the commutator switches has reduced the switching to the ultimate minimum of channels (when bivalued signals are used), namely, to logarithm-base-two of the number (2^m) of stored information bits. Because of the push-pull inputs, the actual number of driving tubes is doubled. Also, one or two tubes are required for restoring the commutators. In all $2m$ + (1 or 2), tubes are required for the address circuits. In addition, write-in and read-out circuits for the information are required. These circuits are in the nature of simple amplifiers.

The intensity of the induced currents in the matrix lines depends on the value of the primary currents driving the commutator switch, since the selected core of the commutator acts to a great extent like a conventional current transformer when it is heavily loaded by the matrix lines. Consequently, this intensity may be adjusted to have the optimum value for the matrix operation by controlling the primary currents. Faster turn-over of the cores of the commutator can be obtained when they are not loaded so heavily, and a greater proportion of the primary current is used for their excitation. This can be accomplished by impedances in series with the matrix lines. A resistance is employed for this purpose as shown in Figure 4.

Effects of the Departure from Ideal Characteristics of the Cores

For the sake of simplicity, it has been assumed thus far that the hysteresis loop of the core material is perfectly rectangular, that the magnetizing force within the material is always proportional to the applied currents as it would be in the absence of eddy currents, that no other disturbing effects exist in the cores when the flux is changing rapidly, and that all cores have uniform properties. In the operation of actual materials, there is considerable departure from these ideal assumptions.

A significant hysteresis curve of materials that were tested is shown in Figure 5. This is a minor loop described when the maximum magnetomotive force H_M, or tip H, is adjusted so as to obtain optimum discrimination under the two-to-one driving system, i.e., essentially when the ratio of the total change of flux, ΔB, to the change $\Delta B_{1/2}$ obtained for $\frac{1}{2}$ H_M is maximum. The departure from ideal rectangularity has two detrimental effects in the information storing matrix: demagnetization of unselected cores due to accesses to other cores, and presence of unwanted signals in the reading windings. These effects and means to minimize them will now be described.

Consider a core at its remanant induction, represented by point N, Figure 5. A current pulse, in direction P, equal to half (for the case of the 2-to-1 excitation system) of the total current corresponding to H_M, will cause the induction to describe half a minor loop and leave the core at a remanant induction such as that represented by point N_1. If a demagnetizing current pulse is applied again, a new half minor loop will be described, and there will be a further loss of remanant induction. A large number of such demagnetizing pulses could occur in a matrix driven directly by tubes, for a long run of entries to other cores on the same matrix lines. This would result in an asymptotic remanant induction which could be disastrously small for some matrials.

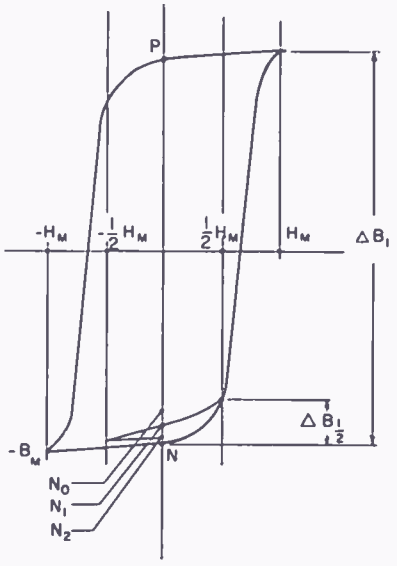

Fig. 5—Typical hysteresis loop.

This cumulative demagnetizing effect is greatly minimized—if not completely eliminated—by the pulse schedule inherent in the drive by means of magnetic commutator switches. It will be recalled that for every access, any selected line is first subjected to a P pulse, then an N pulse. Consequently, the partial demagnetization of any unselected core from N to N_1 will be immediately followed by a remagnetization, completing the minor loop to such a point as N_2. This point is very close to the original point N. The asymptotic remanance due to the repetition of this minor loop is equivalent to that resulting from a small alternating-current disturbance which is known to produce only a small permanent demagnetization. In the case of the use of an inhibiting pulse in the two step schedule, an additional opposing pulse following every inhibiting pulse is necessary to prevent cumulative demagnetization of unselected cores in the whole matrix.

Unwanted voltages are produced in the reading winding when the selected core is driven in the standard positive interrogating direction. They are due in part to the small change of flux in the selected core when it happens to be in state P, but mostly to the additive effects of the change of flux in all unselected cores which are partially excited, i.e., the cores on the selected lines and also in the rest of the matrix when a third common switching or inhibiting winding is used. These additive effects can be greatly reduced by using a reading winding in which the direction of linkage changes polarity at every core on every line, i.e., the pattern of polarities is like a checkerboard. It is easy to see that with this arrangement the unwanted voltages from all unselected cores tend to cancel each other except from two cores on the selected lines. The latter voltages tend to reduce both the wanted and unwanted signals from the selected core and hence improve discrimination ratio. With perfect uniformity of magnetic properties, linear dependence of induction near remanance, and identical time variation of flux for all cores and for both polarities, the cancellation system would be perfect and no unwanted signal would be obtained in the reading winding. For a given dispersion of magnetic properties, the deterioration of the ratio of wanted to unwanted signal will grow only as the square root of the number of contributing cores, i.e., the square root of the side of the matrix with a regular double coincident system, or linearly with the side with a triple-coincidence or compensation system.

It is seen that appreciable departure from an ideal rectangular hysteresis loop can be tolerated, since there are simple remedies for cumulative, partial demagnetizations on unselected cores, and for additive effects of the contributions to the deterioration of the reading signal. These remedies are effective only when the properties from core to core are very uniform. The uniformity is in fact an important prerequisite even when the loops are nearly rectangular, particularly in as far as the coercive force is concerned.

The commutator switch operation is less sensitive to the magnetic properties of the core than is that of the information storing matrix. The significant merit factor is the ratio of remanant induction to the induction obtained at maximum excitation, i.e., B_r/B_M. When this ratio departs from its ideal value of unity, some voltages are induced in the unselected cores in the opposite direction from the voltage on the selected cores. When the commutator drives an information storing matrix, these voltages are in the right direction to improve the operation of the matrix. The amplitude of these voltages, different from

line to line, is not optimum, but still, in practical cases, these opposing voltages will induce currents which are somewhat helpful.

The eddy currents induced in the cores due to the rapid changes of flux play a dominant role in the operation of the information storing matrix. The dissipation of power is not as significant as the fact that these currents oppose the effects of the externally applied current and slow down the rate of change of flux. As a result, a certain time elapses between the application of a current step and the completion of the change of flux corresponding to that current. This delay in switching time of the core is in part detrimental, because it limits the speed at which the memory system can be operated, and is in part beneficial, because it provides a means of time discrimination, in addition to amplitude discrimination, between wanted and unwanted reading signals.

The equations describing the change of flux within a material with nonlinear B-H characteristic, when driven by a step current pulse in the inevitable presence of eddy currents, are difficult to solve. When many simplifying assumptions are made, however, it is possible to obtain a qualitative idea of the solution. This was done by Mr. W. N. Papian in his master's thesis.[5]

Typical experimental behavior of a core wound with 5 wraps of $\frac{1}{8}$-mil 4-79 Permalloy under pulse conditions is illustrated by the photographs of the traces of an oscilloscope, Figure 6. These were obtained from a secondary winding when alternate polarity current pulses of about .4 microsecond rise, 10 microseconds duration and .3 microsecond decay were applied to the primary. The voltage pulse, for different current amplitudes is seen to have different shapes. For all amplitudes, there is an initial sharp rise, followed by a decay to zero. The switch-over time, i.e., the duration up to the end of any flux change in the core, varies with increasing current amplitude. At first it is short, then it increases and passes through a maximum to become shorter and shorter. The striking feature of the middle range of drives is the two maxima of the voltage pulse shape.

The broad aspects of this behavior can be understood in terms of the well known retarding effects of the inducted eddy currents. The change of flux is delayed by an amount increasing with electrical conductivity and magnetic permeability of the material. In materials with a very rectangular loop, there are two distinct ranges of permeability values with an abrupt transition between them, the ratio between these values being a thousand to one, or more. For a low magnetizing

[5] W. N. Papian, "A Coincident-Current Magnetic Memory Unit," Master's Thesis, Electrical Engineering Department, Massachusetts Institute of Technology, August, 1951.

force, only the low permeability region is traversed by the core, the consequent damping of eddy currents is small and a sharp voltage pulse is produced. For higher magnetizing forces the high permeability region is encountered and the greater damping causes the voltage pulse to have a long bell-shaped waveform. Thus the voltage pulse is the composite of these two pulses and has two distinct maxima. For still higher magnetizing forces the delays due to the damping of the eddy currents become shorter because these opposing currents become

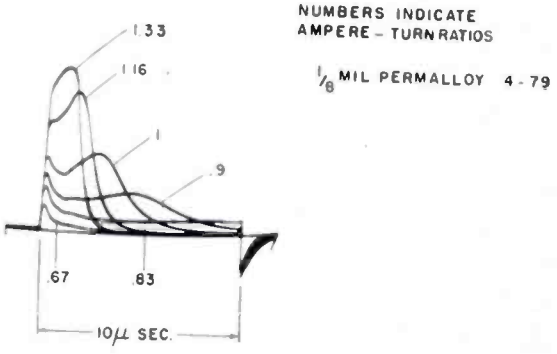

Fig. 6—Voltage output for various amplitudes of current.

relatively smaller with respect to the drive. This causes the two pulses to merge and form a single pulse. The family of voltage wave forms of Figure 6, taken with increasing magnetizing force, illustrates these effects. (Similar double peaks in the voltage shape, observed at the trailing edge of very intense current pulses, may be accounted for by departures from linearity of the hysteresis loop in the region from high saturation to remanance. This nonlinearity is not as pronounced as the transition from unsaturated to saturated induction occurring at the leading edge of the pulse, but the relative importance of the eddy currents is enormously greater since the external magnetizing force is removed.)

Experimental Results

The above observations made with symmetrical excitations of different amplitudes are illustrative of the behavior of the core but are not directly applicable when the cores are used in the coincident matrix. Indeed, they refer to family of symmetrical hysteresis loops, whereas minor unsymmetrical loops play an essential role in the application at hand.

As a guide in the design of actual devices, empirical data was taken in conditions approximating those of actual operation as closely as

possible. Typical results of such tests on a single core are the voltage traces displayed on an oscilloscope as shown on Figure 7. A schedule of pulses of different amplitudes and polarities as shown on the figure is applied to the core $(P - \frac{N}{2} - - \frac{N}{2} - P - N)$ and the resulting induced voltages are displayed on an oscilloscope synchronized so that the traces are superimposed. It will be noticed that two successive partial demagnetizations cause only a small loss of flux. This flux is measured by the sum of the areas under the two successive voltage traces or the area of the single remagnetizing full amplitude pulse P. The contribution to the reading signal of the cores on the unselected lines can be

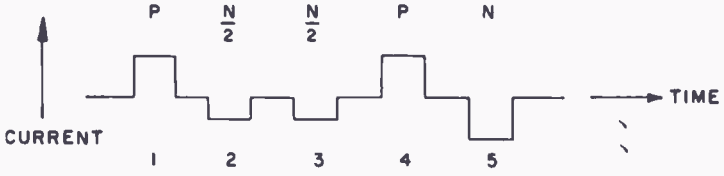

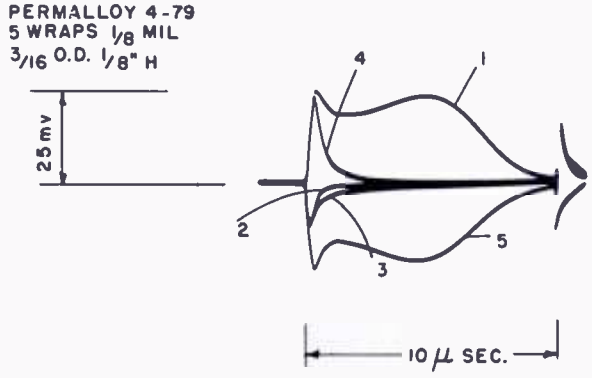

Fig. 7—Typical voltages from single core.

appreciated also by the voltage traces due to the demagnetizing half-current pulses. The amplitude of the voltage from the interrogated reversing core passes through a maximum. At that instant, voltages from half-excited cores on the same lines have decayed to a very small value. Consequently, if the reading signal is sampled or strobed, at the right instant, a very high ratio of wanted to unwanted signals can be obtained. This shows that time differences between wanted and unwanted signals considerably improve the discrimination obtained from amplitude differences alone. As a matter of interest, similar traces for a three-to-one driving system are shown in Figure 8.

Several materials were used in the tests. Nickel-iron alloys (Delta-

max) were found to have very long switching time. Silectron, a silicon steel alloy obtained from Allegheny Steel Co., provided the first material with which workable information-holding matrices and commutator switches were built. Most of the recent work was done with cores wound with 5 wraps of 1/8-mil Permalloy 4-79, cores of 3/16-inch diameter 1/8-inch high, obtained from Magnetics, Inc.

Throughout the research work, experiments were made on the possible use of ferrospinel magnetic cores. Owing to their low electrical conductivity, the eddy currents are considerably smaller than in metallic cores and the switching times much shorter. Switching times of a fraction of a microsecond have been observed for most samples. Some

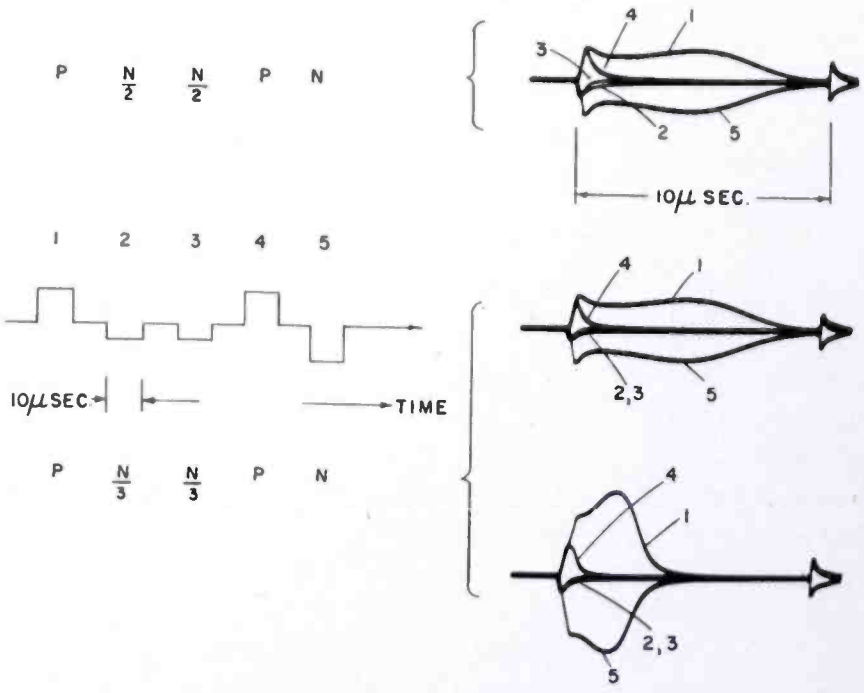

Fig. 8—Typical voltages for three-to-one excitation.

materials with reasonably rectangular loops which promise to be suitable for the memory unit have recently been made available by General Ceramics Co.

Memory Unit with 256 Information Bits

A whole memory unit was made to operate successfully. It consists of a matrix 16 × 16 lines, i.e., 256 storing cores, driven by two commutator switches of 16 cores each. All the cores were wound with 5 wraps Permalloy 4-79 1/8-mil thick, 1/8-inch high on 3/16-inch ceramic spools. These cores were mounted between two perforated bakelite sheets, as shown in Figure 9. Single-turn windings were made by

threading a wire in and out alternately through the holes of the plate. The reading winding was wound so as to link the cores according to polarities in a checkerboard pattern. The commutator switches were wound with two-turn windings for the P coils and $(4-1)2=6$ turns for the N windings. Eight turns were used for restoring and for the driving windings.

At first, the unit was tested by sending appropriate trains of pulses to the binary address channels selected through manual switches and to the commutator restoring windings. Typical output voltage pulses from the selected core, obtained from the reading winding, showed that the ratio of wanted to unwanted signal at the appropriate strobing

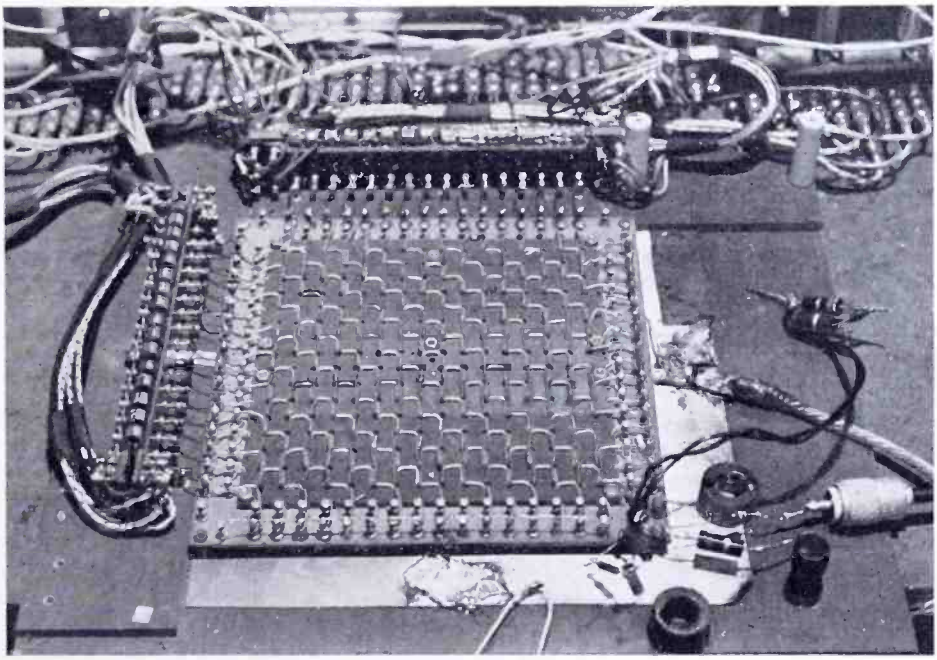

Fig. 9—Operating unit—Permalloy cores.

instant was higher than for a similar ratio obtained on a single core by itself. This is due to the cancellation effects of the checkerboard reading winding mentioned previously. Considerable variations of pulses from core to core were observed, so that one strobing instant, necessarily the same for all, had to be chosen so as to optimize the signals from the cores with extreme properties.

A circuit was built to scan through the elements of the memory unit. Figure 10 shows the experimental circuit setup. The reading circuit was connected to appropriate restoring circuits so as to read non-destructively. The results of the read-out were displayed on a cathode-ray tube whose horizontal and vertical deflections were in proportion to the binary ordinal numbers of the matrix lines. The beam was keyed

by the reading circuit. In order to introduce any arbitrarily chosen pattern of information into the memory system, it was found convenient to use a manual setting as follows: At first all cores are magnetized in direction N. A metallic wire probe is inserted in any core which it is desired to magnetize in direction P. The signal between the probe and a metal plate backing the matrix is introduced into the reading restoring circuit so as to inhibit restoration. When the scanning circuit excites the selected core, it is left in state P instead of being restored to N because of the inhibiting pulse from the probe. Figure 11 shows a pattern of information stored in the magnetic matrix as it appears on the cathode-ray tube.

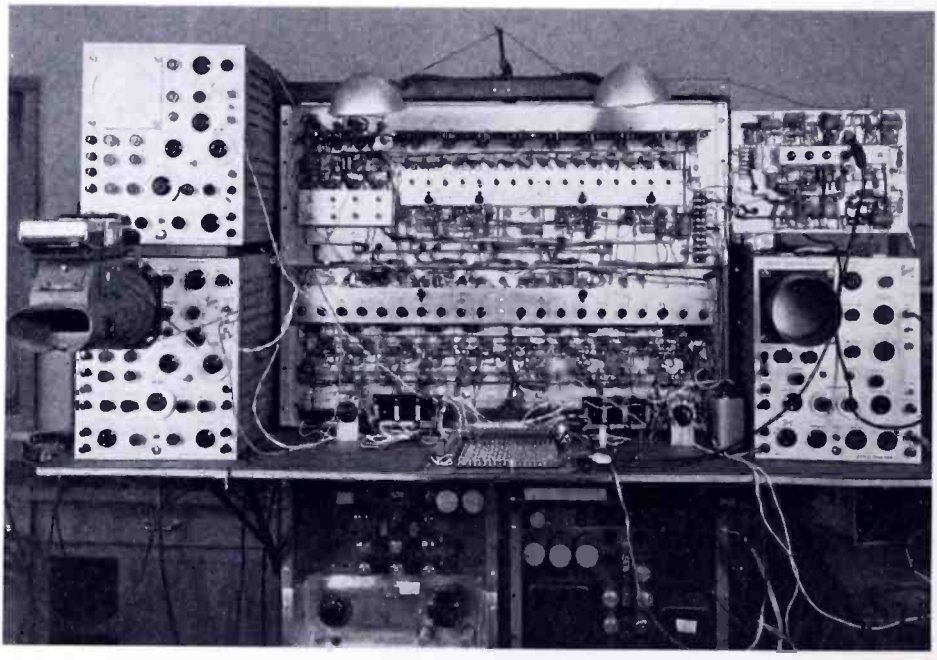

Fig. 10—Experimental circuit setup.

The turn-over time of the cores in this system was from 5 to 8 microseconds, corresponding to an access time of 15 to 24 microseconds, since a 3-step schedule was used.

About .45 ampere turn is required to turn over a core in the matrix. The commutator switch has two turns in each P winding (6 turns on the N winding). About 250 milliamperes are required in the selecting lines of the commutator.

Conclusions

Theoretical considerations, confirmed by early experiments, indicate that magnetic cores are inherently suitable building blocks for a memory system with ideal properties. Two natural states of remanent

magnetization provide indefinite storage without the use of external holding power, and nonlinear properties allow multi-coincident switching. These properties allow great simplicity in construction and extreme reliability in operation.

An operative memory system has been built, and although its storage capacity of 256 information bits is rather modest, it demonstrates the principles of switching and operating schedules applicable to systems of any capacity. A natural extension of present-day techniques should be sufficient to obtain capacities in the thousands or tens of thousands.

The recent development of ferrospinel magnetic materials with rectangular hysteresis loops opens possibilities of reducing the access time by a factor of ten (i.e., 2 or 3 microseconds). Also, it is possible to visualize a reduction of the cost of these cores to a fraction of a cent.

Consequently, it is probable that in the more distant future it will be feasible to build extremely reliable and simple memory units with

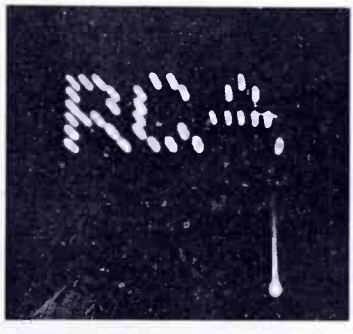

Fig. 11—Cathode-ray-tube display.

capacities of millions of bits of information, with access times of a few microseconds. This will require, of course, a great effort in the development of both the system and the materials. These possibilities may be viewed in the same light as those offered by the transistors; both are due to solid state devices invading the field of electronics, hitherto dominated by vacuum tubes.

ACKNOWLEDGMENTS

Many members of the RCA Laboratories, in particular M. Rosenberg, contributed to the project. It was greatly facilitated by the assistance of Lars Person, American-Scandinavian trainee at the Laboratories. It was possible due to the constant supervising interests of V. K. Zworykin.

It was facilitated by information on materials received from the M.I.T. Group and, in particular, W. N. Papian. Indispensable assistance was received from material suppliers, in particular Allegheny Ludlum Steel Co.; Armco, Magnetics, Inc.; and General Ceramics Co.

A 7000-MEGACYCLE DEVELOPMENTAL MAGNETRON FOR FREQUENCY MODULATION*

By

H. K. JENNY

Tube Department, RCA Victor Division,
Harrison, N. J.

Summary—A developmental magnetron designed primarily for use in 7000-megacycle microwave relay systems is described. This tunable continuous-wave magnetron delivers a power output of 10 watts and is capable of handling frequency deviations up to 16 megacycles without amplitude modulation. Circuit elements included within the tube are discussed, and equivalent circuits are presented which facilitate determination of tuning and modulation curves. Performance data is included to show the effects of applied voltages, magnetic fields, and tuner setting on power output, efficiency, frequency, and modulation.

INTRODUCTION

THE use of magnetrons in microwave relay systems has been limited, to date, because such tubes generally are not designed to be used for frequency modulation. This article describes a developmental tunable continuous-wave magnetron designed for frequency-modulation (FM) service in applications requiring power outputs of up to ten watts. This FM magnetron, shown in Figure 1, operates in the region from 6575 to 6875 megacycles and can handle frequency deviations up to 16 megacycles, at rates up to 5 megacycles, without resulting amplitude modulation. The frequency-modulator system incorporated in the tube accomplishes both modulation and frequency stabilization of the output signal. This tube can be used in systems requiring amplitude modulation, frequency modulation, or phase modulation, and allows additional frequency control for stabilization. It has been designed to replace the lower-output tubes now in general use, thereby increasing the range and reliability of transmitted signals.

Besides having frequency-modulation characteristics, tubes designed for use in fixed transmitter and relay equipment must also contribute to low investment and maintenance costs for the over-all system. A tube contributes to reduced costs when it operates with good efficiency and at low voltage, when it has reasonably long life, and when replacement is relatively easy. The efficiency of the develop-

* Decimal Classification: R355.912.11.

mental FM magnetron is approximately 30 to 40 per cent, as compared with efficiencies of less than 10 per cent for commercially available klystrons and traveling-wave tubes having comparable power-output ratings. The magnetron operates at a voltage of 550 volts, or about half the voltage required for klystrons or traveling-wave tubes. The cathode of the magnetron is operated at a low current density, 0.150 ampere per square centimeter, to assure long life. Tube replacement costs are minimized by incorporating the magnet and tuner mechanisms

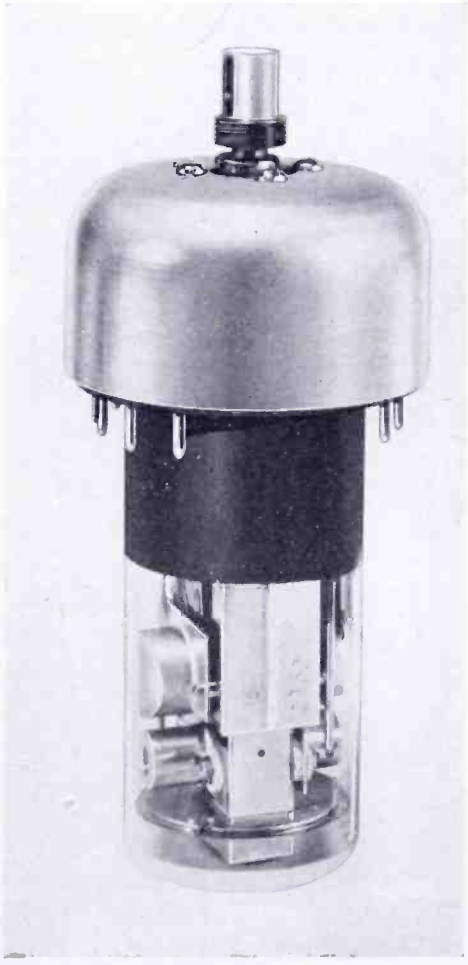

Fig. 1—Developmental tunable continuous-wave magnetron.

in the associated equipment and designing the tube to plug into the equipment as a conventional tube plugs into a socket. Figure 2 shows the tube inserted into a socket which is mounted with the permanent magnet in the equipment. The tuner may be screwed on after the tube is inserted, or, if desired, may be mounted and adjusted before the tube is inserted into the equipment.

Design Considerations

A tunable magnetron for frequency-modulation operation includes many circuit elements. Such a tube acts as an oscillator-buffer-modulator requiring a low-frequency signal at the input terminals and an antenna at the output terminals. In the developmental FM magnetron, all parts of the tube except the magnetron cathode, the modulation guns, and the tuning plunger are incorporated in one subassembly which can be varied during manufacture to cover different frequency bands. The tube consists of three major parts enclosed in a single evacuated envelope: the magnetron system; the tuning-cavity system; and the modulator system.

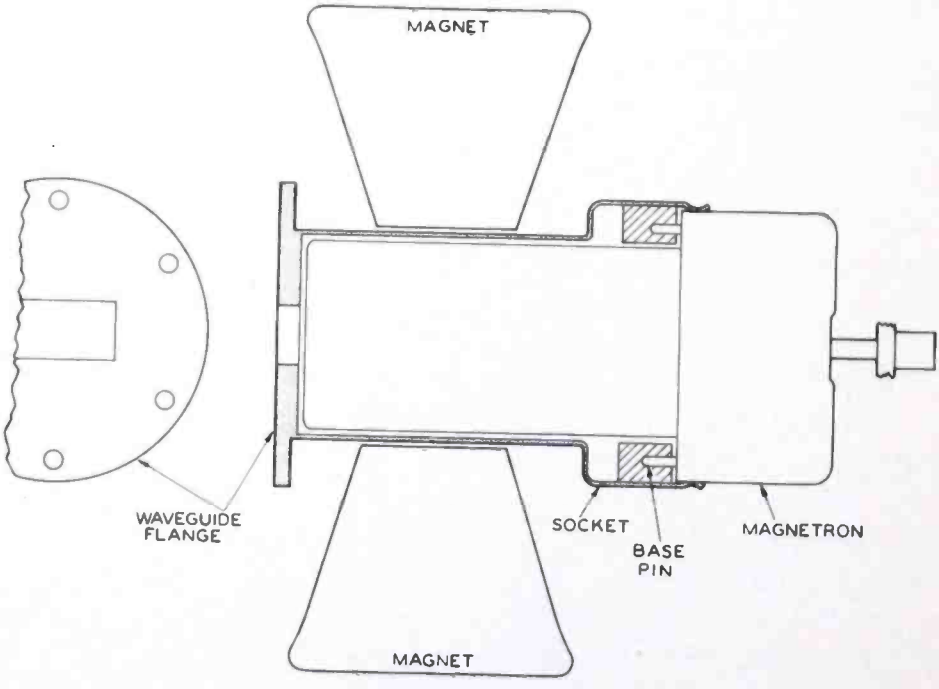

Fig. 2—Plug-in-type socket for the magnetron. This socket is mounted with a permanent magnet in the equipment.

A. Magnetron System

The magnetron is a 24-vane double-strapped system. The high number of vanes allows operation at low voltage and low current density. As mentioned previously, this tube operates at a voltage of 550 volts and a current density of 150 milliamperes per square centimeter, and delivers a power output of 10 watts with efficiencies of 30 to 40 per cent. Operational data for the magnetron system will be discussed later.

B. Coupled Tuning-Cavity System

Mechanical tuning of this developmental FM magnetron is accomplished by changing the dimensions of a separate tuning cavity which is coupled closely to the magnetron system and is incorporated in the same evacuated envelope.

The technique used to achieve frequency modulation is the spiral-beam method described by Smith and Shulman.[1] The beam, to be applied most efficiently, must interact with a maximum of stored energy. The separate tuning-cavity-to-magnetron coupling is so designed that the cavity stores approximately the same amount of energy as is stored in the magnetron resonant system. The electric field in the cavity is concentrated in the region between the two modulator electrodes through which the modulating beam passes. A modulation

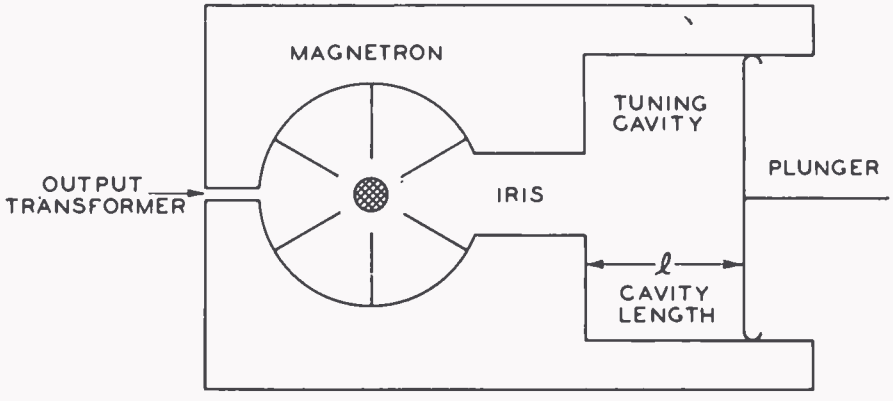

Fig. 3—Equivalent circuit for developmental FM magnetron showing magnetron system with coupled tuning-cavity system.

factor of almost 0.5 can be obtained; i.e., change of resonant frequency in the cavity produces about half as much change in the frequency of the entire resonant system.

The primary objective in the design of the tuning cavity and the coupling element to the magnetron system is to achieve good operation in the correct mode over the required tuning range. A simplified equivalent circuit for the magnetron and tuning-cavity systems is shown in Figure 3. The magnetron system is coupled closely through an iris to a ridge-type wave guide tuning cavity a half wave length long. As mentioned above, field concentration exists in the center of the cavity, where the electric field is at a maximum. One end of the cavity is short-circuited by a choke-type noncontacting movable

[1] L. P. Smith and C. I. Shulman, "Frequency Modulation and Control by Electron Beams," *Proc. I.R.E.*, Vol. 35, pp. 644-657, July, 1947.

plunger which allows tuning over the required frequency range. No losses are assumed in the equivalent circuit because losses have little effect in determining the frequency. The accuracy of the equivalent circuit shown in Figure 3 is limited; it is best close to the resonant frequency of the magnetron system alone.

1. Tuning Curves—The condition for resonance of the entire system shown in Figure 3 is $b_m + b_i + b_c = 0$, where b_m is the magnetron susceptance, b_i is the iris susceptance, and b_c is the cavity susceptance. Figure 4 shows the susceptance of the magnetron, the iris, and the cavity, as computed from the equivalent circuits. The magnetron susceptance b_m, in mhos, is equal to

$$b_m = \frac{\lambda}{2\pi c\, L_m\, N} \left[\frac{N\left(\frac{\lambda_0}{\lambda}\right)^2 - (N-1)}{1 - \left(\frac{\lambda_0}{\lambda}\right)^2} \right],$$

and

$$\frac{d\, b_m}{d\, \lambda} = -\frac{1}{2\pi c\, L_m\, N \left[1 - \left(\frac{\lambda_0}{\lambda}\right)^2\right]^2} \left[N\left(\frac{\lambda_0}{\lambda}\right)^4 + (3-2N)\left(\frac{\lambda_0}{\lambda}\right)^2 + (N-1) \right],$$

where N = the number of cavities in the magnetron,

λ = the operating wave length in centimeters,

λ_0 = the magnetron resonant wave length in centimeters $= 2\pi c \sqrt{L_m\, C_m}$,

C_m = the capacitance of a single magnetron cavity in farads,

L_m = the inductance of a single magnetron cavity in henries,

c = the velocity of light in centimeters per second.

The iris susceptance b_i, in mhos, is equal to

$$b_i = \sqrt{\frac{C_i}{L_i}} \frac{\lambda}{\lambda_i} \left[\left(\frac{\lambda_i}{\lambda}\right)^2 - 1 \right],$$

and

$$\frac{db_i}{d\lambda} = -\sqrt{\frac{C_i}{L_i}}\frac{1}{\lambda_i}\left[\left(\frac{\lambda_i}{\lambda}\right)^2 + 1\right],$$

where C_i = the iris capacitance in farads,

L_i = the iris inductance in henries,

λ_i = the resonant wave length of the iris in centimeters $= 2\pi c\sqrt{L_i C_i}$.

The cavity susceptance b_c, in mhos, is equal to

$$b_c = \frac{1}{377}\frac{w}{a}\frac{\lambda}{\lambda_g}\cot\frac{2\pi l}{\lambda_g},$$

and

$$\frac{db_c}{d\lambda} = \frac{w}{377a\lambda}\left[\left(\frac{\lambda_g}{\lambda} - \frac{\lambda}{\lambda_g}\right)\left(\cot\frac{2\pi l}{\lambda_g}\right) - \left(\frac{2\pi l}{\lambda}\operatorname{cosec}^2\frac{2\pi l}{\lambda_g}\right)\right],$$

where w = ridge spacing in the cavity in centimeters,

a = ridge height in centimeters,

λ_g = guide wave length in centimeters,

l = cavity length in centimeters.

When the susceptance values have been determined either by calculation or by measurement, the tuning curves can be computed. Figure 5 shows the graphical solution of the resonance equation for one position of the tuning plunger. It is apparent that there are three possible π modes, in addition to other tube modes which are spaced farther away and can be neglected in this analysis. Figure 6 shows the tuning curve plotted as a function of the cavity length. The method of graphical solution demonstrated in Figures 5 and 6 makes possible the determination of a tuning curve with desired tuning rate (i.e., ratio of frequency change to change in plunger position or cavity length), linearity, and separation from the adjacent modes.

Because of the modulator electrodes incorporated in the tuning cavity, the best mode of operation for this FM magnetron is the one giving the magnetron resonant frequency when the tuning plunger is half a wave length from the iris. This mode is called the main mode, therefore, and the two adjacent π modes are called the upper and

lower modes. Although a new π mode is obtained for every movement of the tuning plunger of approximately half a wave length, these modes are not pertinent to the analysis and will not be discussed.

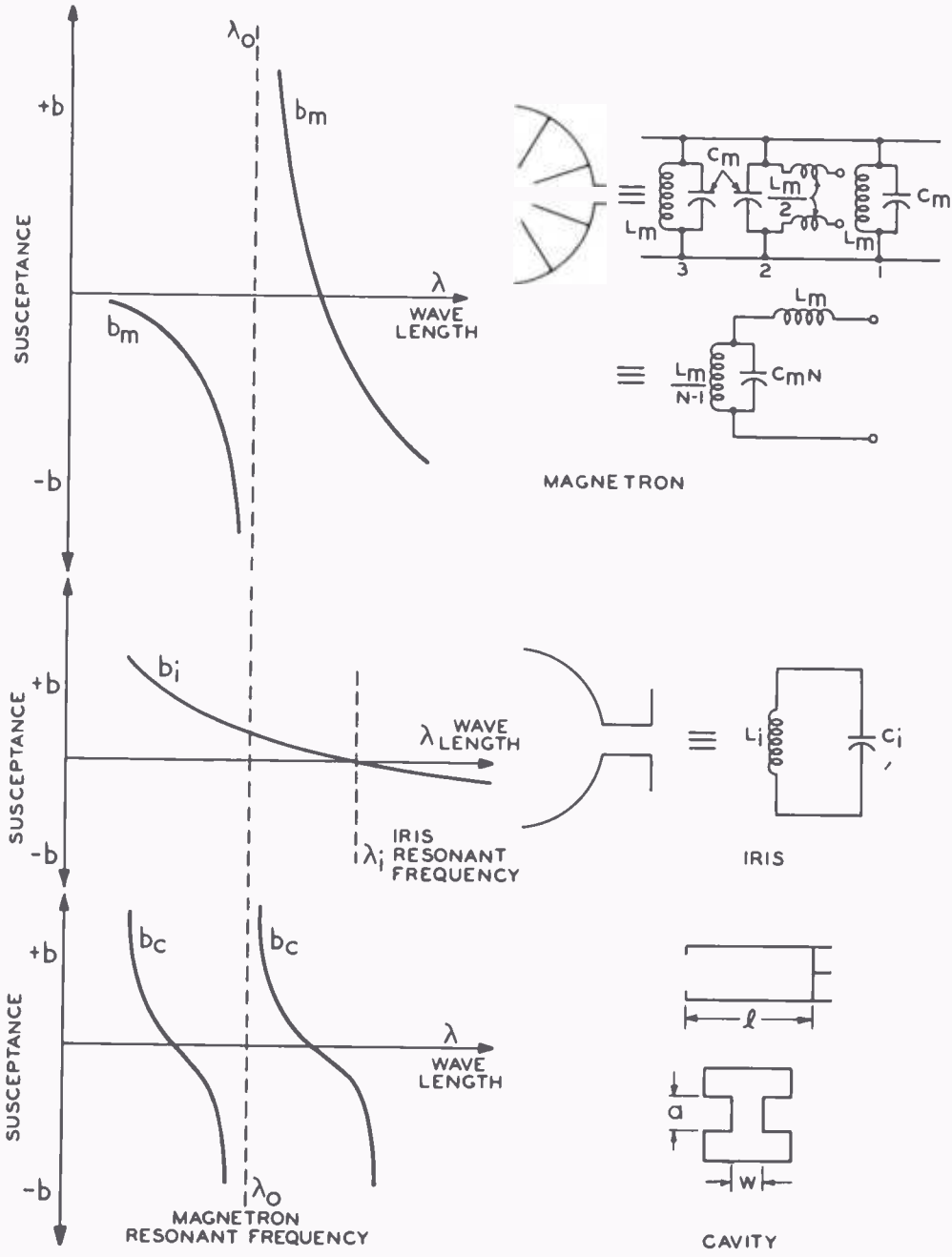

Fig. 4—Curves showing magnetron susceptance at iris opening, iris susceptance, and cavity susceptance.

The tuning curve is influenced by both the length and the inductance-capacitance ratio of the coupling iris. For constant magnetron

and cavity geometries, the longest slot length tends to bring the lower mode very close to the main mode, while the shortest length brings the upper mode very close to the main mode. An intermediate length which spaces the upper and lower modes evenly about the main mode is desirable for stable operation.

A high ratio of inductance to capacitance in the iris, or no iris at all, reduces the tuning rate sharply at wave lengths below the magnetron resonant wave length, λ_0. A very low ratio of inductance to capacitance, on the other hand, reduces the tuning rate at wave lengths above the magnetron resonance point. An optimum value between these extremes can be found which gives a fairly linear tuning curve.

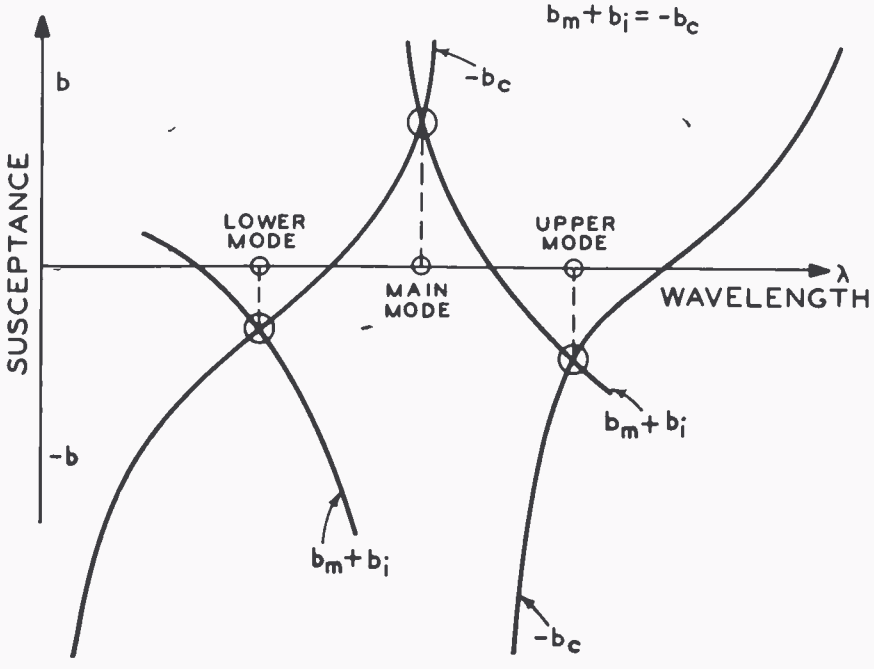

Fig. 5—Curves showing resonant frequencies for one position of the tuning plunger.

2. Mode Selection—The determination of the mode in which the tube will oscillate involves such factors as the ratio of the stored energy in the magnetron, iris, and cavity to the stored energy in the magnetron alone, losses in the circuits, power or energy coupled out of the tube, direct-current operating voltages, and the effects of the magnetron space charge. The mode of operation may be closely approximated, however, from consideration of only the first two of these factors.

The ratio of the stored energy in the magnetron, iris, and cavity to the stored energy in the magnetron alone may be defined as stabiliza-

tion factor, S. If this stored-energy ratio were the only consideration, the tube would tend to oscillate in the mode having the lowest stabilization factor. It is desirable, therefore, to be able to compute the stabilization factor for the desired mode, as well as for its adjacent modes, in order to evaluate possible tuning range.

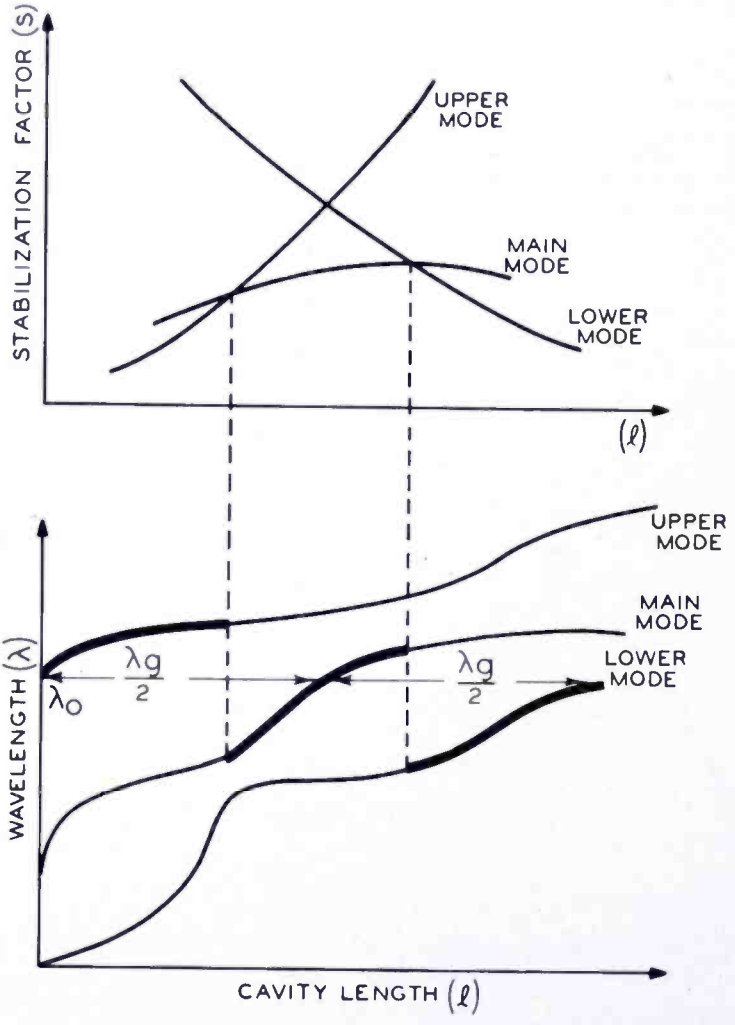

Fig. 6—Tuning curves plotted as a function of cavity length. Stabilization factors for the three π modes are shown in the curves at the top of the figure.

The computation of the stabilization factor may be demonstrated by consideration of a simple parallel resonant circuit. If L is the circuit inductance and C the circuit capacitance, then the circuit susceptance, b, is equal to

$$b = \frac{2\pi cC}{\lambda} - \frac{\lambda}{2\pi cL}.$$

and

$$\frac{db}{d\lambda} = -\frac{2\pi cC}{\lambda^2} - \frac{1}{2\pi cL}.$$

From these two equations, we can find the values of C and L:

$$C = \frac{\lambda}{4\pi c}\left[b - \lambda\left(\frac{db}{d\lambda}\right)\right],$$

$$L = -\frac{\lambda}{\pi c}\left[\frac{1}{b + \lambda\left(\frac{db}{d\lambda}\right)}\right].$$

The stored energy, E_{ST}, in the circuit is given by

$$E_{ST} = \frac{1}{2}V^2C = \frac{1}{8}V^2\frac{\lambda}{\pi c}\left[\lambda\left(\frac{db}{d\lambda}\right) - b\right].$$

The stabilization factor for the entire system can now be expressed as

$$S = 1 + \frac{\lambda\left[\left(\frac{db_c}{d\lambda}\right) + \left(\frac{db_i}{d\lambda}\right)\right] - [b_c + b_i]}{\lambda\left(\frac{db_m}{d\lambda}\right) - b_m}.$$

This equation is valid for all values of frequency represented by the equivalent circuit except that at which the frequency of the entire system is equal to the magnetron resonant frequency; at this frequency, the susceptance values b_m and b_c are infinite.

When the frequency of the entire system is equal to the magnetron resonant frequency, it is of advantage to use reactance values instead of susceptance values to compute the stabilization factor. At the magnetron resonant wave length λ_0, where the susceptance of the entire system becomes infinity, the reactance is equal to zero. The reactance of a series circuit is

$$X = \frac{2\pi cL}{\lambda} - \frac{\lambda}{2\pi cC},$$

and

$$\frac{dX}{d\lambda} = -\frac{2\pi cL}{\lambda^2} - \frac{1}{2\pi cC}.$$

From these two equations, we can find the value of L:

$$L = \frac{\lambda}{4\pi c}\left[X - \lambda\left(\frac{dX}{d\lambda}\right)\right].$$

Thus, when the frequency of the entire system is equal to the magnetron resonant frequency, the stored energy is

$$E_{ST}{}_{(\lambda=\lambda_0)} = \frac{1}{2} I^2 L = \frac{1}{8} I^2 \frac{\lambda_0{}^2}{\pi c}\left(\frac{dX}{d\lambda}\right),$$

and the stabilization factor of the system is

$$S_{(\lambda=\lambda_0)} = 1 + \frac{\dfrac{dX_c}{d\lambda}}{\dfrac{dX_m}{d\lambda}}.$$

The values of dX_c and dX_m at the magnetron resonant frequency are

$$\frac{dX_c}{d\lambda} = -\frac{w}{377a}\frac{\pi}{\lambda_0}\left(\frac{\lambda_g}{\lambda_0}\right)^3,$$

$$\frac{dX_m}{d\lambda} = -\frac{N}{\pi c C_m}.$$

A method of computing or measuring stabilization factors has now been established for all the π modes through the use of susceptance and reactance values and their derivatives. This method is also applicable to equivalent circuits which are much more complex, provided the susceptance values can be obtained analytically or experimentally.

Figure 6 (top) shows a curve of stabilization factors as a function of cavity length for the three π modes. The mode most likely to be excited for a given cavity length, that is, the one having the lowest stabilization factor, is marked on the tuning curve.

As mentioned previously, tube operation in the main mode is desired with a plunger distance of half a wave length from the coupling iris, to accommodate the modulator electrodes. Figure 6 (bottom) shows that, when the plunger is gradually moved out from the coupling slot, the upper mode is most likely to be excited up to the point where its stabilization-factor curve intersects with the curve of the main mode. At the point of intersection, operation jumps to the main mode and continues there until the stabilization factor of the lower mode becomes smaller than that of the main mode. As the plunger is moved farther out, operation will jump to a lower tube mode every time a distance of half a wave length has been traveled.

In actual operation, the point at which mode jump occurs varies

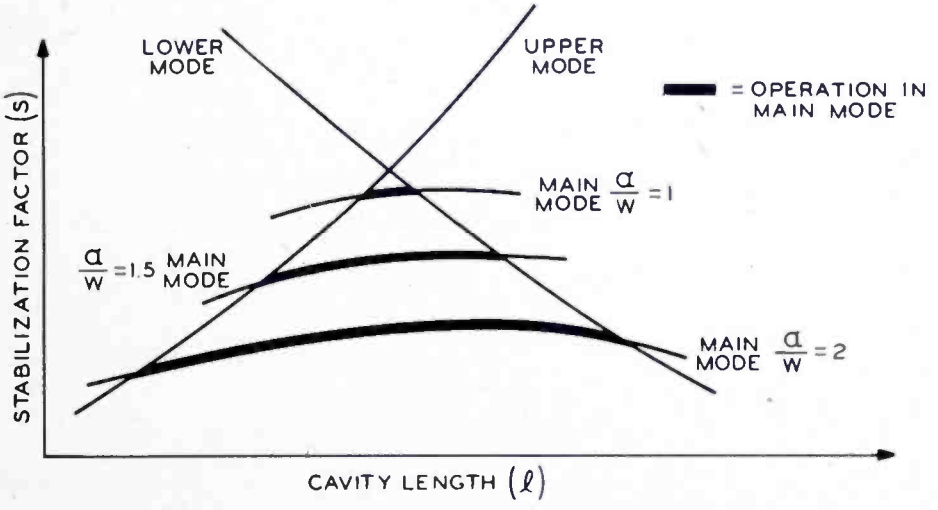

Fig. 7—Curves showing the influence of tuning-cavity parameters on stabilization factors of the three π modes.

according to a hysteresis effect. When tuning is varied continuously in one direction, oscillation in a given mode will continue over a wider range of plunger positions than if the oscillator were started at these positions, even though another mode has a lower stabilization factor.

The influence of cavity parameters on the stabilization factors is shown in Figure 7. The curves illustrate the effects of three different ratios of ridge height, a, to ridge spacing, w. An increase in the ratio of a to w increases the stabilization factor of the main mode and usually decreases the obtainable tuning range of this mode.

C. Tube Modulator System

As mentioned previously, frequency modulation in this developmental magnetron is accomplished by modulation guns enclosed in the same evacuated envelope as the magnetron system and the tuning-

cavity system. The technique used to achieve frequency modulation is the spiral-beam method.[1]

1. Spiral Beam—When a spiral beam is used to achieve frequency modulation, the beam is shot through the capacitive section of a resonant circuit and a magnetic field having the same direction as the beam is applied. The beam then introduces both resistive and reactive components across the capacitance. The values of resistance and reactance introduced are dependent mainly upon beam current, beam velocity, and magnetic field for a given geometry. The electron admittance y_e, in mhos, is equal to

$$y_e = g_e + j\,b_e = \frac{h^2}{4d^2}\,\frac{I_0}{V_0}\left[\frac{1-\cos\theta}{\theta^2} + j\,\frac{\theta-\sin\theta}{\theta^2}\right]$$

where g_e = electron conductance in mhos,

b_e = electron susceptance in mhos,

h = length of space in which the radio-frequency (r-f) field acts on electrons, in centimeters,

d = modulator electrode spacing in centimeters,

I_0 = beam current in amperes,

V_0 = beam voltage in volts,

$\theta = (\omega_c - \omega)\,\lambda T$ = transit angle in radians,

T = electron transit time through h, in seconds,

$\omega_c = \mathrm{H}\dfrac{e}{m}$ = angular frequency of rotation in cycles per second,

ω = angular high frequency in cycles per second,

H = magnetic field in gausses.

A graphical presentation of the above expression with the admittance values plotted as a function of the transit angle θ is shown in Figure 8.

The maximum frequency deviation possible with zero resistive component or zero amplitude modulation occurs when the transit angle θ is equal to $\pm 2\pi$; the value of the maximum deviation is

$$\Delta f_{\text{cavity}} = \mp\,\frac{h^2}{16\pi d^2}\,\frac{I_0}{V_0}\,\frac{1}{2\pi C_0},$$

where C_0 is the total capacitance of the cavity.

The frequency deviation of the magnetron–cavity combination (Δf_{system}) is given by the product of the deviation of the cavity alone (Δf_{cavity}), as given above, and the tuning rate (TR):

$$\Delta f_{system} = TR\, \Delta f_{cavity}\,.$$

The tuning rate at the resonant frequency of the magnetron system can be determined from the equations given previously to be

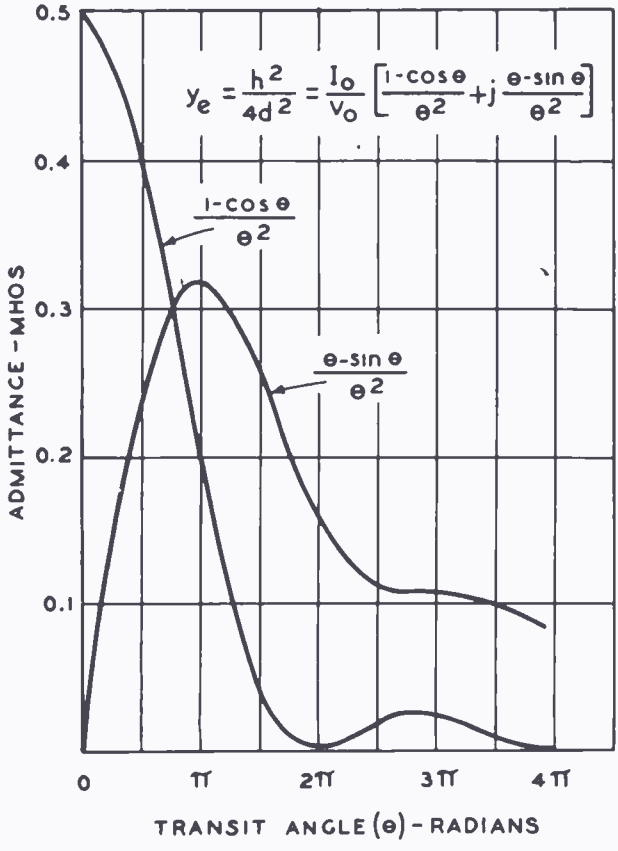

Fig. 8—Curves showing electron admittance as a function of transit angle θ.

$$TR_{(\lambda=\lambda_0)} = \frac{1}{1 + \dfrac{\dfrac{dXm}{d\lambda}}{\dfrac{dXc}{d\lambda}}}\,.$$

2. Physical Configuration of the Modulator System—A diagram of the modulator system of the developmental FM magnetron is shown

in Figure 9. A shield (1) is set into the ridge-type tuning-cavity wall to allow mounting of the two modulator guns. The guns are mounted opposite each other in front of the magnetic pole pieces. Focusing of the beam is accomplished mainly by the large magnetic field. Each gun is a tetrode-type system with an oxide-coated cathode used as emitter. In front of the cathode is a negative aperture-type control grid which permits modulation control without requiring any driving power. The control grid is followed by an accelerating grid which operates at 300 volts and determines the magnitude of the beam current. Shield 1 and the structure beyond it are maintained at a low potential in order to permit adequate frequency deviation. The voltage of this portion of the structure is referred to as the beam voltage.

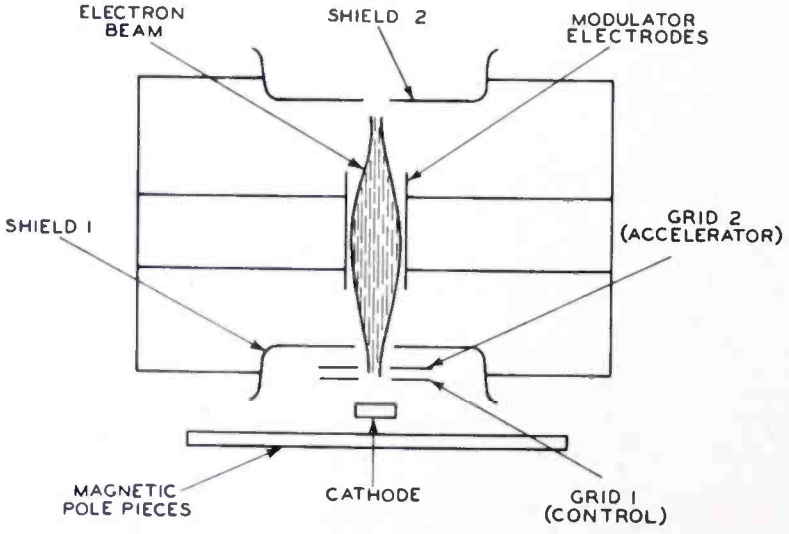

Fig. 9—Diagram of the modulator system.

When the beam enters the r-f field region between the modulator electrodes, it expands until it reaches the center of the electrodes, picking up energy from the field. In the second half of the region, the beam contracts and leaves the r-f field with the same shape and velocity it had upon entering the field. The beam has stored energy for a time, acting as a pure reactance, but the energy taken from the field is all returned. The beam current is then collected on the opposite shield (2). The driving power required for modulation is determined only by the grid input capacitance, which in this tube is 8 micromicrofarads.

Operational Data

A. *Magnetron Performance*

Figure 10 shows the performance chart for this developmental FM

magnetron with magnetic field strength as the parameter. In operation, the field strength of the magnet is determined by modulation considerations so that the spiral beam modulator is operated at the points of least amplitude modulation ($\theta = \pm 2\pi$). The curve of magnetic field strength chosen for this tube is marked on the performance chart.

The power output of this tube is approximately 10 watts at 550 volts, 50 milliamperes, and efficiency of about 35 per cent. At these operating conditions, the cathode current density is 150 milliamperes per square centimeter. Both nickel-mesh and matrix-type oxide-coated cathodes have been used with good results. Life-test results on

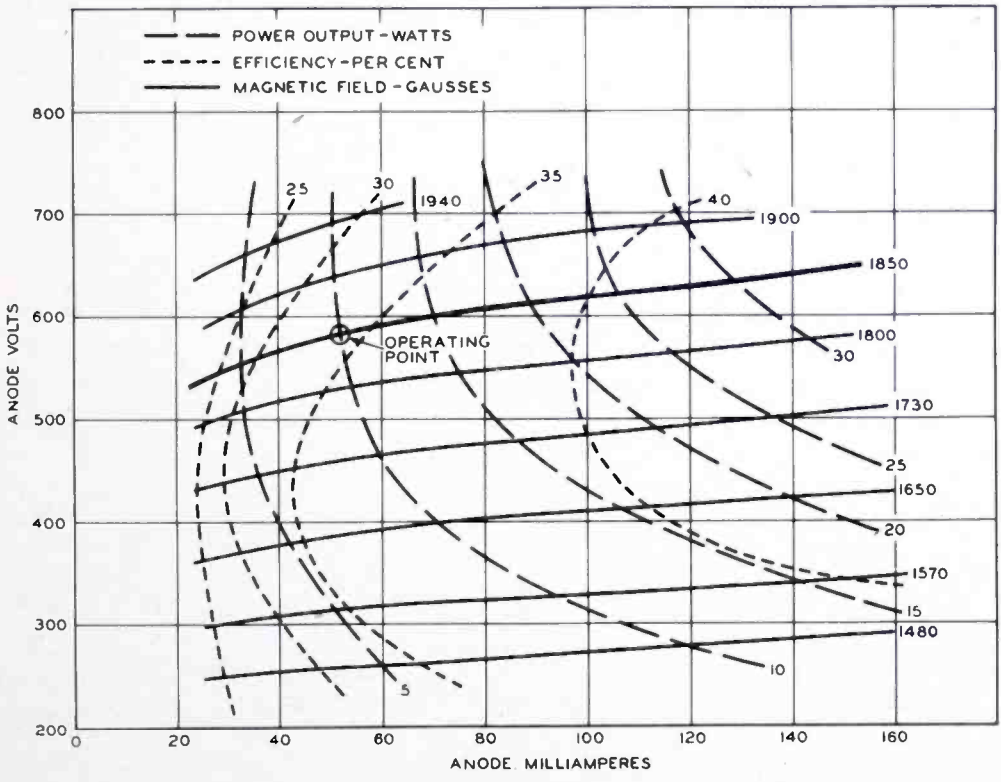

Fig. 10—Performance chart for the developmental FM magnetron with magnetic field strength as the parameter.

developmental tubes have been satisfactory to more than 5000 hours, with a few tubes operating more than 7000 hours. Poorer tubes having a life of only a few hundred to a few thousand hours also were encountered, but it is evident that careful quality control during production will result in a long-life tube.

The Rieke diagram taken at the operating point, which is shown in Figure 11, shows power output and frequency as a function of tube loading. Figure 12 shows frequency and power output plotted as a

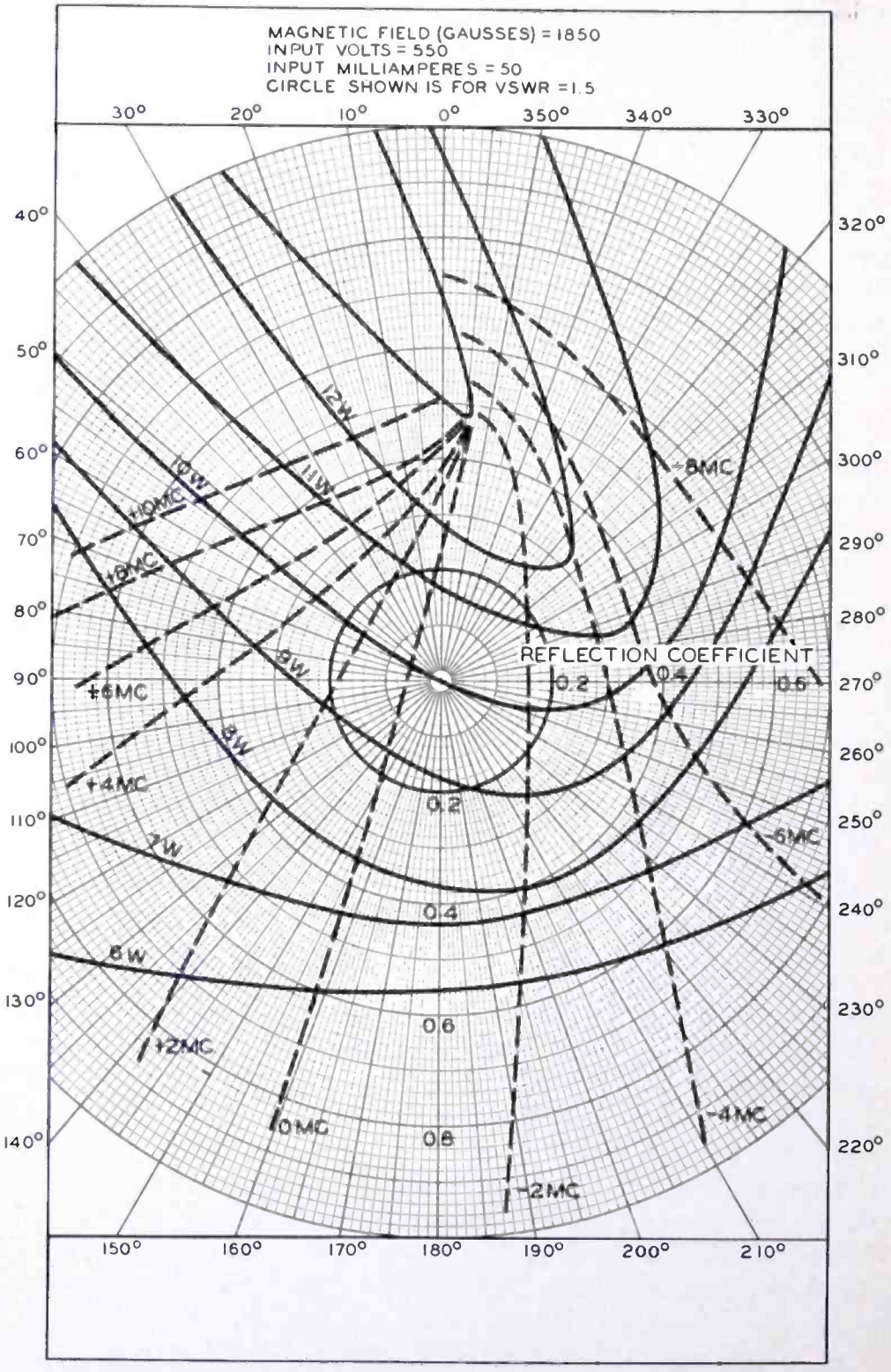

Fig. 11—Rieke diagram for the developmental FM magnetron, taken at the operating point.

function of cavity length for mechanical tuning. For the microwave application for which this tube was designed, a tuning range of 300 megacycles is required. The loading of this tube is such that the output power is practically constant over this 4.5-per-cent tuning range. Coverage of adjacent bands with this magnetron is possible with a change of only one subassembly during manufacture.

B. Modulator Performance

Experimental modulation curves for this tube are shown in Figure

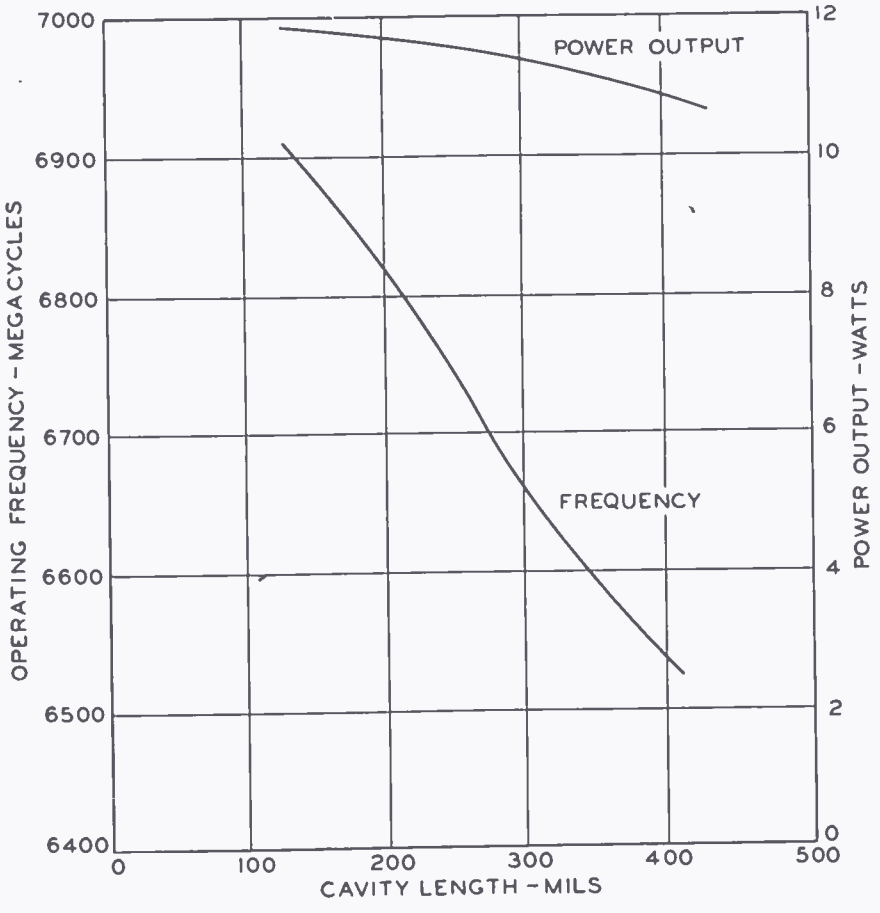

Fig. 12—Curves showing frequency and power output as a function of cavity length.

13. The energy-storing component is plotted directly as frequency deviation of the tube in megacycles per milliampere, and the energy-absorbing component is shown as amplitude modulation in per cent. For practical tube operation, only the magnetic field yielding best frequency modulation and no additional amplitude modulation is applied. Because low magnetron plate voltage is desired, a transit angle

θ equal to -2π was chosen for operation. With this angle, frequency modulation is one-half of the maximum obtainable deviation, which occurs when the transit angle θ is equal to $\pm\pi$ and brings about appreciable amplitude modulation. If the modulator is driven from cutoff to a certain beam current for special applications, the frequency increases with increasing modulator current. If a decrease in frequency is required, the magnetic field is adjusted to make the transit angle θ equal to $+2\pi$. The results shown in Figure 13 were obtained with the beam voltage equal to 45 volts and an accelerator voltage of 300 volts.

Frequency deviation is a function of the ratio of accelerator voltage to beam voltage. Usually a high total frequency deviation is required

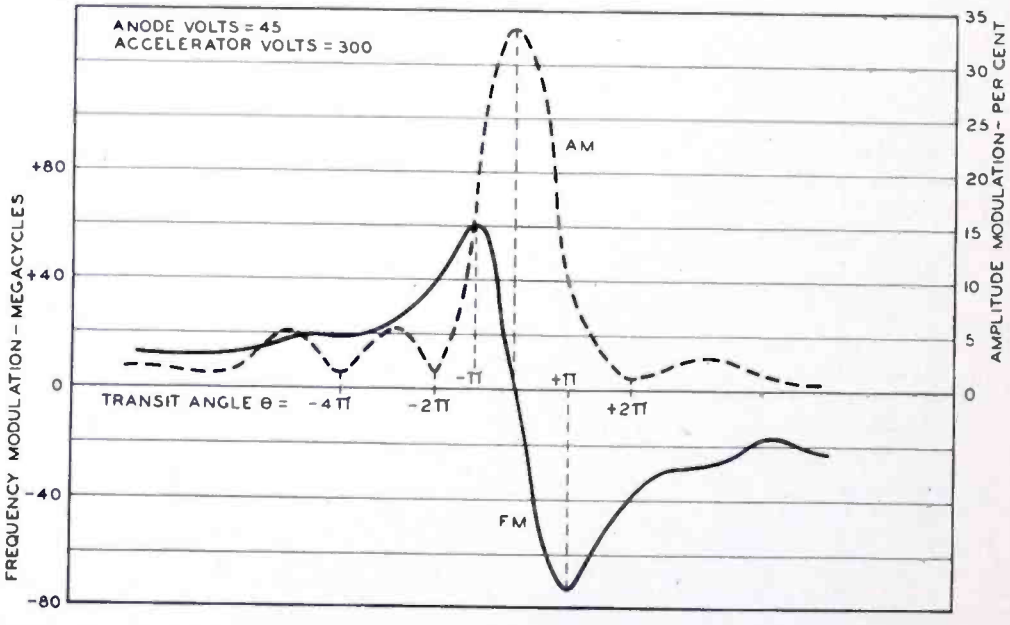

Fig. 13—Curves showing amplitude modulation and frequency modulation as a function of the transit angle θ.

rather than a high deviation per unit of beam current. The frequency deviation per unit of beam current increases as the ratio of accelerator voltage to beam voltage increases. The total obtainable current, on the other hand, increases with a decreasing voltage ratio because both emission and focusing improve. The best operating point is the one giving maximum deviation per unit of beam current and enough total current so that the desired deviation is obtained as the control grid is varied from zero bias to cutoff. A deviation of 40 megacycles with some amplitude modulation ($\theta = -\pi$) and of 20 megacycles with no amplitude modulation ($\theta = -2\pi$) may be obtained with an accelerator

voltage of 300 volts and a ratio of accelerator voltage to beam voltage of 6.7.

Figure 14 shows the modulation curves for the two modulator guns in a developmental FM magnetron, with frequency deviation plotted as a function of the negative modulator grid voltage. Two methods of operation of the guns are possible:

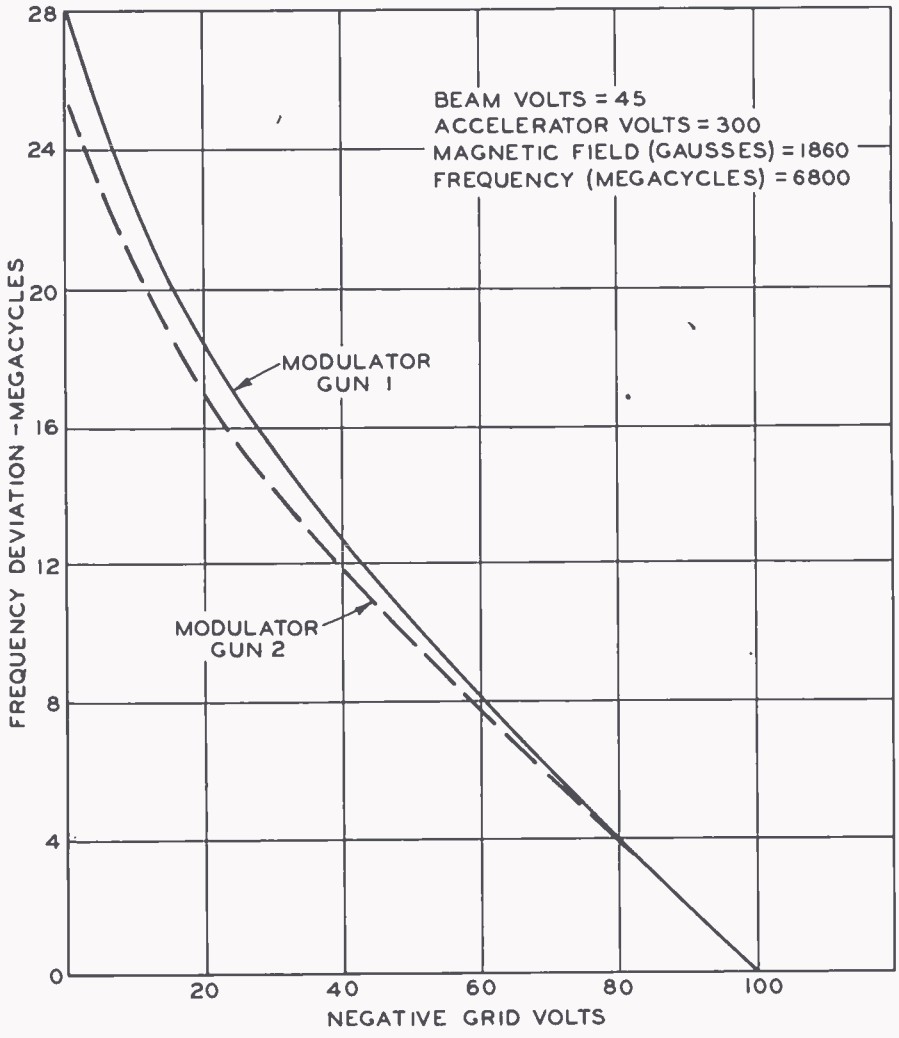

Fig. 14—Curves showing frequency deviation as a function of control-grid voltage for the two modulating guns of a developmental FM magnetron.

a) One gun is operated; the second is inoperative. When the life of the first gun has deteriorated below useful limits, the second gun is switched on and operated.

b) Both guns are operated simultaneously at one-half the operating current of one gun. The lowered cathode current density should increase life.

The recommended method of operation will be determined from life-test results.

This tube is designed to give maximum frequency deviation in the center of the band. In other words, a maximum of stored energy is concentrated between the modulator electrodes. As soon as the tuning plunger is displaced, however, the point of maximum stored energy also is displaced from the center. Thus, the frequency deviation decreases when the tube is tuned to either side of the center point. The allowable decrease in frequency deviation determines the tuning range possible for the tube, because these limits are narrower than the boundaries given by mode jumps. A second limit is given by operation with a fixed magnetic field (permanent magnet) over the tuning range.

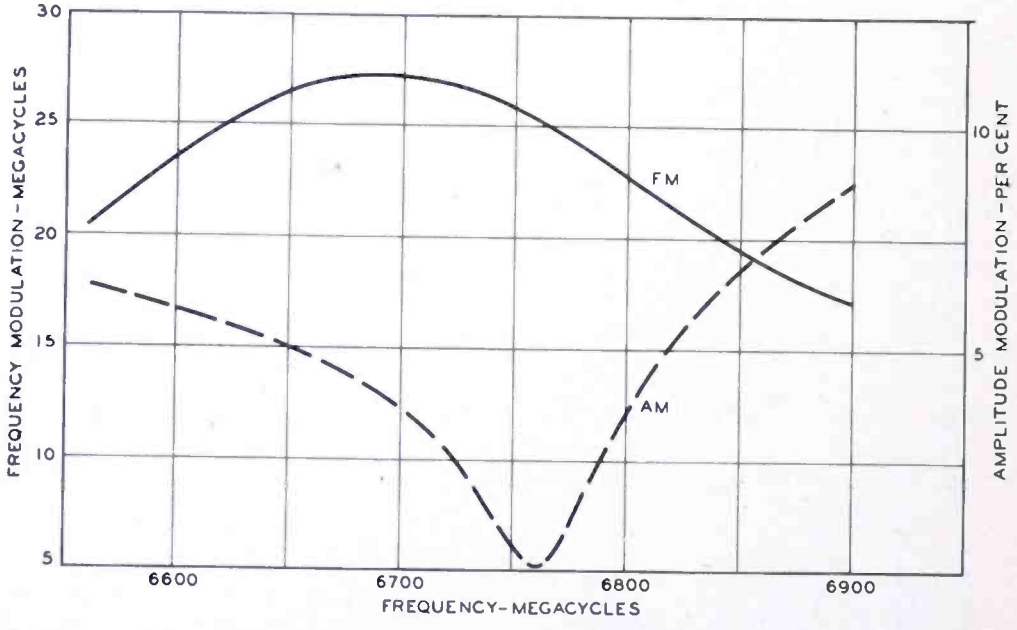

Fig. 15—Curves showing frequency deviation and amplitude modulation as a function of operating frequency.

Because there is only one point at which no amplitude modulation occurs, $(\theta = \pm 2\pi)$, tuning will also introduce a certain amount of amplitude modulation. Figure 15 shows the combined effects of the changes in frequency deviation and in amplitude modulation over the tuning range. Over the desired 4.5-per-cent tuning range, the frequency deviation varies by 25 per cent and amplitude modulation up to 8 per cent is introduced.

C. Miscellaneous

Other data on the performance of the developmental FM magnetron is given below.

Magnetron Pushing Figures	
Current Pushing	0.25 Mc/ma
Voltage Pushing	0.25 Mc/v
Magnetic Field Pushing	0.003 Mc/gauss
Temperature Stability	
Frequency Shift	0.21 Mc/°C
Total Warm-up Drift	6 Mc
Tuning Rate	
Plunger Displacement	1.4 Mc/mil
Modulation Rate	
Negative Grid Voltage	0.4 Mc/v
Magnetic Field	1850 gausses

ACKNOWLEDGMENTS

Acknowledgment is given to B. B. Brown, Manager of the Special Development Group, L. Kovach, Project Engineer, and staff and shop members who contributed much toward the development of the frequency-modulated magnetron.

SOME NEW ULTRA-HIGH-FREQUENCY POWER TUBES*

By

P. T. Smith

Research Department, RCA Laboratories Division,
Princeton, N. J.

Summary—Experimental grounded-grid triodes and grounded-cathode tetrodes with identical cathodes and equivalent grids are described. The triodes may be operated at 900 megacycles with approximately the same power gain and output as at low frequencies. This operation may be obtained with cathode emission densities compatible with long life. The tetrodes under grounded-cathode operation are not as high in power gain, but offer some advantages when high-level modulation is required. Grounded-grid operation of the tetrodes, although not tested, is believed to retain the high-level modulation advantage and improve the power gain. The triode, of course, has the important advantage of a simpler construction.

Introduction

THIS paper presents a study of grid-controlled power-amplifier tubes. Because the specific objective was television transmission between 500 and 900 megacycles, certain performance characteristics had to be attained. Two of the more important of these factors are wide band width and low input-to-output circuit coupling (feedback).

One can relate the power output W, band width $\Delta\omega$, and effective output circuit capacitance C, by

$$W = \frac{K I^2}{\Delta\omega C}.$$

where I is the fundamental component of the plate current. The problems which confront the tube engineer become more apparent if this relation is expressed in terms of $\bar{J}$, the average current density of the peak of the plate current pulse and the effective output capacitance C' per unit area of anode. The capacitance associated with the external circuit and of ineffective portions of the anode must be appropriately absorbed in C'. The above formula then becomes

* Decimal Classification: R334 × R310.

$$W = \frac{K'}{\Delta\omega} \frac{(\bar{J})^2 A}{C'}.$$

It is clear that at low frequencies the current density $\bar{J}$ is ultimately limited by the choice of cathode and the desired life. The grid–anode spacing is determined primarily by space charge considerations and C' can be kept low. However, as the grid–anode transit time is increased the fundamental component of the anode current at high frequencies decreases rapidly.[1] Since C' also decreases with increasing spacing, but less rapidly, there is an optimum grid–anode spacing. While the basic large-signal theory exists,[2,3] it is not in a form which readily allows one to determine this spacing for a given set of conditions. Care and ingenuity must be exercised in order to arrive at the optimum compromise.

The second factor, feedback, if ignored in the tube design, may lead to unnecessary difficulties for the transmitting engineer and loss of power gain. It is important in television transmitters[4] since it gives rise to a serious distortion of the apparent band-pass characteristic of the output circuit. This leads to an appreciable loss of resolution in the picture.

Other grid-controlled tubes have been developed which give good

---

[1] In a triode, the effective fundamental component of the plate current at UHF depends upon 9 parameters; frequency, cathode-to-grid spacing, input radio-frequency voltage, bias, grid turns per inch, grid wire size, plate direct-current voltage, output radio-frequency voltage, and grid-to-anode spacing. In a tetrode there are four more; the screen potential, grid-to-screen spacing, screen grid turns per inch, and wire diameter. As a consequence, no simple description may be expected. The main reduction in the fundamental component with large transit angles in the anode region results from a widening of the current pulse.

[2] Chao-Chen Wang, "Large-Signal High-Frequency Electronics of Thermionic Vacuum Tubes," *Proc. I.R.E.*, Vol. 29, p. 200, April, 1941.

[3] A. D. Sutherland, unpublished work, done as part of his doctorate thesis requirements at the University of Illinois. He is now on active duty with the U. S. Navy; however, he was associated with the author at the RCA Laboratories during part of this program.

[4] The importance of capacitive feedback in a television transmitter was first pointed out to the writer by T. L. Gottier while he was with the RCA Laboratories. His conclusions were later confirmed by L. S. Nergaard. When the familiar

$$\frac{\omega C g_m R_1 R_2}{2}$$

is very much less than 1, the relative distortion of the upper and lower sidebands are given by ± the above expression. C is the plate-to-control-grid capacitance in a grounded-cathode tetrode or plate-to-cathode capacitance of a grounded-grid triode.

ultra-high-frequency (UHF) performance at low-power levels[5-9] and one at a high-power level.[10] The tubes described here yield output power of the order of 5 to 10 kilowatts and the feedback is at least an order of magnitude less than that of earlier tubes.

During the course of this investigation a large number of triodes and tetrodes were built and tested. Since they used identical cathodes and equivalent grids with the same cathode-to-grid spacing, a comparison of their performance is significant. The triodes were operated in a grounded-grid circuit. Between 500 and 600 megacycles they gave approximately the same power output and gain as the grounded-cathode tetrodes. The tetrodes, however, offer advantages if high-level modulation is required. This low power gain of the tetrodes may be attributed to current intercepted by the screen and greater input circuit losses relative to those in the triodes. At 900 megacycles the transit-time loading of the grid circuit of the tetrodes became important and the relative power gain of the triodes was even greater.

A grounded-grid tetrode was considered but the close-spaced triodes, because of their simplicity, seemed better; furthermore, it was established that triodes could be built with a high order of shielding.

The first tubes made in this study had glass-to-metal seals, but the dielectric losses in the glass proved to be a limiting factor. Because of the superior properties of available ceramics, an investigation of the use of silver-soldered ceramics was started. Satisfactory techniques, based on the titanium-hydride method due to R. J. Bondley,* were developed and used in some of the tubes described in this paper.

Consideration of the mechanical and circuit problems involved in a 5- to 10-kilowatt UHF grid-controlled tube leaves little choice but

---

[5] W. G. Wagener, "500-Mc Transmitting Tetrode Design Considerations," *Proc. I.R.E.*, Vol. 36, p. 611, May, 1948.

[6] W. P. Bennett, E. A. Eshbach, C. E. Haller, and W. B. Keyes, "A New 100-Watt Triode for 1000 Megacycles," *Proc. I.R.E.*, Vol. 36, p. 1296, October, 1948.

[7] R. R. Law, W. B. Whalley, and R. P. Stone, "Developmental Television Transmitter for 500-900 Megacycles," *RCA Review*, Vol. 9, p. 643, December, 1948.

[8] C. E. Fay, D. A. S. Hale, and R. J. Kircher, "A 1.5-kw 500-Megacycle Grounded-Grid Triode," *Proc. I.R.E.*, Vol. 39, p. 800, July, 1951.

[9] GE power tetrode for UHF transmitters with ceramic construction, the GL-6019.

[10] W. W. Salisbury, "The Resnatron," *Electronics*, Vol. 19, p. 92, February, 1946.

* General Electric Company, Schenectady, N. Y.

to arrange the electrodes in concentric cylinders. These experimental tubes used a demountable copper gasket seal, which not only facilitated the development of the tubes but also made possible the determination of the effects of small changes in a given structure.

CATHODES

Thoria-on-tantalum cathodes were used. For a given coating thickness the life of this type of cathode is determined almost entirely by the operating temperature. Although the detailed mechanism by which the thoria coating disappears is unknown, experimental data show that the rate of loss increases rapidly with temperature. Nevertheless, commercial tubes have been operated at temperatures which permit electron emission densities in excess of 2 amperes per square centimeter with good life. Tantalum as a base metal allows a cathode which readily meets the structural and circuit requirements of the tubes. However, considerable care is required during processing in order to prevent the formation of a resistive interface.[11] With improperly processed tubes, the effect showed up as a loss in power gain.

The cathode structure used in these tubes was relatively inefficient, since only a small fraction of the radiating surface was available for electron emission. Only this part of the elements was coated with thoria. Both ends of the elements were rigidly mounted and the thermal expansion was taken up by the flexible tab at one end as indicated in Figure 1. Properly mounted test structures could be turned on and off several thousand times without any measurable deformation. Because proper mounting was somewhat critical, it is probable that the same cathode, with one end free and with opposing heating current flow in adjacent elements, would be superior and could also be designed to operate more efficiently.

ANODES

The anodes had only 14.5 square centimeters of surface exposed to electron bombardment. They were capable of dissipating 10 kilo-

[11] This is probably one of the reasons for some of the discrepancies in the experimental data which have appeared in the literature. In fact, it was generally assumed for a long time that thoria could not be used on tantalum for good electron emission. Electrophoretic coatings on tantalum show a marked decrease in emission in comparison with sprayed or painted cathodes and have a visible interface. Also, a minute trace of tantalum oxide mixed in with the thoria coating severely poisons the cathode. Although a large amount of oxygen can be taken up by tantalum without the formation of an oxide, too rapid breakdown of the cathode apparently does form an oxide layer.

watts with water cooling because of an efficient system of water channels which greatly increased the water-to-metal surface. A flow of 1.5 gallons per minute was attained with about 50 pounds per square inch pressure in a series channel arrangement. A multiplicity of other designs, which may be operated at lower pressures and greater flow, are also possible using parallel channels. The proper design may be chosen to meet the cooling systems requirements of the transmitting engineers. The important factor, according to these experiences, is the fact that the speed of flow in the channels must be well above the Reynold's number necessary for turbulent flow.

TETRODES

A number of experimental tetrodes were built and tested. A typical tube is shown in cross section in Figure 2. This tube used the cathode,

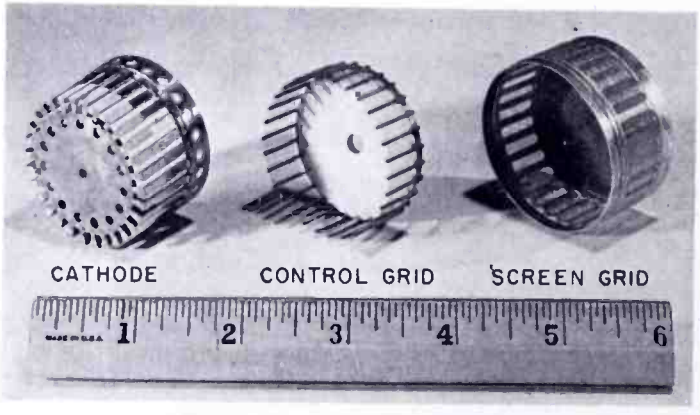

Fig. 1—Tetrode elements.

grid, and screen grid shown in Figure 1. The cathode elements were supported by (6) and (13). (Numbers in parentheses refer to Figure 2.) Several arrangements of heating current flow were employed. With element (6) divided into three equal segments and fed by leads (7), a three-phase Y was used, the neutral lead being element (13). A single-phase, center-tapped, cathode was achieved by dividing element (6) into two equal segments and using (13) as the direct-current ground.

In both of these arrangements the lead (13) functioned as the outer conductor of the coaxial-line input circuit. The center conductor (1) of this line served also as the control-grid support (3). This arrangement allowed grounded-cathode tetrode operation, the screen grid being bypassed to the cathode by the capacitance between elements (5) and (6). A dielectric of either vacuum or mica was used in this condenser. An extension of (6) by the cylinder (7) allowed the equivalent of a low-impedance quarter-wave transmission line at 900

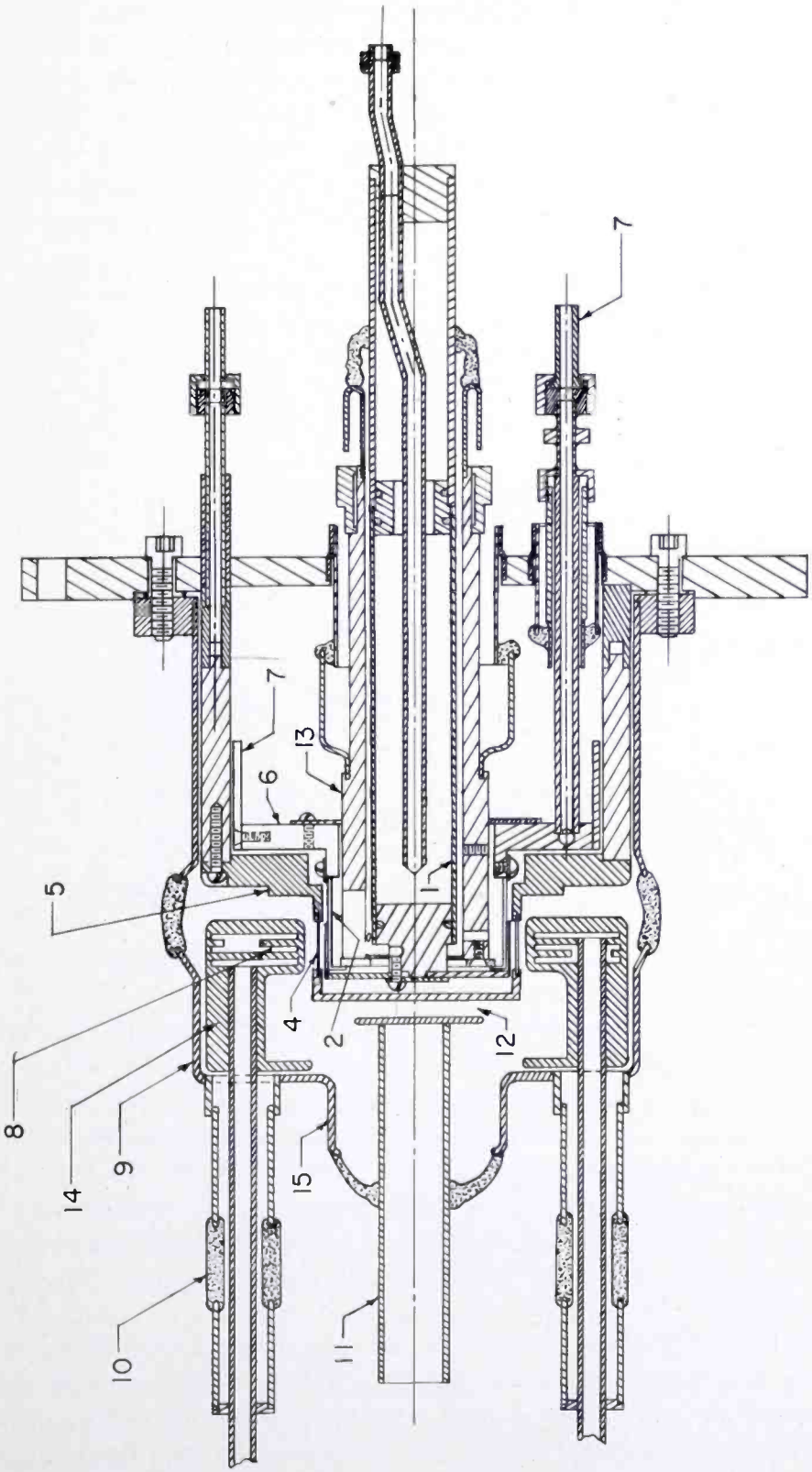

Fig. 2—Cross section of a tetrode with internal bypass condenser for the output cavity.

megacycles. In practice it was found that the elimination of (7) and the use of a thin sheet of mica between (5) and (6) was preferable. A capacitance of 500 micromicrofarads or more could be attained by this means. The effectiveness of this bypass condenser was demonstrated by cold tests which showed no changes in the circuit constants with an electrical short between (5) and (6). This was not true with the quarter-wave-line bypass, since it was tightly coupled to the external parts of the tube and cathode leads.

In the first tetrodes, the anode (8) was mounted by four leads, which are insulated by the glass (10). The close spacing between (9) and (14) allowed a low-impedance blocking condenser for direct-current insulation in the output cavity. This feature was later abandoned, with (9) and (14) directly connected together; direct-current

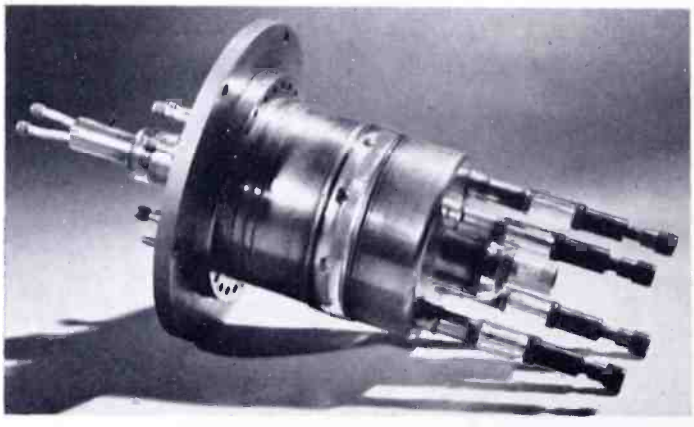

Fig. 3—Photograph of a tetrode with internal bypass condenser.

insulation was achieved with an external blocking condenser in the output cavity.

In all of the tubes, shunt loading of the output circuit was attained through the capacitance (12) and the loaded coaxial line formed by a continuation of the elements (11) and (15). Since the capacitance (12) is proper for a matched line at only one frequency, suitable transformer sections were required in the external line. This can be done between 500 and 900 megacycles with the addition of negligible stored energy to the circuit. The photograph of a completed tube is shown in Figure 3. This tube has an internal blocking condenser for the output cavity.

In the first tetrodes a complete beaming array was used as shown in Figure 4. These tubes operated with the control grid at negative voltages and most of the convection current was beamed between the screen wires. Their performance was very good at low frequencies but at 600 megacycles a useful power gain of less than 10 was realized.

The large driving power was required because of the losses in the input circuit. At 900 megacycles, transit-time effects become very important, so the beaming structure was abandoned in favor of small-wire grids with a large number of turns per inch. The decrease in the required radio-frequency grid voltage more than compensated for the increased grid and screen electron interception.

A large number of structures were tried but the control grid and screen grid shown in Figure 1 represented about the best compromise. This screen grid has 6-mil aligned wires on both the inside and outside of the copper shell. This provides excellent shielding, with a minimum of screen current, and well defined regions between the control grid and screen and between the screen and anode.

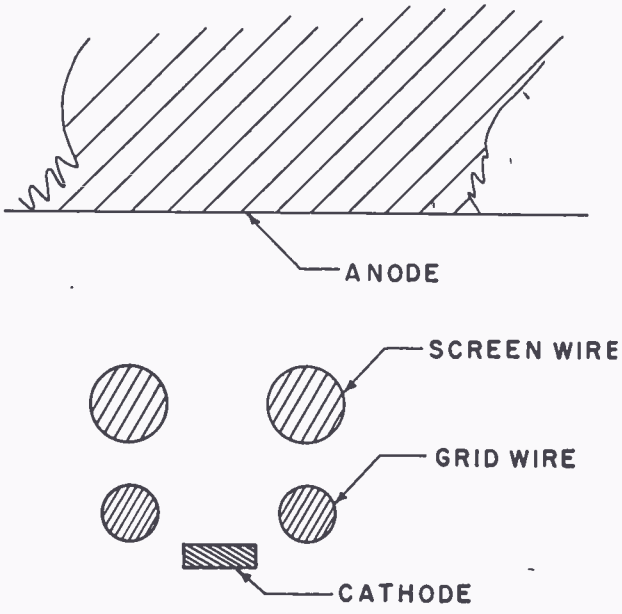

Fig. 4—The cathode–grid array used in the first experimental tetrodes.

Most of the tests of the tetrodes were made at 576 megacycles. At this frequency the tubes with the elements shown in Figure 1 were suitable for 5 kilowatts of peak power with the output cavity loaded for an 8-megacycle band width. Under these conditions the plate efficiency was about 50 per cent. The limiting factor in these tests was the dielectric losses in the glass of the anode seal. The losses in the kovar of the seals were greatly reduced by a gold surface with chrome oxide under the glass.

With 5 kilowatts output, the useful power gain was between 12 and 15. Approximately half of the driving power was absorbed in circuit losses, so the actual tube gain was between 20 and 30. A simple quarter-wave cavity circuit was used up to about 950 megacycles but,

as a result of a mechanically broken seal, only preliminary data was obtained at the higher frequencies. The tubes showed an increase in gain with power level but it was apparent that the power gain at this frequency would certainly not be above 10 at a 5-kilowatt output.

In the meantime work on a grounded-grid triode had been started and the ceramic seal techniques had reached the point which allowed their use in tubes. Also, the conclusion had been reached that ceramics should be used in place of glass and that if a tetrode were required at UHF, it should be designed for grounded-grid operation. Grounded-grid operation would allow a larger power gain at 900 megacycles and also permit high-level modulation. Considering the greater simplicity of the triodes, no further work was done on the tetrodes.

Grounded-Grid Triodes

The cross section of a grounded-grid triode utilizing glass-to-kovar seals is shown in Figure 5. The kovar had a gold surface with chromium oxide under the glass in order to cut down the radio-frequency losses. Figure 6 is a photograph of a completed tube. The anode assembly may appear to be complicated but it allowed easy cleaning and preparation of the glassed parts before the anode was mounted. The main purposes of these experimental tubes using glass seals were to provide the means for a study of UHF performance, and to supply the information necessary for good commercial tube designs. The glass-seal tube was suitable for a 5-kilowatt television transmitter with an 8-megacycle band width at 600 megacycles and with decreasing power up to 900 megacycles. The limitation in power was determined by the dielectric losses in the glass when cooled with forced air. As with the tetrode, a simple quarter-wave cavity output circuit was usable up to 950 megacycles.

The cross section of a silver-soldered ceramic-seal triode is shown in Figure 7, with a subassembly in Figure 8. The completed tube shown in Figure 9 delivered 5 kilowatts at 576 megacycles without forced air cooling of the seals, and 5 kilowatts at 900 megacycles with forced air cooling. However, the thermal conductivity of the metal at the ceramic seal was low so that, since the equilibrium temperature distribution was a quadratic function of the distances from the surfaces of the ceramics, even small losses caused mechanical forces enough to break the ceramics. New techniques were therefore developed which resulted in a tenfold increase in the thermal conductivity of the metal. It is assumed that a triode using these improved ceramic seals could be rated at 10 kilowatts up to 900 megacycles. This power would be attained at 900 megacycles with a maximum electron-emission

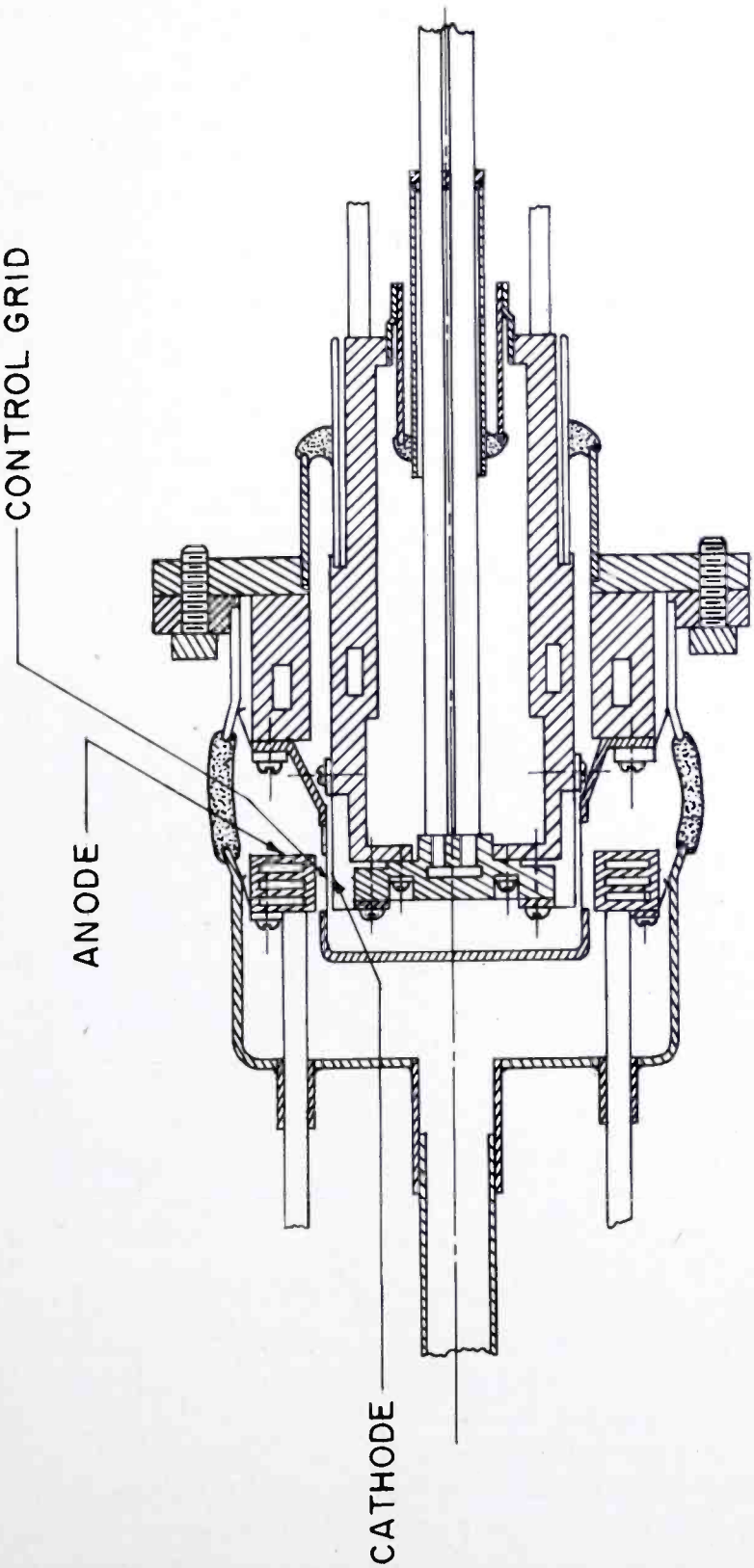

Fig. 5—Grounded-grid triode using glass–kovar seals.

density of less than 2 amperes per square centimeter, so that good life should be realized.

With 5 kilowatts output, the actual tube gain dropped a little between 500 and 900 megacycles because of circuit losses and transit-time effects between the control grid and anode. With a 0.015-inch cathode-to-grid spacing, the useful power gain was about 12 at 900 megacycles and the tube gain was better than 15, or between 60 and 70 per cent of the low-frequency value. With a grid-to-anode spacing of 0.080 inch, the apparent plate efficiency was 64 per cent at 864 megacycles, with 5 kilowatts of useful power and 0.55 kilowatt loss in the circuit. In terms of useful power, the efficiency was about 57 per cent. These data were obtained with an 8-megacycle band width. In a commercial tube, better output circuit efficiencies should be possible,

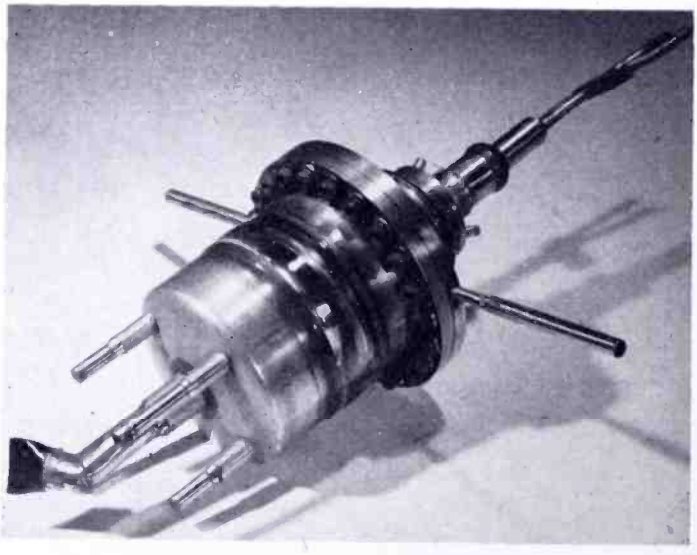

Fig. 6—Photograph of a completed triode as shown in Figure 5.

since over half of the above losses were due to undesirable circuit features associated with the demountable seal.

Theoretical Considerations

While this paper is not intended to be a comprehensive study of grid-controlled tubes, it is fruitful to compare the performance of the tubes with large-signal theory.

Wang[2] was the first to give a rigorous description of a plane diode when large impulsive voltages and currents are involved. A. D. Sutherland[3] has more recently solved the problem of the plane diode with a cathode having unlimited emission when driven by a voltage

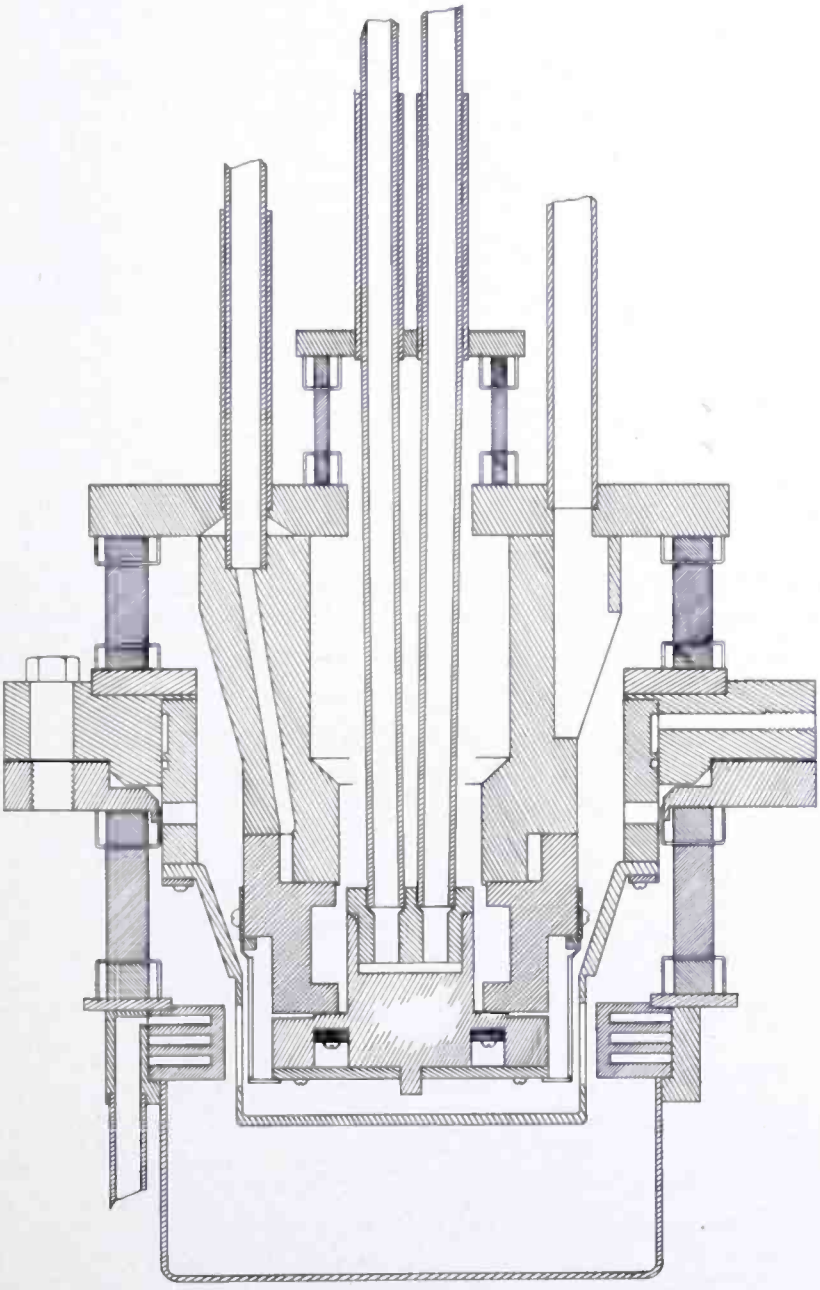

Fig. 7—Ceramic insulated triode.

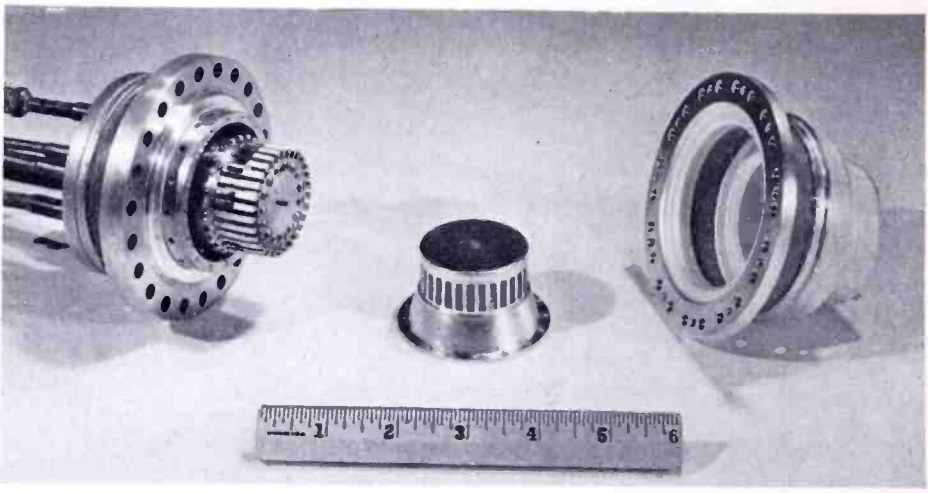

Fig. 8—Subassembly of a ceramic triode.

$V\sin\omega t$. Their approaches are similar, differing mainly in methods and choice of dimensionless parameters.

It is not necessary to go into the details of the theory in this paper. It is sufficient to point out that either Wang's or Sutherland's theory accurately predicts the performance of these triodes if we assume a discontinuity at the grid plane and use their computed convection currents at the grid plane to define the current in a second diode between grid and anode. These assumptions are not at all valid if an open-mesh grid or high-plate-conductance triode is considered. The only rigorous approach in this case would require a treatment of the triode as a unit.

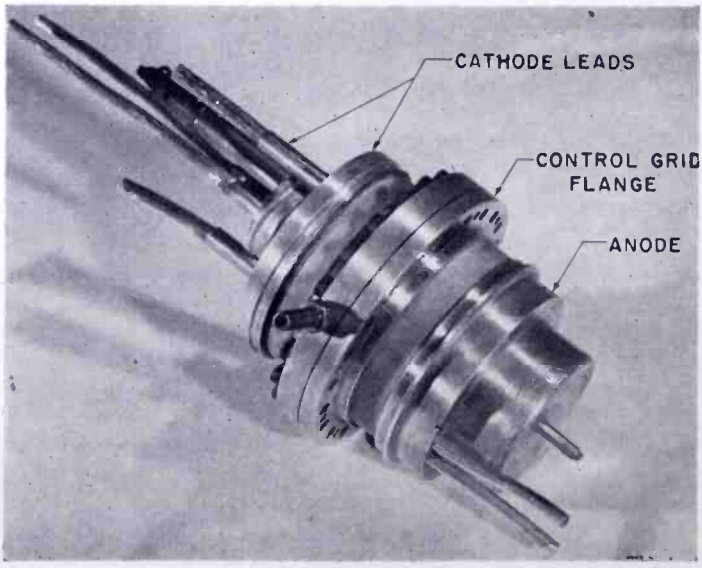

Fig. 9—Completed ceramic insulated grounded-grid UHF triode.

The theory, in conjunction with the data obtained with these tubes, leads to three major conclusions concerning the operation of grid-controlled power tubes at higher frequencies: First, large transit angles in the cathode-grid region merely cause a phase shift of the fundamental component of the convection currents with little loss in amplitude. This prevails so long as all of the charge is swept out of the cathode-grid region during each cycle. When there is a carry-over of charge from previous cycles, the fundamental component is considerably lower than at low frequencies with the same voltage and spacing. Second, the lower power output or efficiency at ultra-high frequencies is a consequence of large transit angles between grid and anode or screen and anode.[12] The third factor, which is important in design considerations, is the fact that the electron emission demands on the cathode increase with frequency. This is illustrated by an examination of the electron dynamics at an unlimited-emission cathode of a plane diode, driven by a voltage $V\sin\omega t$ as the frequency is increased with constant V.

If we consider a single cycle, the emission density at $\omega t = 0$ equals the displacement current density and is proportional to the frequency. The transit angle of this group of electrons from cathode to anode is finite and as they move across the diode they influence the emission from the cathode until they reach the anode. There is a frequency at which the charge associated with these electrons becomes so great, and the transit angle so large, that the driving voltage cannot support any increase in emission for $\omega t > 0$. Above this frequency the maximum cathode current occurs at $\omega t = 0$ and, in the hypothetical tube with unlimited emission, increases directly with the frequency until all of the charge is not removed from the diode before the next cycle starts. At this critical frequency the emission from the cathode is about 2.16 times the direct-current emission for the same voltage. For complete space-charge-limited operation in practical tubes, the cathode must be capable of this emission.

In the tubes described in this paper the increase of required cathode emission with frequency was not serious for a 5-kilowatt

---

[12] If we assume either Wang's or Sutherland's grid plane phenomena to define the current pulse entering the grid-anode region, we can compute the effective fundamental component of the plate current pulse. Even if space-charge effects are negligible, the procedure is tedious and requires trial and error methods. Transit angles of the order of 60 degrees can reduce the fundamental component of the current pulse by as much as 15 per cent, with an additional phase shift of the order of 30 degrees. The largest error arises from the interception of current by the grid, which is not defined by data taken under static conditions. Very good agreement with experimental data was obtained as far as power output is concerned, but the phase shifts were not measured.

television transmitter at 900 megacycles, since the emission density of 1.5 amperes per square centimeter was only about 15 per cent greater than that required at low frequencies. Most of this increase could be accounted for by the decrease of the fundamental component of the plate current pulse during its transit from grid to anode.

With comparable spacings these considerations may be very important if lower emission densities are employed. For example, with a spacing of 0.015 inch between cathode and grid and an emission density of 0.5 ampere per square centimeter at low frequencies, the same power output would require an emission density of at least 0.75 ampere per square centimeter at 900 megacycles.

Conclusion

Grounded-grid triodes with grid-to-cathode spacings of the order of 0.015 inch can be built and operated at 900 megacycles with approximately the same output and nearly the same power gain as at low frequencies. This performance can be attained with cathode emission densities compatible with long life. The experimental triodes described in this paper illustrate the essential factors necessary for this performance and form the basis for the design of a commercial ceramic insulated model which can be jig assembled with a high order of precision. At 900 megacycles, with the construction used in this group of tubes, the useful power gain of the triode was greater than that of the tetrode with grounded cathode; it is believed that a tetrode designed for grounded-grid operation would permit at least as high a power gain as that of the triodes. The choice between these two must, therefore, be made on the basis of simplicity of tube construction, modulation requirements, and similar considerations.

Acknowledgments

The author wishes to express his appreciation to A. D. Sutherland, formerly of RCA Laboratories Division at Princeton, N. J., for the many discussions on UHF tubes and for his aid in some of the circuit problems. Credit is also due to Karl B. Persson, who did most of the basic experimental work which led to the techniques used in making the ceramic insulated triodes, while at the RCA Laboratories at Princeton, N. J. as a Scandinavian-American Foundation Fellow. The author is indebted to L. D. Armstrong of RCA Laboratories Division at Princeton, N. J., who perfected the ceramic-to-metal seal techniques and used them in the construction of the triode described in this paper.

AN ANALYSIS OF THE INJECTION LOCKING OF MAGNETRONS USED IN AMPLITUDE-MODULATED TRANSMITTERS*

By

J. S. Donal, Jr. and K. K. N. Chang

Research Department, RCA Laboratories Division, Princeton, N. J.

Summary—An analysis of the injection locking of a plate-modulated single-loop magnetron is presented. For simplicity, the useful load is assumed to be matched to the transmission line and the synchronizing current is injected at a plane at a distance $\lambda/2$ from the magnetron. The pushing curve and the Rieke diagram of the magnetron are used to calculate the radio-frequency phase modulation during the amplitude-modulation cycle. The power output required of the locking amplifier is related to the injection current, the power in the load and the phase modulation. Using a particular magnetron as an example, together with a locking amplifier capable of a power output of 10 per cent of the peak system output, the expected radio-frequency phase modulation is found to be about ± 20 degrees for an amplitude-modulation factor of 0.74.

Introduction

IT IS DIFFICULT to obtain carrier powers above a few kilowatts with conventional amplifiers designed for frequencies above 500 megacycles. Traveling-wave tubes and klystrons have not yet come into general use for this purpose. While the magnetron oscillator can provide very large amounts of continuous-wave power, with high efficiency, it has certain disadvantages compared to amplifiers for use in the production of amplitude modulation. Modulation by absorption, for example, results in a very low average efficiency during the modulation cycle. Plate modulation of a magnetron gives a high average efficiency, since the input to the oscillator is varied, but it is accompanied by severe frequency modulation.

A system using a plate-modulated magnetron has been investigated experimentally. Good linearity and depth of modulation were obtained,[1] and the band width was roughly that associated with the loaded Q. To prevent frequency modulation, a system of feed-back phase control

* Decimal Classification: R355.912.1.

[1] J. S. Donal, Jr. and K. K. N. Chang, "The Plate Modulation of CW Magnetrons," to be published.

requiring less than one watt of control power has been applied with considerable success to such a modulated magnetron operating in the 800-megacycle range.[2] L. L. Koros[3] has devised a different system for the phase control of a continuous-wave magnetron during plate modulation, by injection of a stabilizing signal. Both systems not only synchronize the magnetron to a crystal-controlled source, but establish a definite phase relation between the radio-frequency (r-f) voltages of the magnetron and the control amplifier. The frequency change accompanying plate modulation is effectively suppressed and converted into a phase modulation that is usually much less than ± 90 degrees and is independent of the modulation frequency, at least for low modulation frequencies. The Koros arrangement used a small locking amplifier, potentially capable of a power output of roughly 10 per cent of the peak system output. Excellent linearity was found experimentally. The minimum power to which the locked magnetron could be modulated was substantially reduced compared to the unlocked case.

The success achieved by Koros has prompted the further consideration of injection locking from an analytical standpoint. In the present paper the locking process is described in terms that permit the designing of an effective r-f circuit which is easy to adjust. Procedures are developed for the prediction of system performance as a function of the requirements placed upon the locking oscillator. The performance is calculated from only that experimental data normally available for a magnetron. Although the present treatment considers the locking of a magnetron with only one output loop, and is limited to the cases in which the useful load is matched to the line supplying it and the injection current is introduced at the plane of the magnetron, the analytical methods described are applicable to more general cases. The methods will be extended to other circuit arrangements at a later date.

Considerable emphasis has been placed upon procedures for the calculation of the expected r-f phase modulation. This performance characteristic is of importance in many practical systems. As an example, it has been shown by D. G. Moore of these laboratories that excessive r-f phase modulation seriously degrades square-wave reproduction in any wide-band system when vestigial side-band transmission is used.

---

[2] D. S. Bond, D. G. Moore, and J. S. Donal, Jr., "Experimental AM Transmitter Employing a Crystal-Controlled FM-Beam Magnetron," to be published.

[3] L. L. Koros, "Frequency Control of Modulated Magnetrons by Resonant Injection System," *RCA Review*, Vol. 13, pp. 47-57, March, 1952.

Locking Process

J. C. Slater[4] developed the basic theory most applicable to the phasing of microwave oscillators, particularly magnetrons. E. E. David, Jr.[5,6] extended this theory and applied it to the analysis of a specific circuit which was applicable to the phase control of a microwave oscillator by a reference source. The analysis of the circuit (superficially similar to that of Figure 1) was simplified by the assumptions that the locking signal propagates only toward the magnetron and the magnetron signal propagates only toward the load. David experimentally satisfied these assumptions by placing a directional coupler at the junction. This caused a large loss of locking power, a result avoided by the circuits employed by Koros and treated here. Nevertheless, David's analysis and experimental results are of great interest.

David showed that the locking signal adds terms to both the susceptance and conductance equations that express the conditions for oscillation. The new susceptance term holds the frequency constant by correcting for the changes in electronic susceptance caused by plate modulation. The conductance term gives the unavoidable simultaneous change in loading of the magnetron.

It would perhaps be more illuminating to describe locking in the following qualitative manner. The locking amplifier sends a wave of fixed frequency to the magnetron. For phase comparison purposes the phase of this wave at the magnetron may be taken as reference phase. If the magnetron tries to increase its frequency, its outgoing wave advances in phase. The result is a relative lag in phase between the wave incident on the magnetron (the locking signal) and the voltage wave from the magnetron. However, a lagging incident wave, analogous to that reflected from a capacitive load, always adds positive susceptance to the resonant system and reduces the magnetron frequency. If the effect is insufficient, the magnetron will continue to advance its relative phase until the angle opens up to the point where the susceptance presented to the magnetron exactly corrects the change in susceptance that produced the original frequency increase. Thus, an equilibrium state is reached in which there is a fixed phase angle

---

[4] J. C. Slater, "The Phasing of Magnetrons," Technical Report No. 35, Research Laboratory of Electronics, Massachusetts Institute of Technology, April 3, 1947.

[5] E. E. David, Jr., "Locking Phenomena in Microwave Oscillators," Technical Report No. 63, Research Laboratory of Electronics, Massachusetts Institute of Technology, April 8, 1948.

[6] E. E. David, Jr., "Some Aspects of R-F Phase Control in Microwave Oscillators," Technical Report No. 100, Research Laboratory of Electronics, Massachusetts Institute of Technology, June 11, 1949.

between the wave from the magnetron and the wave from the locking source. Since there is the fixed phase relation, the magnetron frequency is synchronous with that of the locking source.

Use of the Rieke Diagram

It is shown below that both the power output of the locking source and the locked-system phase modulation can be calculated if one can determine the complex reflection coefficients presented at the magnetron during plate modulation. Both components of the load admittance can be determined by use of the Rieke diagram. Only the load susceptance will be considered for the moment, since the contribution of the conductance portion of the effective load depends upon the locking current in a manner discussed in detail later.

The condition for resonance of the system may be written in the approximate form

$$b_e + 2C\,(\omega - \omega_0) + K\,B_L = 0 \qquad (1)$$

where b_e is the electronic susceptance, B_L is the normalized load susceptance, C is the tank capacitance and K is a coupling factor. The operating and cold-resonance angular frequencies are ω and ω_0, respectively. If K, B_L and C are known, the changes in b_e, corresponding to changes in ω during the plate modulation, can be calculated. This information yields the values of B_L that must be presented by the locking source if ω is to be constant.

A much simpler procedure is available, for the determination of the values of B_L required for locking, if use is made of the Rieke diagram. This diagram is usually a plot of the frequency and power output, as a function of either the complex reflection coefficient or the VSWR and phase, at an arbitrary plane in the line outside of the magnetron. For present purposes it is assumed that this plane is so chosen that the frequency contours are parallel to the B_L contours of the admittance chart, or all make the same angle with these contours. The contours of the usual Smith chart[7] then give the values of B_L and G_L presented at the magnetron reference plane. A diagram of this type, with additional data used later, is shown in Figure 3. Two examples of the use of such a chart will be given.

First, assume that the magnetron is operating into a matched nonresonant load and that the frequency is decreased two megacycles by means of an internal tuner. The locking system will correct this

[7] P. H. Smith, "Transmission Line Calculator," *Electronics*, Vol. 12, pp. 29-31, January, 1939.

frequency change if it presents a load lying at any point on the contour marked "+ 2 mc" in Figure 3.* Conversely, if the frequency is corrected, the load must be at some point on this "+ 2 mc" contour. The vector ρ, representing the new reflection coefficient, must terminate on this contour. If another condition governing ρ can be found from circuit theory, the phase angle of the reflection coefficient and the phase change of the load voltage can be determined.

As a second example it is again assumed that the magnetron is operated into a matched load, but that the plate voltage is decreased by an amount which would reduce the unlocked magnetron frequency by two megacycles. The locking system can then eliminate this frequency change by presenting a load lying at any point on the "+ 2 mc" contour of Figure 3. This assumes that the distribution of the frequency contours on the Rieke diagram is unaltered by the reduction in plate current. This assumption, which has been made in this analysis, can be shown to be reasonable.** It eliminates the necessity for taking a large amount of experimental data.

It is obvious that the use of the Rieke diagram effects a great simplification. It gives the locus of possible loads, presented by the locking oscillator, that will maintain the magnetron frequency constant. It makes it unnecessary to determine the tank capacitance and the coupling factor. In addition, the experimental data takes account of the well-known variation of b_e in Equation (1) with the load conductance, an effect which causes the frequency contours to cut across the B_L contours at a slight angle.

Analysis of a Locking Circuit

An effective locking circuit for a magnetron with a single coupling loop is shown in Figure 1. The locking amplifier injects a current I at a junction placed at a distance l from the magnetron reference plane. The current I does not need to be constant. The line to the load is assumed to be terminated in its characteristic admittance, Y_o. The powers in the branches and the phase of the voltage across the

---

* This procedure neglects a very small change in the distribution of the frequency contours due to the change in tank capacitance.

** The approximation in Equation (1) is valid when ω does not differ by more than a few megacycles from ω_0. If b_e is replaced by ωC_e, solving Equation (1) for ω and substituting known values of C, ω, and ω_0 shows that the plate current swing during deep modulation alters the electronic capacitance, C_e, by about a factor of two. This causes a change in the distribution of frequency contours, along constant-conductance contours, by only a few per cent.

junction can be determined in terms of I and the reflection coefficient at the junction.

a. Phase Modulation

At the magnetron reference plane, the reflection coefficient looking toward the load may be defined in the usual manner as

$$\vec{\rho}(x_1) = |\rho|\, e^{j\phi}. \tag{2}$$

At the plane of the junction, looking toward the magnetron,

$$\overleftarrow{\rho}(x_0) = \frac{1}{\vec{\rho}(x_0)} = \frac{1}{|\rho|\, e^{j(\phi + 2\beta l)}} = \frac{1}{|\rho|\, e^{j\phi'}}, \tag{3}$$

where $\phi' = \phi + 2\beta l$ is the phase of the reflection coefficient at the junction.

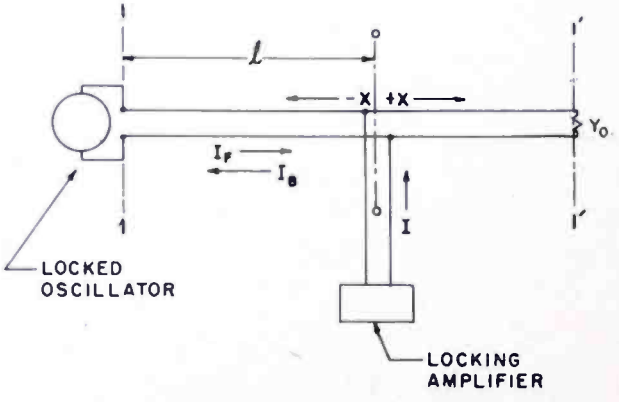

Fig. 1—Schematic diagram of circuit analyzed.

At the junction, the normalized admittance looking toward the magnetron is

$$\overleftarrow{Y}(x_0) = \frac{1 - \overleftarrow{\rho}(x_0)}{1 + \overleftarrow{\rho}(x_0)} = \frac{-1 + |\rho|\, e^{j\phi'}}{1 + |\rho|\, e^{j\phi'}}. \tag{4}$$

The total admittance at the junction, no longer normalized, is

$$Y_T = \overleftarrow{Y}(x_0) \cdot Y_0 + Y_0, \tag{5}$$

so that the junction voltage, which makes an angle θ with I, is

$$e_3 \angle \theta = \frac{I}{Y_T} = \frac{I}{(\overleftarrow{Y}(x_0) + 1)\, Y_0} = \frac{1 + |\rho|\, e^{j\phi'}}{2\, Y_0\, |\rho|\, e^{j\phi'}} \cdot I$$

$$= \frac{I}{2\, Y_0\, |\rho|} \cdot e^{-j\phi'} + \frac{I}{2\, Y_0}. \qquad (6)$$

The magnitude and phase of the voltage at the junction are found from the vector diagram of Figure 2. The determination of I will be considered next.

Koros[3] used a grounded-grid triode as a doubler for the output stage of the locking amplifier. For the purposes of this analysis it is assumed that the 6161 is used as the doubler. L. S. Nergaard of these laboratories has shown that, under quite normal conditions of operation and with an input power of about 200 watts, the second-harmonic component of the plate current of the 6161 as a doubler could have a

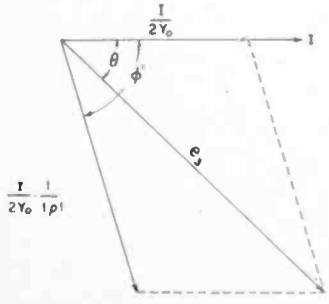

Fig. 2—Vector diagram giving e_3 and θ in terms of $|\rho|$ and ϕ'.

value of 0.3 ampere and would be substantially independent of the load. The maximum power output would be somewhat in excess of 100 watts. It is shown in the Appendix that, under these conditions, a simple circuit can be designed that will inject a current I of one ampere at the junction. This current can be made constant during the cycle of plate modulation of the magnetron, and constant in phase with respect to the grid drive of the doubler stage. Since this grid drive may be taken as reference phase, there is no additional phase modulation contributed by the locking-amplifier branch of Figure 1.

From the preceding paragraph, the desired phase modulation of the r-f voltage across the load can be calculated if the variations in θ during the modulation cycle can be determined. This point-by-point determination of θ forms the subject of the next section.

b. Branch Powers

From Equation (6) the power output of the locking amplifier and the power in the load are given by

$$P_{l_1} = Re\,[e_3 I^*] = Re\left[\frac{1 + |\rho'|\,e^{j\phi}}{2\,Y_0\,|\rho|\,e^{j\phi}}\,II^*\right] = \frac{2\,Y_0\,|\rho'|}{I^2}\,(\cos\phi' + |\rho'|), \quad (7)$$

$$P_l = Re\,[e_3(e_3\,Y_0)^*] = \frac{1 + 2\,|\rho|\cos\phi' + |\rho|^2}{4\,Y_0\,|\rho|^2}\cdot I^2. \quad (8)$$

Although the derivations will not be given, an application of ordinary circuit theory to Figure 1 yields the following powers and currents.

Currents indicated in Figure 1:

$$I_F\,(x) = \frac{I}{2\rho}\,e^{-j\beta x}, \quad (9)$$

$$I_B\,(x) = -\frac{I}{2}\,e^{j\beta x}. \quad (10)$$

Corresponding powers:

$$P_F = \frac{|\,I_F\,(x)\,|^2}{Y_0} = \frac{I^2}{4\,Y_0}\cdot\frac{1}{|\rho|^2}, \quad (11)$$

$$P_B = \frac{|\,I_B\,(x)\,|^2}{Y_0} = -\frac{I^2}{4\,Y_0}. \quad (12)$$

Net power in the line between the magnetron and the junction:

$$P_0 = \frac{|\,I_F\,(x)\,|^2}{Y_0}\,(1 - |\rho|^2) = \frac{I^2}{4\,Y_0}\,\frac{(1 - |\rho|^2)}{|\rho|^2}. \quad (13)$$

Point-by-Point Calculation of Phase Modulation

It has been shown that the determination of the phase modulation requires only a knowledge of the variations of θ (Equation (6)) during the modulation cycle. If $|\rho|$ and ϕ can be determined at the magnetron reference plane, $|\rho|$ and ϕ' at the junction may be calculated. The variations of θ, and the phase modulation, are then obtainable by

vector diagrams such as Figure 2. As a simplification, an l (Figure 1) of $n\lambda/2$ has been used in this treatment. This is convenient, also, in that $\phi' = \phi$ on the chart.

In any practical system it is desirable to calculate the phase modulation as a function of the amplitude of the modulation envelope. For this reason the power in the load was chosen as the independent variable. The type of developmental magnetron (the A-128)[8] used by Koros was chosen to illustrate the procedure. Figure 4 is a representative pushing curve, and Figures 3 and 5 are representative Rieke

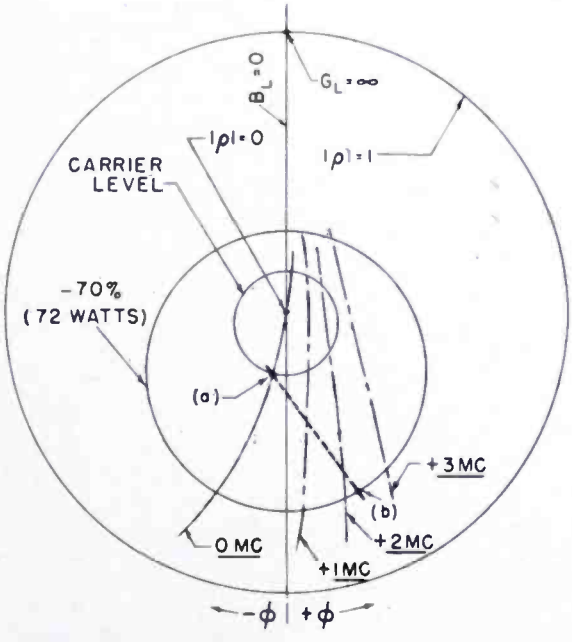

Fig. 3—Portion of Rieke diagram with two possible locked operating points.

diagrams, for this tube. A carrier level of 340 watts was assumed and P_L was calculated for various modulation factors, expressed as percentage voltage modulation down from the peaks. From Equation (8) the possible combinations of $\phi = \phi'$ and $|\rho|$ yielding each P_L were determined. As an example, the values of $|\rho|$ and ϕ on the "carrier" contour of Figure 3 satisfy Equation (8) for $P_L = 340$ watts. Modulation, about a carrier level of 340 watts, to a peak power of 808 watts and to a minimum power of 72 watts corresponds to a voltage modulation of 70 per cent down from peak voltage. The "— 70%" contour of Figure 3 is obtained from Equation (8) for the minimum power of 72

[8] J. S. Donal, Jr., R. R. Bush, C. L. Cuccia, and H. R. Hegbar, "A 1-Kilowatt Frequency-Modulated Magnetron for 900 Megacycles," *Proc. I.R.E.*, Vol. 35, pp. 664-669, July, 1947.

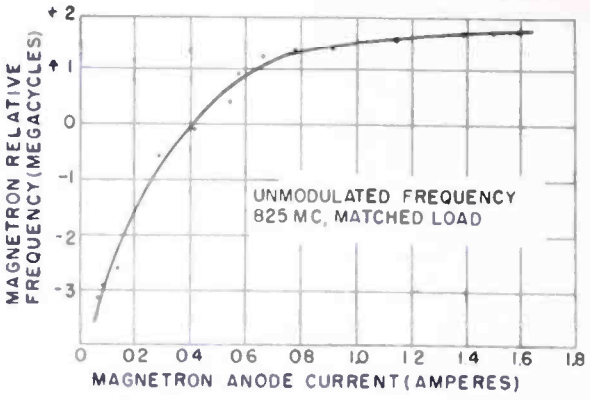

Fig. 4—Dynamic pushing curve of A-128 developmental magnetron.

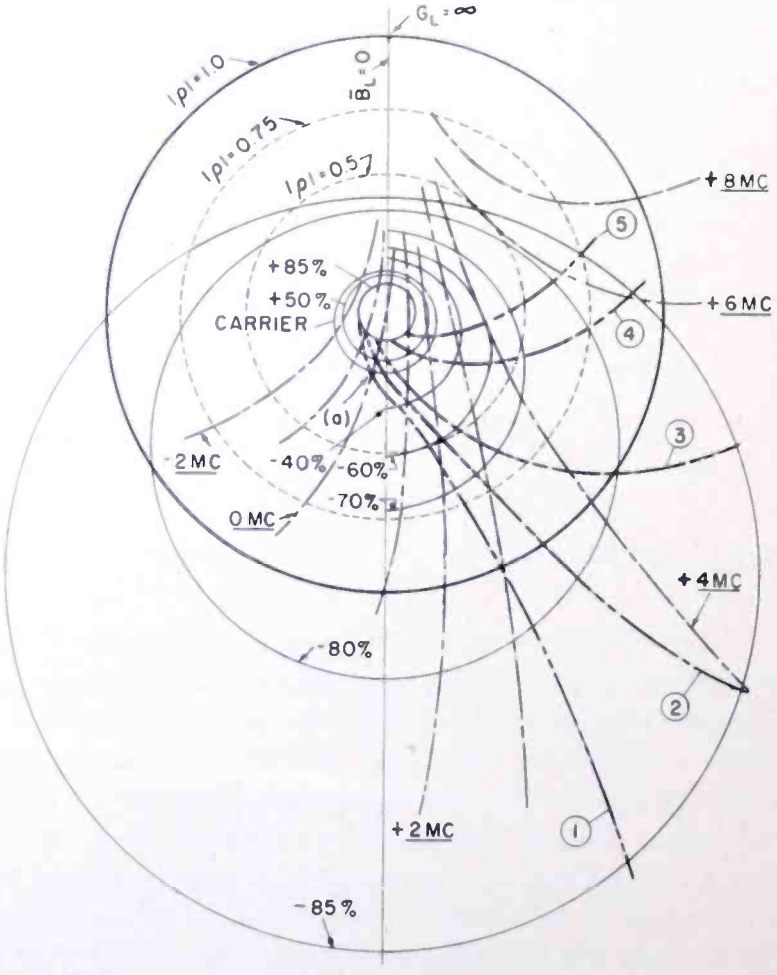

Fig. 5—Rieke diagram with superimposed P_L contours and paths of operating points. The heavy dashed lines are paths of operating points. When P_L is varied from the value for the "+ 85%" P_L contour to that for the "— 85%" contour, for example, the sinusoidal r-f voltage modulation is from the peak value to 15 per cent of peak, about a carrier level of 340 watts.

watts. At carrier level and at 72 watts in the load the magnetron will see combinations of $|\rho|$ and ϕ lying on the respective contours of Figure 3. However, since each such combination gives a different θ, the actual operating points on the P_L contours are required in order to determine the phase modulation.

The determination of successive operating points on Figure 3 would require a knowledge of the magnetron pushing (variation of frequency with plate current) for all loads. This data can be shown to be the equivalent of Rieke-diagram frequency contours at all currents. Therefore, since it has already been assumed that the Rieke diagrams are independent of current, it must now be assumed that the pushing is independent of loading.* In addition, the straightforward determination of the operating points would require a knowledge of the magnetron current. This, in turn, would require a measurement of magnetron efficiency for each plate current and for all possible loads as a parameter. Such magnetron data is not usually available. However, there is a simple alternative means for obtaining the current. Koros[3] found the r-f voltage across the load to be a linear function of the input voltage to the plate modulator, V_{in}. The grid voltage of the tetrode modulator[1, 3] developed for this service is varied over a substantial range. Under these conditions the dynamic characteristic, except at very high modulation frequencies, is

$$i_m = K_1 V_{in}^{3/2}, \tag{14}$$

where i_m is the plate current of the magnetron. It is obvious, therefore, that

$$i_m = K_2 P_L^{3/4}. \tag{15}$$

If the magnetron current is measured for one value of load power, it is known for each P_L during the modulation cycle. If the exponent in Equation (14) were different, the exponent in Equation (15) would have another value, but the general procedure would be the same.

It is now a simple matter to determine the operating points and the phase modulation during a modulation cycle. The magnetron currents are obtained from Equation (15) for a series of values of P_L above and below carrier level. As an example, assume that the magnetron tuner is adjusted to give a carrier-level operating point at (a) on the 0-megacycles frequency contour of Figure 3. Assume that the mag-

* For present purposes, the assumption that $\partial C_e/\partial i$ is independent of loading is not unreasonable when the magnetron is *locked*. The usual measured variation of unlocked pushing with the degree of mismatch of the load to the line is enhanced by the change in electrical length of the line to the load.

netron plate current is reduced to give 72 watts in the load, corresponding to the "— 70%" contour of Figure 3. The potential (unlocked) change in frequency is determined, for the two values of plate current, from a pushing curve such as that of Figure 4 for the magnetron to be used. If this change in frequency is —2.3 megacycles, as an example, *the operating point at 72 watts must be on the "+2.3mc" frequency contour and, therefore, at its intersection with the 72-watt* P_L *contour.* This point is shown at (b) in Figure 3. Points (a) and (b) of Figure 3 give two of the combinations of $|\rho|$ and ϕ at the magnetron reference plane, during a modulation cycle, for the particular case of the loading (a) at carrier level. The path of operating points is completed by the same procedure.

Five such paths, corresponding to five assumed tuner positions and, therefore, to five equivalent loads at carrier level, are shown in the more complete diagram of Figure 5. Two of these go outside the $|\rho| = 1$ circle. The frequency contours are extended by maintaining their angle of intersection with the B_L contours. Each P_L contour of Figure 5 intersects the frequency contours at two points. For the circuit used by David, only the lower intercepts are stable operating points.[4] This is probably equally true for the circuit considered here and only lower intercepts have been employed.

From the values of $|\rho|$ and $\phi = \phi'$ found on the paths of Figure 5, θ was determined by use of Figure 2. The values of θ are plotted for the indicated paths in Figure 6. The peak-to-peak changes in θ are the phase modulation for 85 per cent amplitude modulation. The phase modulation for lower percentages of amplitude modulation can be found from the intersection of the phase curves with the lines extending from the reference sine wave.

Several conclusions have been drawn from consideration of data such as that shown in Figures 5 and 6:

(a) The phase modulation is roughly proportional to the modulation factor until, for some paths, the phase change begins to flatten and the phase modulation begins to acquire harmonic components.

(b) The phase modulation is a sensitive function of the magnetron tuning, for the tuning determines, at any load power, the total loading presented to the locked oscillator to adjust its frequency to that of the locking source. If, for any path of Figure 5, the P_L contour fails to intersect the frequency contour required to correct the pushing, the system will break out of lock. The magnetron must then be retuned so that another path is chosen. This path will usually result in greater phase modulation.

(c) If the magnetron breaks synchronism for a path of Figure 5, the effect can be eliminated by increasing the locking current I. This

may require a larger locking amplifier. However, if break-out is not encountered with the original current, the construction of graphical representations such as Figures 5 and 6 has shown that the minimum attainable phase modulation is not necessarily reduced.

(d) The minimum peak-to-peak r-f phase modulation shown in Figure 6 is ± 15 degrees. If synchronization is not broken, a path can be found for which the phase change, from the top to the bottom of the amplitude-modulation cycle, is zero. However, there will usually be substantial phase deviations in other parts of the cycle. Thus, for curve 5 of Figure 6 the maximum deviation occurs for modulation between the "+ 85%" and "— 60%" points. The shape of the phase-

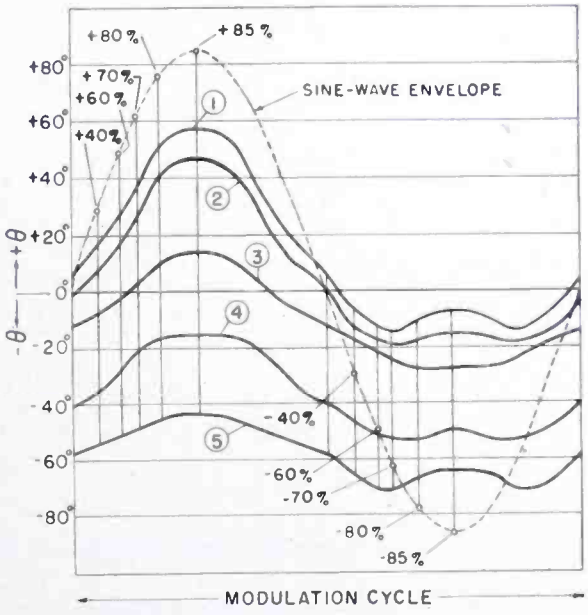

Fig. 6—R-f phase modulation for the paths of Figure 5. The phase modulation is the variation in θ during the amplitude-modulation cycle. The peak-to-peak variations plotted occur when the modulation is 85 per cent down from peak voltage. For lower depths of modulation, such as 80 per cent down from peak voltage, the phase modulation is the difference in θ corresponding to the intersections of the phase curves with the vertical lines extended from the "+ 80%" and "— 80%" points on the sine wave.

modulation curve is a sensitive function of the pushing curve and Rieke diagram of the magnetron in question. Therefore, even for a magnetron having a Rieke diagram and pushing similar to those of the tube used as an example, and for an amplifier of the power output assumed, one should not count on a phase modulation less than about ± 20 degrees. If the magnetron has higher pushing or lower pulling, or if the shape of either the Rieke diagram or the pushing curve is altered substantially, the phase modulation might be increased further.

Requirements Placed Upon the Locking Amplifier

From Equations (10) and (12) the current and power going toward the magnetron are constant. The power output of the locking amplifier varies over a wide range, however. From Equation (7) it may be very high when $|\rho|$ and $\phi = \phi'$ are small. It would be roughly 150 watts, for example, at point (a) of Figure 5. On the other hand, P_{LA} is zero wherever $\cos\phi = -|\rho|$. P_{LA} is negative when $\cos\phi < -|\rho|$ and in this case the locking amplifier absorbs power. In general, P_{LA} is greatly reduced near the bottom of the amplitude-modulation cycle.

It is clear that the power output of the locking amplifier can have widely different values for the same frequency-correcting susceptance presented to the magnetron. However, the output of the amplifier cannot be ignored even though its magnitude is not of primary importance. As an example, if P_{LA} is negative the sum of the power absorbed and the input power may exceed the dissipation limits of the locking amplifier. For other points on Figure 5, P_{LA} might exceed the maximum possible output of the locking tube. However, it can be shown that this latter limit is not rigid, for if an attempt is made to exceed the available P_{LA}, the current I will drop. If the overloading is not severe, the resulting increase in phase modulation is not great. In general, a path of low phase modulation on Figure 5 can be chosen such that the limits discussed here are not exceeded. If it is found by analysis that this is not the case, a larger locking amplifier must be used.

Choice of a Locking Amplifier for a New Magnetron

In the preceding sections a particular example has been treated. A magnetron with the pushing of Figure 4 and the Rieke diagram of Figure 5 was modulated about a carrier power of 340 watts. A locking amplifier capable of injecting a constant current of 1 ampere at the junction of Figure 1 yielded the predicted phase modulations of Figure 6.

As a new example, it is assumed that another magnetron is to be modulated about a carrier with ten times the power of that of the earlier tube. Similarly, a new locking amplifier is chosen with a tenfold increase in plate dissipation. The circuit (Figure 7) is adjusted to inject a current of $\sqrt{10}$ amperes instead of 1 ampere. From Equation (8) it is evident that the P_L contours of Figure 5 will be unchanged, with the exception that each will correspond to ten times its original power. It is assumed that the unlocked frequency changes of the new magnetron are identical with those (Figure 4) of the old tube when

the carrier frequencies are made identical and the data is plotted as a function of modulation factor about this carrier. If the example is further simplified to include identical Rieke diagrams, it is obvious that the phase modulation will be identical with that of Figure 6. The locking amplifier will be operated with the same margin of safety. Its output power will be variable. As in the original example, for which the output of the locking amplifier was about 100 watts, it will again be possible to supply the necessary injection current if the output of the amplifier is very roughly 10 per cent of the peak power in the load.

The above case is, of course, an oversimplification. If the experimentally determined pushing and Rieke diagrams of the new magnetron are different from those assumed, the phase modulation can be calculated by the procedures described earlier. If the pushing of the new tube is increased, or if the frequency contours of the new Rieke

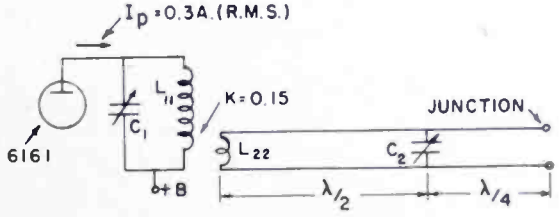

Fig. 7—Locking-branch circuit.

diagram are more widely separated (lower pulling), breakout may occur for some paths, since the required frequency contour will not be intersected. Breakout can be eliminated by adjusting the circuit to give a higher locking current. However, if for any reason the paths of desirably low phase modulation result in overloading of the locking amplifier, a larger amplifier must be chosen.

Attainable Depth of Modulation

At least one developmental magnetron, the 1-kilowatt A-128, has been found to be capable of plate modulation,[1] unsynchronized, to a minimum power of 40 or 50 watts. Koros[3] has found that, when this tube is locked to a reference source, it can be modulated to zero power. The remaining load power of only a few watts is supplied by the locking amplifier. This is an improvement of considerable practical importance.

In this analysis, P_L was taken as the independent variable. It can be shown that *if* P_L goes to zero, all of the paths of Figure 5 converge

to a point corresponding to a short circuit presented at the junction. However, the analysis cannot predict that this will happen in practice, for when the magnetron stops oscillating it becomes a passive circuit, presenting an impedance which is a function of L, C, ω, Q and the coupling parameters. Near resonance, for example, it would present substantially an open circuit, with the result that the output of the locking amplifier, and the power in the load, would be high. Fortunately, it appears that the trend of the magnetron impedance toward a short circuit is not interrupted until the power in the load is very low.

Phase Modulation as a Function of Modulation Frequency

This analysis takes no account of effects arising at high modulation frequencies. At low modulation frequencies it predicts that the phase modulation will be independent of modulation frequency and that the frequency modulation will be proportional to the modulation frequency. The phase modulation should be in phase with the amplitude modulation.

Other observations[1] suggest that at high modulation frequencies the unlocked frequency change may shift in phase and may be no longer in phase with the amplitude modulation. This effect should be observable experimentally as a progressive shift in phase of the locked phase modulation with respect to the envelope amplitude.

David[9] has predicted that the locked phase modulation should decrease at high modulation frequencies. This conclusion was confirmed experimentally. David considered this to be a disadvantage if the object of the locking is to control an out-phase modulation system. It would be a distinct advantage, however, when minimum phase modulation is desired.

Conclusions

This analysis shows that a plate-modulated magnetron can be synchronized with a crystal controlled source by means of a simple circuit that is relatively easy to construct and adjust. As demonstrated experimentally by Koros, the locking amplifier required may be considerably smaller than that demanded by the circuit proposed originally by David.

The phase modulation of the voltage across the load, with respect to the synchronizing signal as a reference, may be calculated by a point-by-point procedure. The powers in the circuit branches can be

[9] E. E. David, Jr., "Some Aspects of RF Phase Control in Microwave Oscillators," Doctoral Thesis, Massachusetts Institute of Technology, May, 1950.

determined. While the instantaneous power output of the locking amplifier is of secondary importance in the synchronizing process, the circuit must be adjusted so that the limitations of the amplifier are not exceeded. The analytical procedure permits a reasonably accurate choice of a locking amplifier for use with a new magnetron. The calculations require only the magnetron performance chart, the Rieke diagram at rated current, and the dynamic pushing curve taken with a matched load.

Although this paper treats only the one-loop magnetron and assumes that the passive load is matched to the line and the locking current is injected at the magnetron plane, the analytical procedure is applicable to more general cases. With the above assumptions, if the pushing and Rieke diagram of a new magnetron are similar to those of the tube used as an example, and if the output of the locking amplifier is about 10 per cent of the peak power output of the system, the minimum attainable system phase modulation should be roughly ± 20 degrees for a modulation factor of 0.74.

A system using a synchronized plate-modulated magnetron can be adjusted by peaking to have an r-f band width in excess of that associated with the loaded Q. The linearity and depth of modulation have been found to be very good. Phase and frequency control systems of the type analyzed should make the plate-modulated magnetron a practical tube for use in high efficiency amplitude-modulated transmitters.

Acknowledgment

L. L. Koros of the RCA Victor Division in Camden has been most cooperative in discussions of his experimental work. L. S. Nergaard of the RCA Laboratories Division in Princeton gave generously of his time and, in particular, contributed the analysis of triode operation referred to in the text.

Appendix

Nergaard showed that the second harmonic component of the plate current of the 6161, used as a doubler, could safely have a value of 0.3 ampere, and would be substantially constant during the magnetron modulation cycle. It was felt to be desirable to design a locking-branch circuit which would inject a constant current I at the junction. The circuit should introduce no system phase modulation in addition to that described in the text and associated with variations in θ. Variations in I would, in general, result in additional phase modulation. This would not only be difficult to calculate but might degrade the system performance.

The circuit of Figure 7 was chosen to inject a constant current of one ampere. The tank inductive reactance, $j\omega L_{11}$, was made $j32$ ohms for resonance with the tube capacitance at 825 megacycles. A reasonable size of coupling loop gave $K = 0.15$ and a value of $j\omega L_{22}$ of $j50$ ohms. C_2 is a stub adjusted to give a capacitive reactance.

By application of nodal-admittance analysis to an intermediate circuit, Figure 7 can be reduced to Figure 8. Z_1 is the equivalent impedance of the tank capacitive susceptance in parallel with an inductive susceptance of $-j0.0281$ mhos arising from the coupling. Z_2 is $j261$ ohms. Z_3 is the impedance of $j60.1$ ohms in parallel with the reactance of C_2 of Figure 7. Z_4 is the impedance presented across C_2 of Figure 7 by the complex load, at the junction, due to the magnetron in parallel with the 50-ohm passive load.

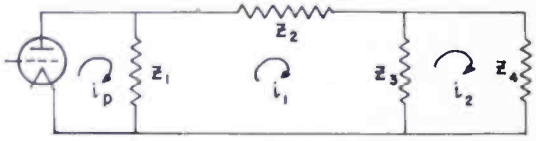

Fig. 8—Simplified equivalent circuit of locking branch.

The mesh equations for Figure 8 may be solved to give

$$i_1 = \frac{i_p Z_1 (Z_4 + Z_3)}{Z_4 (Z_1 + Z_2 + Z_3) + Z_3 (Z_1 + Z_2)}. \tag{16}$$

It is assumed that I_R, which is the current in the load Z_4 is to be one ampere. At Z_3, which is distant $\lambda/4$ from Z_4, the voltage is

$$V_s = -j Z_0 I_R = -j 50 \text{ volts}. \tag{17}$$

If $-j1$ ohms is chosen for the reactance of C_2, the 60 ohms in parallel with it can be neglected and $Z_3 = -j1$ ohms. From a consideration of the paths of Figure 5, the total impedances presented at the junction can be calculated. After transformation of these impedances by the quarter-wave line of Figure 7, the resulting Z_4 is always 10 ohms or more, so that i_2 can be neglected compared to i_1. Therefore

$$i_1 = \frac{V_s}{Z_3} = 50 \text{ amperes}. \tag{18}$$

Z_3 may be neglected, compared to Z_4, in Equation (16), which becomes

$$i_1 = \frac{i_p Z_1}{Z_1 + Z_2 + Z_3}. \tag{19}$$

Substituting the known values and solving for Z_1 yields $Z_1 = j261$ ohms. But Z_1 represents the impedance of the tank capacitive susceptance in parallel with a known inductive susceptance. The unknown tank capacitive reactance is found to be $-j31.3$ ohms compared to the original $-j32$ ohms. The result shows that the tank must be detuned to produce the desired one ampere at the junction. Since Z_3 is made small compared to Z_4, i_1 is constant. As a result, V_s is constant and the junction current (I_R of Equation (17)) is constant. From Equations (17), (18), and (19) it can be seen that the phase of the injected current with respect to i_p is independent of Z_4. Since i_p is constant during the modulation cycle, its phase, with respect to the grid drive, must be constant. Therefore, there is no phase modulation introduced by the locking branch of Figure 1.

RCA TECHNICAL PAPERS†

First Quarter, 1952

Any request for copies of papers listed herein should be addressed to the publication to which credited.*

"Admissions and Transfers," R. F. Guy, *Proc. I.R.E.* (February) ... 1952
"Air Weather Ahead," R. F. Guy, *Radio-Electronics* (January) 1952
"AM Transmitter Design," M. H. Hutt, *Rad. and Tele. News* (January) 1952
"Assembly-Line TV Studios," M. Rettinger, *Broadcast News* (January-February) 1952
"A Band-Pass Mechanical Filter for 100 Kilocycles," L. L. Burns, Jr., *RCA Review* (March) 1952
"Circuit Stability in Guided Missiles," R. L. Kelly, *Electronics* (March) 1952
"Design and Adjustment of Kinescope Centering Magnets and Ion-Trap Magnets," *RCA Application Note AN-152* (March) 1952
"Design Considerations for Minimizing Ripple and Interference Effects in Horizontal-Deflection Circuits," *RCA Application Note AN-151* (March) 1952
"Design Data for Horizontal Rhombic Antennas," E. A. Laport, *RCA Review* (March) 1952
"A Developmental Portable Television Pickup Station," L. E. Flory, W. S. Pike, J. E. Dilley, and J. M. Morgan, *RCA Review* (March) 1952
"Efficient TV Service in the Customer's Home," W. M. Tomlin, *Radio-Electronics* (March) 1952
"An Experimental High-Transconductance Tube Using Space-Charge Deflection of the Electron Beam," J. T. Wallmark, *Proc. I.R.E.* (January) 1952
"Factors Affecting the Quality of Kinerecording," P. J. Herbst, R. O. Drew, and J. M. Brumbaugh, *Jour. S.M.P.T.E.* (February) 1952
"Ferrite Applications in Electronic Components," B. V. Vonderschmitt, M. J. Obert, and H. B. Stott, *Electronics* (March) 1952
"Frequency Control of Modulated Magnetrons by Resonant Injection System," L. L. Koros, *RCA Licensee Bulletin LB-855* (February 8) 1952
"Frequency Control of Modulated Magnetrons by Resonant Injection System," L. L. Koros, *RCA Review* (March) 1952
"Frequency Stability for Television Offset Carrier Operation," P. J. Herbst and E. M. Washburn, *RCA Review* (March) 1952
"Heat-Transmitting Mirror," G. L. Dimmick and M. E. Widdop, *Jour. S.M.P.T.E.* (January) 1952
"High-Silica Fluosilicic Acids: Specific Reactions and the Equilibrium with Silica," S. M. Thomsen, *Jour. Amer. Chem. Soc.*.. 1952
"A High-Voltage Electron-Trap Rectifier," E. G. Linder, J. H. Coleman, and E. G. Apgar, *Proceedings of the National Electronics Conference* (February) 1952
"Image Gradation, Graininess and Sharpness in Television and Motion Picture Systems (Part II)," O. H. Schade, *Jour. S.M.P.T.E.* (March) 1952

† Report all corrections or additions to RCA Review, Radio Corporation of America, RCA Laboratories Division, Princeton, N. J.
* *RCA Licensee Bulletins* are not published and are issued only as a service to licensees of the Radio Corporation of America.

"Image Orthicon Color Television Camera Optical System," L. T. Sachtleben, D. J. Parker, G. L. Allee, and E. Kornstein, *RCA Review* (March) 1952
"Improved Television Picture Performance," H. N. Kozanowski, *Broadcast News* (January-February) 1952
"Inexpensive Square-Wave Generator," G. W. Gray, *Electronics* (February) 1952
"Master Monitor for Video Monitoring," N. P. Kellaway, *TV Eng.* (March) 1952
Musical Engineering, H. F. Olson, McGraw-Hill Book Company, Inc., New York, N. Y. 1952
"The NBC New York Color Television Field Test Studio," J. R. DeBaun, R. A. Monfort, and A. A. Walsh, *RCA Review* (March) 1952
"A New Master Monitor," N. P. Kellaway, *Broadcast News* (March-April) 1952
"New Principle for Electronic Volume Compression," H. E. Haynes, *Jour. S.M.P.T.E.* (February) 1952
"A New Television Camera for Studio and Field Use," A. Reisz, *Broadcast News* (March-April) 1952
"A New UHF Television Antenna, TFU-24-B," O. O. Fiet, *Broadcast News* (March-April) 1952
"Originative and Intensifier Activators in MgO Phosphors," R. H. Bube and K. F. Stripp, *Jour. Chem. Phys.* (January) 1952
"Performance of the Vidicon, a Small Developmental Television Camera Tube," B. H. Vine, R. B. Janes, and F. S. Veith, *RCA Review* (March) 1952
"Pictorial Radio, Part I," C. D. Tuska, *Jour. Frank. Inst.* (January) 1952
"Pictorial Radio, Part II," C. D. Tuska, *Jour. Frank. Inst.* (February) 1952
"Power-Increase Conversions," F. E. Talmage, *TV Eng.* (January) 1952
Radio Antenna Engineering, E. A. Laport, McGraw-Hill Book Company, Inc., New York, N. Y. 1952
"The RCA Color Television Camera Chain," J. D. Spradlin, *RCA Review* (March) 1952
"Reducing Outage at WNBT and WNBC-FM," L. A. Looney and F. C. Everett, *Electronics* (January) 1952
"Regulated 1,600-Ampere Filament Supply," A. W. Vance and C. C. Shumard, *Electronics* (February) 1952
"A Scientist Looks at Television in Relation to Its Social Aspects," V. K. Zworykin, Section of *Technion Yearbook*, 1951 1952
"Standards Conversion of Television Signals," V. K. Zworykin, and E. G. Ramberg, *Electronics* (January) 1952
"The Stratford, Conn. UHF TV Tests," R. J. Hall, *Service* (March) 1952
"Sweep Frequency Generator for UHF Television Band," J. A. Cornell, and J. F. Sterner, *Tele-Tech* (February) 1952
"Television in Medicine and Biology," V. K. Zworykin, and L. E. Flory, *Elec. Eng.* (January) 1952
"TT-25AL/20AH Conversion Equipments," F. E. Talmage, *Broadcast News* (January-February) 1952
"The 'Twomobile', a 144-Mc. Transceiver," H. W. Brown, Jr., *Ham Tips* (January-February) 1952
"UHF Receiving Antennas," E. O. Johnson and J. D. Callaghan, *Electronics* (January) 1952
"Vibrating-Plate Viscometer," J. G. Woodward, *Electronics* (February) 1952

AUTHORS

KERN K. N. CHANG received the B.S. degree from the National Central University, Nanking, China, in 1940, and the M.S. degree in Electrical Engineering from the University of Michigan in 1948. From 1940 to 1945, he was associated with the Central Radio Manufacturing Works, Kunming, China, working on radio receivers, and from 1945 to 1947, he was a radio instructor in the Office of Strategic Service, U. S. Army, China Theatre. Since 1948, Mr. Chang has been at RCA Laboratories Division, Princeton, N. J., where he is presently engaged in work on the use of magnetrons in amplitude-modulated transmitters. Mr. Chang is a Member of Sigma Xi.

JOHN S. DONAL, JR. received the A.B. degree from Swarthmore College in 1926 and the Ph.D. degree in Physics from the University of Michigan in 1930. From 1930 to 1936, he was associated with the Johnson Foundation for Research in Medical Physics and with the department of Pharmacology of the University of Pennsylvania. In 1936, he joined the Research Laboratories of the RCA Manufacturing Company, Inc., and is now associated with RCA Laboratories Division, Princeton, N. J., where he is engaged in research on microwave transmitting tubes and their modulation. Dr. Donal is a Member of Sigma Xi, Sigma Tau, the American Physical Society, and a Senior Member of the Institute of Radio Engineers.

JESS EPSTEIN received the E.E. degree and the M.S. degree in Physics from the University of Cincinnati in 1932 and 1934. From 1934 to 1935, he was an instructor in Physics at the Cincinnati College of Pharmacy. In 1935, he joined the research division of RCA Manufacturing Company at Camden, N. J., and was transferred to RCA Laboratories Division at Princeton, N. J., in 1942, where he is now engaged in work on antennas, transmission lines and propagation. Mr. Epstein is a Member of Sigma Xi, and a Senior Member of the Institute of Radio Engineers.

HANS K. JENNY received the M.S. degree in Electrical Engineering from the Swiss Federal Institute of Technology in Zurich, Switzerland in 1943. He remained there from 1944 to 1946 as assistant to Professor Dr. F. Tank, head of the Institute of High Frequency. In 1946 he joined the Tube Department of the Radio Corporation of America in Lancaster, Pa., and has since been engaged in the development of microwave tubes. Since moving to Harrison, N. J. with the Special Development Group in 1950, he has been in charge of the tube design unit. Mr. Jenny is a Senior Member of the Institute of Radio Engineers.

EDWARD O. JOHNSON received the B.S. degree in Electrical Engineering from Pratt Institute of Brooklyn in 1948. From 1941-1945 he served as an electronic technician in the U. S. Navy. In 1948 he joined the RCA Laboratories Division, Princeton, N. J., where he is now engaged in work on gaseous electronics. Mr. Johnson is a Member of the Institute of Radio Engineers.

LOUIS MALTER received the B.S. degree from the College of the City of New York in 1926 and the M.A. and PhD. degrees in Physics from Cornell University in 1931 and 1936, respectively. He taught Physics at the College of the City of New York from 1926 to 1928. He was with the Acoustic Research and Photophone Divisions of Radio Corporation of America from 1928 to 1930, and during the Summer of 1931. From 1933 to 1942 he was with RCA Manufacturing Company at Camden, N. J., and from 1942 to 1943 with RCA Laboratories Division at Princeton, N. J. From 1943 to 1946, he was in charge of the Special Development Division of RCA Manufacturing Company at Lancaster, Pa. From May 1946 to December 1947 he was in charge of the Vacuum Tube Research Section of the Naval Research Laboratory, Washington, D.C. In December 1947 he returned to the RCA Laboratories where he is now engaged in research on gaseous electronics. Dr. Malter is a Fellow of the American Physical Society, a Senior Member of the Institute of Radio Engineers, a Member of the American Association for the Advancement of Science, and a Member of Sigma Xi.

DONALD W. PETERSON received the B.S. degree in E.E. from the University of Wisconsin in 1936. In that year, he joined the Service Department of RCA Manufacturing Company, Camden, N. J., shifting to the research division of that company in 1939. In 1942 he was transferred to RCA Laboratories Division in Princeton, N. J., where he is currently engaged in work on antennas, transmission lines and propagation. Mr. Peterson is a Member of Sigma Xi and the Institute of Radio Engineers.

JAN A. RAJCHMAN, received the diploma of Electrical Engineering in 1934 and the degree of Doctor in Technical Sciences in 1938 from the Swiss Federal Institute of Technology. In 1936 he joined the Research Department of the RCA Manufacturing Company in Camden, New Jersey. In 1942 he was transferred to the RCA Laboratories Division in Princeton, New Jersey. Dr. Rajchman is a Senior Member of the Institute of Radio Engineers, a Member of the American Physical Society, Sigma Xi, and the Association for Computing Machinery, and co-recipient of the Levy Medal of the Franklin Institute 1946.

PHILIP T. SMITH received the B.A. degree in Physics from the University of Minnesota in 1927. He was a teaching assistant in physics at that University until 1931, when he received the Ph.D. Degree. From 1931 to 1933 he was a Rockefeller Research Fellow at the University of Minnesota, and the following year, he was a National Research Fellow in physics at Princeton University. He was an instructor of physics at the Massachusetts Institute of Technology until 1937. He joined the Research staff of the RCA Manufacturing Company at Harrison, N. J., remaining until 1942, when he transferred to RCA Laboratories Division at Princeton, N. J., as a research engineer working on UHF problems. Dr. Smith is a Member of the American Physical Society, Sigma Xi, and Gamma Alpha.

WILLIAM M. WEBSTER studied physics at Rensselaer Polytechnic Institute and at Union College as a Navy V-12 student. He received a B.S. degree in Physics in 1945. He was released from active duty in 1946 and joined the RCA Laboratories Division, Princeton, in October of that year. He is currently enrolled in the Graduate School of Princeton University on a part-time basis. Mr. Webster is an Associate Member of the Institute of Radio Engineers.

OAKLEY M. WOODWARD, JR. received the degree of Bachelor of Science in Electrical Engineering from the University of Oklahoma in 1938. He joined the Seismograph Service Corporation of Tulsa, Oklahoma, after graduation. During 1941, he was a research engineer at the RCA Manufacturing Company, Camden, N. J. Since January 1942, he has been with RCA Laboratories Division, Princeton, N. J. Mr. Woodward is a Member of Sigma Xi, and an Associate Member of the Institute of Radio Engineers.